Effects of sample treatment on mixed-layer illite/smectite in X-ray diffractograms and transmission electron micrographs

S. Kelly Sears

Department of Earth and Planetary Sciences
McGill University
Montreal, Quebec

A thesis submitted to the Faculty of Graduate Studies and Research
in partial fulfilment of the requirements for
the degree of Master of Science

July, 1993

Name S. Kelly Sears

Dissertation Abstracts International is arranged by broad, general subject categories Please select the one subject which most nearly describes the content of your dissertation Enter the corresponding four digit code in the spaces provided

Earth Sciences — 0 3 7 2

SUBJECT TERM — SUBJECT CODE

Subject Categories

THE HUMANITIES AND SOCIAL SCIENCES

COMMUNICATIONS AND THE ARTS

Architecture	0729
Art History	0377
Cinema	0900
Dance	0378
Fine Arts	0357
Information Science	0723
Journalism	0391
Library Science	0399
Mass Communications	0708
Music	0413
Speech Communication	0459
Theater	0465

EDUCATION

General	0515
Administration	0514
Adult and Continuing	0516
Agricultural	0517
Art	0273
Bilingual and Multicultural	0282
Business	0688
Community College	0275
Curriculum and Instruction	0727
Early Childhood	0518
Elementary	0524
Finance	0277
Guidance and Counseling	0519
Health	0680
Higher	0745
History of	0520
Home Economics	0278
Industrial	0521
Language and Literature	0279
Mathematics	0280
Music	0522
Philosophy of	0998
Physical	0523
Psychology	0525
Reading	0535
Religious	0527
Sciences	0714
Secondary	0533
Social Sciences	0534
Sociology of	0340
Special	0529
Teacher Training	0530
Technology	0710
Tests and Measurements	0288
Vocational	0747

LANGUAGE, LITERATURE AND LINGUISTICS

Language	
General	0679
Ancient	0289
Linguistics	0290
Modern	0291
Literature	
General	0401
Classical	0294
Comparative	0295
Medieval	0297
Modern	0298
African	0316
American	0591
Asian	0305
Canadian (English)	0352
Canadian (French)	0355
English	0593
Germanic	0311
Latin American	0312
Middle Eastern	0315
Romance	0313
Slavic and East European	0314

PHILOSOPHY, RELIGION AND THEOLOGY

Philosophy	0422
Religion	
General	0318
Biblical Studies	0321
Clergy	0319
History of	0320
Philosophy of	0322
Theology	0469

SOCIAL SCIENCES

American Studies	0323
Anthropology	
Archaeology	0324
Cultural	0326
Physical	0327
Business Administration	
General	0310
Accounting	0272
Banking	0770
Management	0454
Marketing	0338
Canadian Studies	0385
Economics	
General	0501
Agricultural	0503
Commerce Business	0505
Finance	0508
History	0509
Labor	0510
Theory	0511
Folklore	0358
Geography	0366
Gerontology	0351
History	
General	0578
Ancient	0579
Medieval	0581
Modern	0582
Black	0328
African	0331
Asia, Australia and Oceania	0332
Canadian	0334
European	0335
Latin American	0336
Middle Eastern	0333
United States	0337
History of Science	0585
Law	0398
Political Science	
General	0615
International Law and Relations	0616
Public Administration	0617
Recreation	0814
Social Work	0452
Sociology	
General	0626
Criminology and Penology	0627
Demography	0938
Ethnic and Racial Studies	0631
Individual and Family Studies	0628
Industrial and Labor Relations	0629
Public and Social Welfare	0630
Social Structure and Development	0700
Theory and Methods	0344
Transportation	0709
Urban and Regional Planning	0999
Women's Studies	0453

THE SCIENCES AND ENGINEERING

BIOLOGICAL SCIENCES

Agriculture	
General	0473
Agronomy	0285
Animal Culture and Nutrition	0475
Animal Pathology	0476
Food Science and Technology	0359
Forestry and Wildlife	0478
Plant Culture	0479
Plant Pathology	0480
Plant Physiology	0817
Range Management	0777
Wood Technology	0746
Biology	
General	0306
Anatomy	0287
Biostatistics	0308
Botany	0309
Cell	0379
Ecology	0329
Entomology	0353
Genetics	0369
Limnology	0793
Microbiology	0410
Molecular	0307
Neuroscience	0317
Oceanography	0416
Physiology	0433
Radiation	0821
Veterinary Science	0778
Zoology	0472
Biophysics	
General	0786
Medical	0760

EARTH SCIENCES

Biogeochemistry	0425
Geochemistry	0996
Geodesy	0370
Geology	0372
Geophysics	0373
Hydrology	0388
Mineralogy	0411
Paleobotany	0345
Paleoecology	0426
Paleontology	0418
Paleozoology	0985
Palynology	0427
Physical Geography	0368
Physical Oceanography	0415

HEALTH AND ENVIRONMENTAL SCIENCES

Environmental Sciences	0768
Health Sciences	
General	0566
Audiology	0300
Chemotherapy	0992
Dentistry	0567
Education	0350
Hospital Management	0769
Human Development	0758
Immunology	0982
Medicine and Surgery	0564
Mental Health	0347
Nursing	0569
Nutrition	0570
Obstetrics and Gynecology	0380
Occupational Health and Therapy	0354
Ophthalmology	0381
Pathology	0571
Pharmacology	0419
Pharmacy	0572
Physical Therapy	0382
Public Health	0573
Radiology	0574
Recreation	0575
Speech Pathology	0460
Toxicology	0383
Home Economics	0386

PHYSICAL SCIENCES

Pure Sciences

Chemistry	
General	0485
Agricultural	0749
Analytical	0486
Biochemistry	0487
Inorganic	0488
Nuclear	0738
Organic	0490
Pharmaceutical	0491
Physical	0494
Polymer	0495
Radiation	0754
Mathematics	0405
Physics	
General	0605
Acoustics	0986
Astronomy and Astrophysics	0606
Atmospheric Science	0608
Atomic	0748
Electronics and Electricity	0607
Elementary Particles and High Energy	0798
Fluid and Plasma	0759
Molecular	0609
Nuclear	0610
Optics	0752
Radiation	0756
Solid State	0611
Statistics	0463

Applied Sciences

Applied Mechanics	0346
Computer Science	0984
Engineering	
General	0537
Aerospace	0538
Agricultural	0539
Automotive	0540
Biomedical	0541
Chemical	0542
Civil	0543
Electronics and Electrical	0544
Heat and Thermodynamics	0348
Hydraulic	0545
Industrial	0546
Marine	0547
Materials Science	0794
Mechanical	0548
Metallurgy	0743
Mining	0551
Nuclear	0552
Packaging	0549
Petroleum	0765
Sanitary and Municipal	0554
System Science	0790
Geotechnology	0428
Operations Research	0796
Plastics Technology	0795
Textile Technology	0994

PSYCHOLOGY

General	0621
Behavioral	0384
Clinical	0622
Developmental	0620
Experimental	0623
Industrial	0624
Personality	0625
Physiological	0989
Psychobiology	0349
Psychometrics	0632
Social	0451

ABSTRACT

Combined X-ray powder diffraction (XRD) and high-resolution transmission electron microscopy (HRTEM) were used to identify and characterize the clay mineral assemblages in 0.05-0.1 μm and <0.05 μm size fractions separated from shales of three depths (4800, 8700-8750, and 12500-12550 ft) from the Reindeer D-27 well in the Beaufort-Mackenzie area, Arctic Canada. Ethylene-glycol solvated samples indicated a two-component mixed-layer I/S system, whereas glycerol solvation suggested an additional high-charge expandable component. Exchange with octylammonium ($n_c = 8$) and octadecylammonium ($n_c = 18$) ions revealed the presence of five distinct types of layer structures. (1) low-charge smectite-group, (2) high-charge smectite-group or vermiculite, (3) double-layers or rectorite-like, (4) expandable illite, and (5) non-expandable illite. The presence and abundance of each type of layer structure changed with burial depth.

A comparison of untreated and sodium hexametaphosphate-treated <0.05 μm size fractions revealed modifications to the structure of mixed-layer I/S in both ethylene-glycol solvated and alkylammonium-ion exchanged specimens. Changes in peak position, intensity and breadths are apparent in XRD, and these modifications can also be observed in HRTEM. Lattice-fringe images revealed that pretreatment resulted in (1) increased abundance of 2:1 layer silicate packets with expanded interlayers, (2) increased R1-ordered sequences, and (3) thinner packets of non-expanded illite interlayers. The use of sodium hexametaphosphate as a peptizer alters the interlayers and modifies the stacking arrangement of the layer structures. If the primary structure is altered, the disruption may be irreversible.

It is evident therefore, that reliable ratio determination between expandable and non-expandable components in mixed-layer I/S is dependent on characterizing all the components and resolving the effects of chemical pretreatment.

RESUME

Nous avons identifié et caractérisé par diffraction de rayons X (XRD) et par microscopie électronique par transmission à haute résolution (HRTEM), l'association de minéraux argilleux correspondante aux fractions 0.05-0.1 μm et <0.05 μm des schistes argilleux du forage Reindeer D-27 (profondeurs 1453, 2652-2668, et 3810-3826 m) situé au Bassin Beaufort-Mackenzie aux Canada artique.

Les échantillons traité à l'ethylen glycol-solvaté indiquent la présence du system à couches mixtes I/S à deux composants. L'étude après échange à l'ion octylammonium ($n_C=8$) et octadecylammonium ($n_C=18$) montre la présence de 5 types de smectites encouche: (1) smectites à faible charge, (2) smectites ou vermiculite à haute charge, (3) rectorite à double couche, (4) illite expandable, et (5) illite non expandable. La présence et l'abondance de chaque type de structure en couche varie avec la profondeur.

La comparaison des échantillons tel quels et traités par Na-hexametaphosphate (<0.05 μm) a révelé des modifications de la structure à couche mixte I/S dans ceux glycolé-solvatés et dans ceux soumit à l'échange avec l'ion alkylammonium.

La variation de la largeur, de la position et de l'intensité des pics détecté par XRD a été observée en HRTEM aussi Par les images des franges du réseau on réleve: (1) l'augmentation de l'abondance des couches 2:1 avec intercouche expandable, (2) l'augmentation de l'abondancee des séquences ordonneés R1, et (3) la diminution des paquets d'illite intercouche non-expandable.

L'utilisation de l'hexametaphosphate de sodium altère l'intercouche et modifie l'empilement des structures en couche. Le rapport entre composants expandables et non-expandables des couches mixtes I/S dépende de caractéristiques des composants et du traitement chimique soubit.

ACKNOWLEDGEMENTS

Scientific endeavors are never pursued in a vacuum but are accomplished through the collective will, effort and support of numerous institutions and individuals. This manifests itself, financially, intellectually and emotionally to achieve the end results of advancing scientific knowledge and concomitantly furthering personal, intellectual and emotional growth. I am indebted to all those who helped me in my pursuit and attainment of my postgraduate education, and I extend my gratitude and appreciation to the following:

Professor Reinhard Hesse, who supported, supervised and guided me through the travails of my thesis and introduced me to the fascinating, yet complex discipline of clay science, and who taught me self-reliance and self-judgement, and who gave me the freedom to pursue my own goals;

Dr. Hojatollah Vali, for sharing his knowledge and expertise in the field of clay science and the transmission electron microscope (TEM), for being a true supporter and friend, and an indefatigable source of energy, without whom this thesis would have never been completed. Cryofixation and freeze-etching were performed by Dr. Vali at the Technische Universitat Munchen, Garching, Germany,

Professor Alphonso Mucci, for being a member of my committee and contributing constructive criticisms and valuable comments for improving my research, Mr. Tariq Ahmedali, McGill Geochemical Laboratory, for his advice, guidance and willingness to answer all questions and inquiries; Mr. Michael Harrigan, School of Occupational Health, for allowing unrestricted access to the TEM facilities and darkroom, and for lending equipment and giving abundant advice; Dr. Jaehong Ko for helpful suggestions; Dr. Pierpaolo Zuddas, for the last-minute translation of the abstract;

To my fellow students, especially Hugo Chouinard, Saeed Khodabakhsh, Ingo Klaucke, Mark Fay, Xiomara Marquez, Jeanette Roelofsen, Salah Shata and Dong Wang, who helped create a stable environment of friendship and support which sustained itself through difficult periods;

To Sheri Sears for last-minute proofreading;

To the Natural Science and Engineering Research Council (NSERC) of Canada and Petro-Canada Limited for financially supporting my research through graduate scholarships;

I reserve my deepest and most heart-felt gratitude and appreciation to my parents,

Rosamond and Gordon Sears, who gave me the love and support that allowed me to pursue any and all my dreams and aspirations. It is a debt that I can never repay.

"We shall not cease from exploration
And in the end of all our exploring
Will be to arrive where we started
And know the place for the first time" (1)

---

(1) Excerpted from "Little Gidding" by T.S Eliot (1942) Selected poem is from Collected Poems 1909-1962 by T.S Eliot, copyright 1936 by Harcourt Brace Jovanovich, Inc , copyright 1943, 1963, 1964, by T.S. Eliot; copyright 1971, by Esme Valerie Eliot. All rights reserved

TABLE OF CONTENTS

LIST OF FIGURES

CHAPTER 1.0 - Introduction

Shales are the most predominant rock type in many sedimentary basins, but because of their generally heterogeneous and variable mineralogy and extremely fine grain-size, make it difficult to decipher their response to burial diagenesis. Ideally, understanding diagenetic changes requires an *a priori* knowledge of the initial mineralogical composition at deposition, which may not always be available. Investigations into shale diagenesis have shown that variations in mineralogy and composition of minerals with depth may result from changes in provenance, weathering, transport and depositional environment (Pollastro 1990, Bloch and Hutcheon 1992). However, contemporary research has also shown that the originally diverse assemblages at deposition become simpler and converge with depth of burial; smectite and kaolinite diminish, whereas illite and chlorite become enriched with depth (e.g. Hower et al. 1976; Ko 1992; Awwiller 1993).

Clay-diagenetic studies have often relied on "bulk" mineralogical and chemical analysis of shales and clay-size separates, using X-ray powder diffraction (XRD) and some scanning and transmission electron microscopy (STEM) to characterize and define the nature of the diagenetic processes. These processes are often inferred from changes in the relative mineral, elemental and isotopic abundance in different grain-size fractions (Pye et al. 1986). Investigations into clay mineral diagenesis in various sedimentary basins from around the world, such as the Rhinegraben (Heling 1974, 1978), Vienna Basin (Johns and Kurzweil 1979; Horton et al 1985, Johns and McKallip 1989), Paris Basin (Lanson and Champion 1991), various basins of the North Sea (Pearson and Small 1988; Glasman et al. 1989a, 1989b; Jones et al 1989; Hansen and Lindgreen 1987, 1989; Lindgreen and Hansen 1991), Montana basins (McCarty and Thompson 1991), Denver Basin (Elliot et al. 1991), Beaufort-Mackenzie Basin (Powell et al 1978; Ko 1992; Ko and Hesse 1992), and San Joaquin Basin (Ramseyer and Boles 1986) have confirmed initial studies done in the Gulf of Mexico (Burst 1959, 1969; Powers 1967; Perry and Hower 1970, 1972; Hower et al. 1976) that illitic material, smectite-group minerals and illite/smectite (I/S) mixed layers are the most adundant clay minerals and that the principal diagenetic reaction in mudrocks is the illitization of smectite. A major assumption in most burial diagenetic studies is that clay mineral assemblages are in equilibrium with the present thermo-chemical environment and changes in the I/S ratio result from progressive changes in the basin environment through time (Glasmann et al. 1989a).

Significant consequences which may result from the physical, chemical and mineralogical modifications during the smectite-to-illite (S-I) conversion in sedimentary basins include: development of geopressure, hydro-fracturing, hydrocarbon migration, and solute transport. The release of interlayer water in temperature-controlled reactions at great depths during illitization may or may not be an be important flushing mechanism for hydrocarbons and for transporting inorganic and organic substances (Powers 1967; Burst 1969; Bruce 1984).

Despite the increased research activity into mixed-layer I/S within the past two decades, uncertainty remains concerning its structural and compositional state, the definition of 'phase', the characterization of smectite-group minerals, illite and I/S, with emphasis on the existence of interstratification, the composition of the expandable components, the nature of particle boundary coherency, the relevance of short- and long-range order, and sample preparation artifacts (Nadeau et al. 1984a,b,c; Ahn and Peacor 1986a; Eberl et al. 1987; Eberl and Środoń 1988, Huff et al. 1988; Altaner et al. 1988; Altaner and Vergo 1988; Ransom and Helgeson 1989; Ahn and Buseck 1990; Guthrie and Veblen 1989, 1990; Veblen et al. 1990; Reynolds 1991, 1992; Allen 1992; Vali et al. 1993a,b) Warren and Ransom (1992) insisted that it is imperative to determine the stuctural state of mixed-layer I/S, i.e. mixtures of two or more separate phases when interstratified (Garrels 1984; Sass et al. 1987), end-member compositions of one or more solid-solution series (Aagaard and Helgeson 1983), or multi-phase intergrowths (Rosenberg et al. 1990; Aja et al. 1991a,b; Vali et al. 1991).

Illite/smectite has been interpreted using the Markovian model (MacEwan 1956, 1958; Reynolds 1980) which suggested that I/S was a mixture of two layer types, i.e. smectite-group and illite, and stacked perpendicular to the Z-direction within a single crystal or diffracting domain. As a coherent mineral however, it should not be easily broken down into its constituent layers (Reynolds 1992). MacEwan crystallites consist of two thermodynamic phases, smectite-group and illite layers, which behave differently because of differing chemical and structural compositions, and which can separate along smectitic interlayers during sample preparation (Altaner and Vergo 1988; Altaner et al. 1988; Ahn and Peacor 1989; Veblen et al. 1990). Nadeau et al. (1984a,b,c) proposed that disordered mixed-layer I/S was a random mixture of fundamental particles of smectite and illite, whereas ordered mixed-layer I/S consisted solely of fundamental illite layers and was a single thermodynamic phase of constant composition Fundamental illite layers are capable of adsorbing water or organic molecules at their expandable interfaces which mimic a smectite-group component in XRD. From equilibrium studies, Rosenberg et al. (1990) and Aja et al. (1991a,b) argued that mixed-layer I/S consisted of a mixture of multiple, discrete stoichiometric mica-like phases. According to the multiphase model, natural illite was composed of four phases having a composition of S(R0), IS(R1), ISII(R≥3) and I. Lippmann and Johns (1969) suggested that during chemical alteration of an interlayer, modification of the tetrahedral sheets may occur, which can result in the 2:1 layer acquiring a polar character, leaving adjacent layers unmodified. Güven (1991) emphasized the nature of the interlayers in ordered mixed-layer I/S and conceptualized the P-layer model. A polar layer has one tetrahedral sheet with low or no charge (smectitic), whereas the other tetrahedral sheet carries a high charge (illitic). Thus mixed-layer I/S may consist of both polar and non-polar layers.

As diagenetic studies of shales, sandstones and bentonites have illustrated, ambiguities remain concerning the sequence of mineralogical changes, the reaction mechanisms and thermodynamic conditions driving the smectite-to-illite (S-I) conversion. Several mechanisms are proposed: (i) solid-state transformation (layer-by-layer), in which ionic substitutions are inferred to occur within the 2:1 layers (e.g., Hower et al. 1976; Środoń et al. 1986), (ii) dissolution-reprecipitation (neoformation), whereby smectite or smectite-rich I/S dissolves and illite or illite-rich I/S precipitates (e.g., Nadeau et al 1984a,b,c, Yau et al 1987), (iii) mineral-ripening, whereby thicker illite crystals grow at the expense of thinner illite crystals (e g Eberl 1993); and (iv) a combination of the three models (e g , Boles and Franks 1979, Pollastro 1985; Pye et al. 1986; Inoue et al. 1987, 1988).

X-ray powder diffraction is the principal analytical technique employed to identify and characterize I/S. The S-I transition has been inferred from the migration of reflections from lower to higher 2Θ angles, with reflection shape elucidating the development of short and then longer ranges of illite stacking in I/S mixed-layers (Reynolds and Hower 1970; Hoffman and Hower 1979; Reynolds 1980; Bethke et al. 1986). Traditionally, ethylene glycol or glycerol solvation has been routinely used to characterize the expandable component in I/S for XRD analysis, but gives no evidence on the layer charge. However, expandability is dependent on layer charge, type of interlayer cation and relative humidity (RH) (Środoń 1980). These organic molecules may not be able to distinguish between smectite-group and vermiculite components (Malla and Douglas 1987a). Thus, XRD may not be sensitive enough to reveal the degree of compositional or structural heterogeneity in I/S (Drits 1987).

Increasingly, TEM has been used to study the structures and compositions of fine-grained minerals formed under the relatively low temperatures characteristic of sedimentary environments. High-resolution TEM allows the direct observation of layer structures at the scale of illite and smectite-group layers, and can theoretically image both layer heterogeneity and ordering in I/S as well as changes in layer structure. The methods of specimen preparation and focus conditions are significant factors in the differentiation of smectite-group and illite components in I/S as well as in the detection of ordering in HRTEM (Bell 1986; Ahn and Peacor 1986a,b, 1989; Klimentidis and MacKinnon 1986; Hansen and Lindgreen 1987, 1989; Guthrie and Veblen 1989, 1990; Veblen et al. 1990; Ahn and Buseck 1990; Lindgreen and Hansen 1991; Amouric and Olives 1991, Vali et al. 1991, Freed and Peacor 1992). Attempts to reconcile the discrepancies between layer proportions obtained from XRD and TEM (Nadeau and Bain 1985; Eberl and Środoń 1988; Środoń et al. 1990; Środoń et al. 1992; Murakami et al. 1993) have not been entirely successful and the two analytical methods may prove ultimately to be incomparable (Sears and Hesse 1992; Sears et al. 1993a).

Application of the n-alkylammonium ion technique (Lagaly and Weiss 1969, 1970; Lagaly 1981, 1984, 1985) has been increasingly used to both characterize expandable 2:1 layer silicates in TEM (Lee and Peacor 1986; Bell 1986; Klimentidis and MacKinnon 1986: Vali and Köster 1986; Vali and Hesse 1992; Vali et al. 1990, 1991, 1992) and to determine the interlayer-charge density and deduce layer charge of soil and sediment clay minerals in XRD (Lagaly 1979, 1981, Rühlicke and Niederbudde 1985; Malla and Douglas 1987b,c; Laird et al. 1987, 1988, 1989a; Marcks et al. 1989; Ghabru et al. 1989; Chen et al. 1989; Stanjek et al. 1992). There is a systematic arrangement of the large anisometric organic ions in interlayer space of expandable layer silicates which results in a well-defined increase in the interlayer spacing (Lagaly and Weiss 1969). The application of the n-alkylammonium ion-exchange technique to mixed-layer clay minerals has revealed heterogeneous interlayer-charge densities of expandable components in mixed-layer structures (Lagaly 1979; Laird et al. 1989a; Vali and Hesse 1990, Vali et al. 1991; Vali et al. 1992; Sears and Hesse 1992; Sears et al. 1993a). This technique however, has not been used to qualitatively identify the components in mixed-layer I/S on the basis of interlayer-charge densities in a burial diagenetic sequence in both XRD and TEM studies.

An ancillary consequence of the development of the fundamental particle concept of Nadeau et al. (1984a,b,c, 1985) has been the increased awareness and concern for artifacts introduced into mixed-layer I/S by sample preparation techniques especially for XRD and TEM

(Reynolds 1991; 1992). Reynolds (1992) suggested that two types of artifacts may be produced in interstratified I/S clays during preparation (i) a change in the way layers are stacked within a sequence perpendicular to (00*l*), and (ii) a change in the stacking angles (i e rotation) of mica-like stacks which may produce turbostratic defects To aid fine- and ultrafine-particle size separation and promote sample homogeneity using conventional centrifuge techniques, chemical pretreatments and peptizers are used to remove carbonates, organic matter, Fe-oxides and other micro- and crypto-crystalline phases, and to promote stable dispersion of clay suspensions (e g Jackson 1969; Whittig and Allardice 1986, Moore and Reynolds 1989). Previous XRD and TEM studies have demonstrated that aggressive chemical pretreatments will not remove quartz, feldspar, magnetite and other contaminant phases, but may significantly alter the chemical composition and structure of clay minerals and create the appearance of new phases in XRD (Harward et al 1962; Fenner 1966; Jackson 1969; Thorez 1975, 1985, Brewster 1980, Omueti and Lavkulich 1988; Sears and Hesse 1992, Vali et al 1993a) Of primary concern is the potential for the alteration of layer charge and therefore expandability of smectite-group or vermiculite components in mixed-layer clay minerals (Bish and Reynolds 1989) Sodium hexametaphosphate is still used indiscriminantly as a peptizer without considering its effects on the layer structure or the interlayer charge of interstratified I/S (e.g., Bloch and Hutcheon 1992, Bühmann 1992; Reynolds 1992).

It has become imperative to accurately identify the components in mixed-layer I/S in order to unravel reaction mechanisms and sequences of structural and compositional changes in burial diagenetic environments. To achieve these aims, it is necessary to isolate a neoformed component of I/S by separating fine (<0.1 µm) and ultrafine (<0 05-µm) clay-size fractions from shales. However, any investigation of possible artifacts induced in mixed-layer I/S during sample preparation must include a detailed examination and resolution of any effects resulting from chemical pre- and post-treatments by characterizing all the expandable and non-expandable components.

The objectives of this research are,

(1) to identify and characterize the clay mineral assemblages of these ultrafine clay separates using X-ray diffraction (XRD), high resolution transmission electron microscopy (HRTEM) and n-alkylammonium ion-exchange treatment, and,

(2) to compare the effects of the addition of sodium hexametaphosphate as a peptizer on selected samples during clay mineral separation with chemically untreated

fractions.

CHAPTER 2.0 - Beaufort-Mackenzie Area

2.1 Regional Setting

The Beaufort-Mackenzie area, located in northwest Arctic Canada, contains several major depositional basins with estimated recoverable reserves of 1.11×10^9 m^3 of oil and 1.917×10^{12} m^3 of gas (Dixon et al. 1988, 1992b). It is incorporated within part of the foreland thrust-and foldbelt north of latitude 60°N of the eastern Cordilleran Orogenic system (Norris 1985)(Fig. 2.1). The Beaufort-Mackenzie area extends offshore from the Amundsen Gulf at 128°N to the Alaska-Yukon border at 141°W, and onshore from nearly 68°N to the terminus of the Mackenzie Delta's sedimentary cone north of 73°N (Haimila et al. 1990). It is physiographically bounded by the Anderson Plain to the east, the Peel Plateau to the south, the Richardson, British and Barn Mountains to the south and west, and the Porcupine Plateau to the west and northwest (Figs. 2.1 and 2.2). Landward, the Beaufort-Mackenzie area includes the modern Mackenzie River delta, Richards Island, the Tuktoyaktuk Pennisula and the Yukon Coastal Plain, and extends northward and seaward over the Beaufort Sea Shelf and Slope to the southern edge of the Canada Basin (Young et al. 1976; Dixon and Dietrich 1985, Majorowicz et al. 1990). The depositional basins of the Beaufort-Mackenzie area contain a succession of Jurassic to Recent sediments which reach a thickness of at least twenty kilometers, north of the present Mackenzie River delta (R. Stevenson as cited by Majorowicz et al. 1990).

2.2 Geotectonic Evolution

The Mesozoic and Cenozoic tectono-stratigraphic history of the Beaufort-Mackenzie area is due to the complex interaction among three major lithospheric elements; the North American Craton, the Cordilleran Orogen and the Canada Basin (Jones 1980; Dixon and Dietrich 1990). The identification of major interregional unconformities which signify tectono-stratigraphic boundaries, enable the area to be subdivided into four major depositional basins: Brooks-Mackenzie Basin (Hettangian-Aptian), Brooks-Yukon Basin (late Aptian-mid-Albian), Porcupine-Mackenzie Basin (early Cenomanian-early Maastrichtian) and Beaufort-Mackenzie Basin (mid-Maastrichtian-Holocene), each characterized by a dominant structural style and sedimentation pattern (Dixon et al. 1992a).

Although many dynamic models have been proposed to explain the development of the

Canadian Basin (see Lawver and Scotese 1990), consensus exists for the continental margins of the Canadian Arctic to be considered as a rifted (passive) pull-apart margin, with the paleo-pole for rotational rifting located in the Mackenzie delta area (Carey 1958; Tailleur and Broges 1970; Tailleur 1973; Bruce and Parker 1975; Grantz et al. 1979; Grantz and May 1983; Embry and Dixon 1990). The opening of the Canada Basin and the formation of the Beaufort Sea-Mackenzie Delta are are intrinsically linked and yet have very different crustal structures (Jackson et al. 1984; Sweeney 1985; Majorowicz et al. 1990). It appears that the principal structural controls for the incipient development of the Beaufort-Mackenize area were the opening of the Canada Basin and Cordilleran orogenesis which themselves developed in response to subduction in the Pacific and sea-floor spreading in the Atlantic (Smith 1987).

The regional tectonic history is highlighted by the following stages (Dixon and Dietrich 1985; Dixon and Dietrich 1990; Dixon et al. 1992b): in the Jurassic to Early Cretaceous, northern Alaska was adjacent to the Canadian Arctic Islands, and northern Yukon and adjacent Northwest Territories are part of the North America craton with coarse clastics deposited on a broad epicratonic shelf with easterly and southeasterly sources. These deposits are referred to as the Brooks-Mackenzie and Brooks-Yukon basins (Dixon et al. 1992a). Continental rifting began in early Bajocian time creating the Amerasia Basin, followed by rifting, breakup, and formation of the Canada Basin by sea-floor spreading, beginning in Hauterivian (Grantz and May 1983) or Late Albian-Cenomanian time (Embry and Dixon 1990). The onset of continental breakup in the Mackenzie Delta area may be marked by the Middle Hauterivian unconformity at the base of the Mount Goodenough Formation (Dixon 1982). Initiation of thermal subsidence of the newly created continental margins began. In Aptian, extensional tectonics created a series of horst and graben structures, the most prominent of which is the Aklavik Arch Complex (Hubbard et al. 1987; Embry and Dixon 1990). In Late Aptian and Albian, a second extensional phase resulted in a series of east-west trending troughs from the Tuktoyaktuk Peninsula (Kugmallit Trough) to the northern Yukon (Blow, Kuli and Kandit troughs). Coeval with rifting was the development of the Columbian Orogeny and a foredeep was created in front of the paleo-Mackenzie Mountains (Peel Trough). Although sediment was shed principally from the North American craton, westerly-derived coarse clastics began to fill the northern Yukon troughs with sediment gravity-flow deposits. As the Canada Basin continued to develop during the Cenomanian, the Cordilleran Orogen migrated to the north and northeast compressing strata in northern Alaska, northern Yukon and southern Beaufort Sea. During the Cenomanian to Campanian, sedimentation shed from the rising Cordillera to the south and southwest infilled the foreland basins on the craton in northern Yukon and adjacent Northwest Territories. These deposits are referred to as the Porcupine-Mackenzie Basin (Dixon et al. 1992a). There are two unconformities in the Early Cenomanian and Middle Campanian which developed during periods of uplift and erosion and may be related to the termination of sea-floor spreading in the Canada Basin (Grantz et al. 1990). As the Canada Basin developed, compression from the Cordilleran Orogeny during the Late Cretaceous to Paleogene became the dominant force (Dietrich et al. 1989a; 1989b; Hubbard 1988). This resulted in major subsidence during the Late Eocene to Pleistocene.

As a foreland basin developed in front of the Cordilleran Orogen, it was progressively infilled with southerly and southwesterly derived sediments. Along the continental margin of northern Yukon and Northwest Territories, outer shelf to basinal, organic-rich shales were deposited (Boundary Creek and Smoking Hills sequences). In Late Maastrichtian, the depocenter of the clastic sedimentation migrated to the thermally subsiding continental margins, where the combination of tectonic and sediment loading created a thick wedge of Upper Cenomanian to Recent siliciclastic sediments. These deposits are referred to as the Beaufort-Mackenzie Basin (Dixon et al. 1992a).

During this period, hydrocarbons were generated and geopressure developed (Hitchon et al. 1990). In the mid-Eocene, the Laramide Orogeny ended due to changes in Pacific plate motion (McWhae 1986). The final, major tectonic phase, the Camden Orogeny (Hubbard et al. 1987) began in northeastern Alaska in the Neogene and is continuing through to the present creating the Romanzof Uplift and the fold and thrust belt in the northern Yukon and adjacent offshore areas (Grantz et al. 1986; McWhae 1986). At the end of the Miocene, uplift and/or eustatic lowering of sea level caused significant erosion of Cenomanian to Eocene sediments (Bujack and Davies 1981; McNeil et al. 1982, Dixon et al. 1984, Dixon and Dietrich 1990). This resulted in a well-defined angular unconformity to disconformity which was the last major hiatus in the sedimentary history of the Beaufort-Mackenzie area (Dixon and Dietrich 1990). Extensive recharge of meteroic waters at the basin margins is thought to have occurred during this period which may have led to the biodegradation of hydrocarbons (Hitchon et al. 1990).

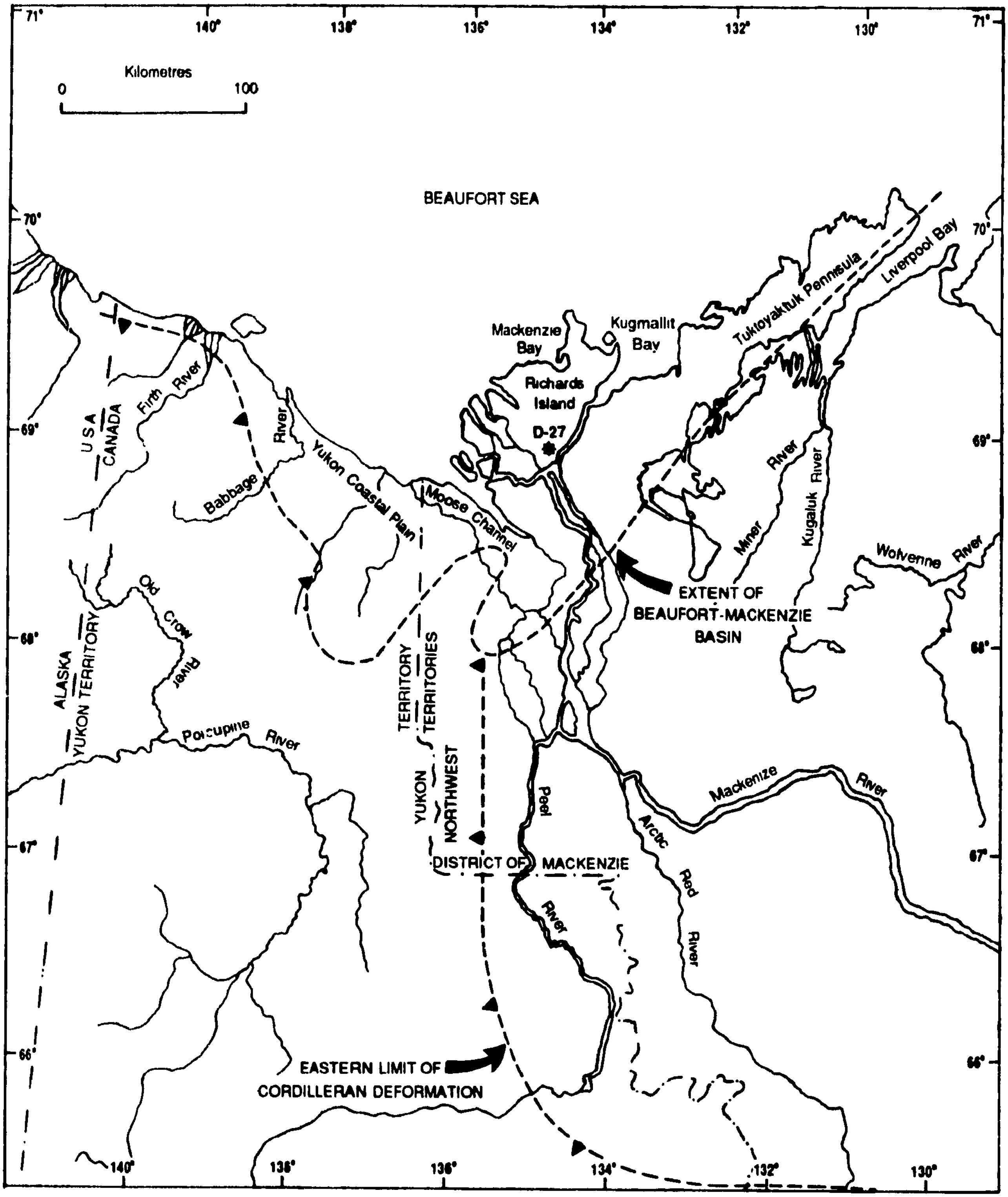
71°
140°
138°
136°
134°
132°
130°
71°
Kilometres
0
100
BEAUFORT SEA
70°
70°
Mackenzie Bay
Kugmallit Bay
Tuktoyaktuk Peninsula
Liverpool Bay
Richards Island
D-27
69°
69°
USA
CANADA
Firth River
Babbage River
Yukon Coastal Plain
Moose Channel
Miner River
Kugaluk River
Wolverine River
EXTENT OF BEAUFORT-MACKENZIE BASIN
Old Crow River
68°
68°
ALASKA
YUKON TERRITORY
YUKON TERRITORY
NORTHWEST TERRITORIES
Porcupine River
Peel River
Mackenize River
Arctic Red River
67°
67°
DISTRICT OF MACKENZIE
66°
66°
EASTERN LIMIT OF CORDILLERAN DEFORMATION
140°
138°
136°
134°
132°
130°

Fig 2.1 Regional extent of the Beaufort-Mackenzie area (after Young et al. 1976, Dixon and Dietrich 1985; Norris 1985; Majorowicz et al 1990).

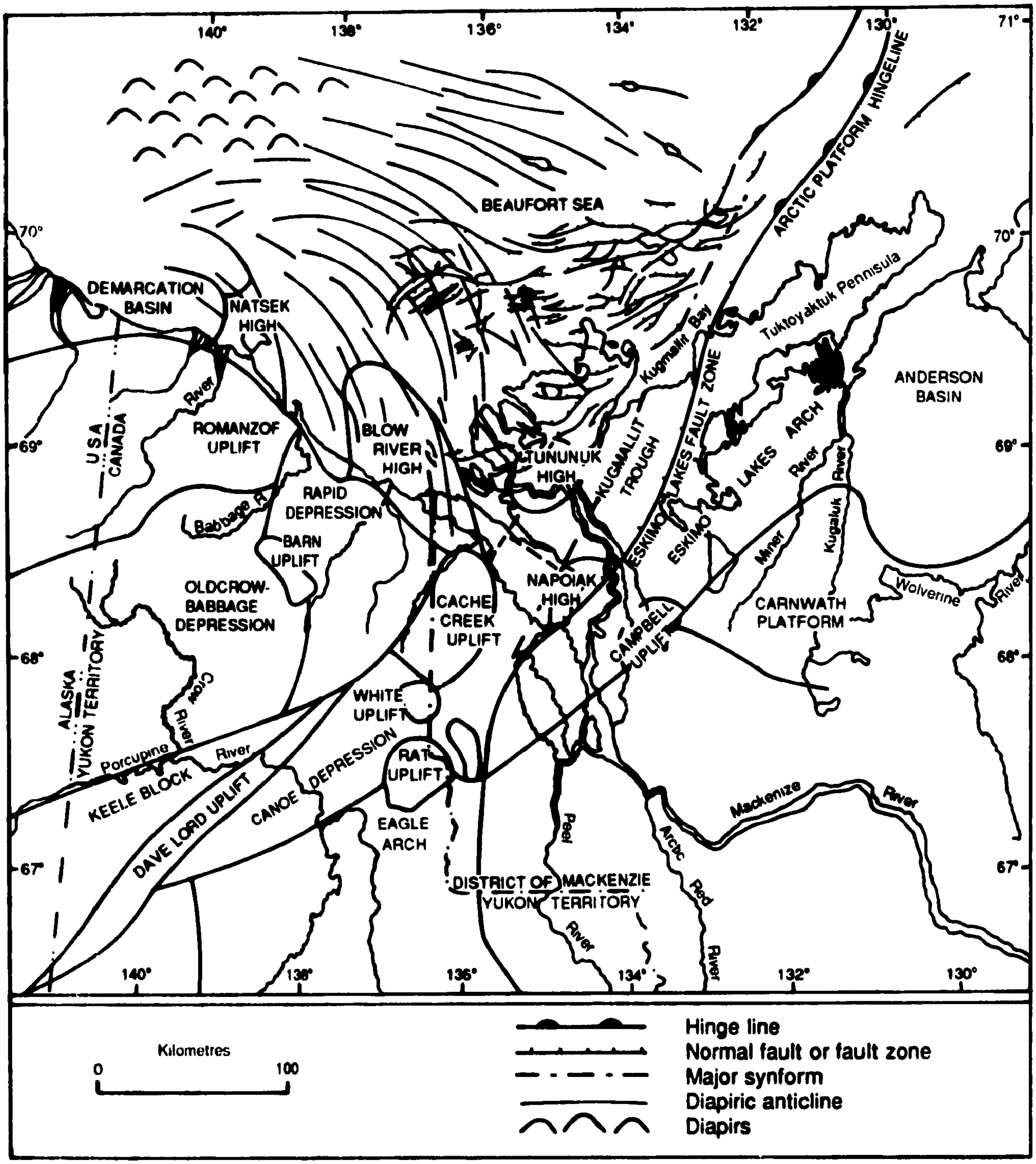
140°
138°
136°
134°
132°
130°
71°
70°
69°
68°
67°
BEAUFORT SEA
ARCTIC PLATFORM HINGELINE
DEMARCATION BASIN
NATSEK HIGH
Kugmallit Bay
Tuktoyaktuk Pennisula
ANDERSON BASIN
USA
CANADA
River
ROMANZOF UPLIFT
BLOW RIVER HIGH
TUNUNUK HIGH
KUGMALLIT TROUGH
LAKES FAULT ZONE
LAKES ARCH
River
River
RAPID DEPRESSION
Babbage R.
BARN UPLIFT
ESKIMO
ESKIMO
Miner
Kugaluk
OLDCROW-BABBAGE DEPRESSION
CACHE CREEK UPLIFT
NAPOIAK HIGH
CAMPBELL UPLIFT
CARNWATH PLATFORM
Wolverine
River
ALASKA
YUKON TERRITORY
Crow
River
WHITE UPLIFT
Porcupine
River
KEELE BLOCK
DAVE LORD UPLIFT
CANOE DEPRESSION
RAT UPLIFT
EAGLE ARCH
Peel
Arctic
Red
Mackenzie
River
DISTRICT OF MACKENZIE
YUKON TERRITORY
River
River
Kilometres
0
100
Hinge line
Normal fault or fault zone
Major synform
Diapiric anticline
Diapirs

Fig. 2.2 Tectonic and structural elements of the Beaufort-Mackenzie area (Dixon and Dietrich 1985; Dixon et al. 1992b; Enachescu 1990).

2.3 Lithostratigraphy

Dixon et al. (1992) re-evaluated their earlier studies and summarized the Upper Cretaceous to Pleistocene sequence stratigraphy of the Beaufort-Mackenzie area. Sediments deposited in the Poorcupine-Mackenzie and Beaufort-Mackenzie basins are characterized as oceanward prograding sequences, often dominated by large deltaic complexes. Regional unconformities and maximum flooding (hiatal) surfaces enable the stratigraphic successions to be sub-divided into transgressive-regressive (depositional) sequences. The descriptions of the eleven sequences in the Upper Cretaceous to Holocene strata of the Beaufort-Mackenzie Basin are summarized from Dixon et al. (1992a).

The lowermost sequences are the Upper Cenomanian to Turonian Boundary Creek and the Santonian to Campanian Smoking Hills sequences, which consist of predominantly organic matter-rich dark grey to black shales interbedded with bentonite beds. They were deposited in a low energy, anoxic, outer shelf to slope environment, characterized by periodic ash falls from local volcanic activity. The following eight sequences represent very thick fluvio-deltaic clastic deposits: The Upper Maastrichtian to Lower Paleocene Fish River Sequence unconformably overlies the Smoking Hills Sequence and represents a thick progradational wedge of shale-dominated deltaic strata which overlie prodelta shelf sands and shales. The Fish River depositional facies range from deep-water sediments, gravity flow deposits, through slope and shelf shales to delta front and delta plain sandstones and shales (Dixon et al. 1992b). The Upper Paleocene to Lower Eocene Aklak Sequence is the lower member of the previously named Reindeer Sequence (Dietrich et al. 1989b). It consists predominantly of interbedded sandstone, conglomerate, siltstone, shale and coal, deposited in a delta-plain to delta-front environment with fluvial channel deposits. The Lower to Middle Eocene Taglu Sequence is the upper unit of the Reindeer Supersequence (Dietrich et al. 1989b) and consists predominantly of interbedded shale and sandstone deposited in delta plain and delta front to deep slope or inter-fan environments. The Middle to Upper Eocene Richards Sequence conformably overlies the Taglu sequence and is comprised predominantly of shale and siltstone of prodelta and shelf origin with localized sandstone and conglomeratic beds. Extensive erosion occurred during the Late Eocene The Oligocene Kugmallit Sequence conformably to unconformably overlies the Richards Sequence. It represents progradational deposits ranging from delta plain conglomerate, gravel and sandstone to offshore basinal shale. It contains the Kopanoar subsequence consisting

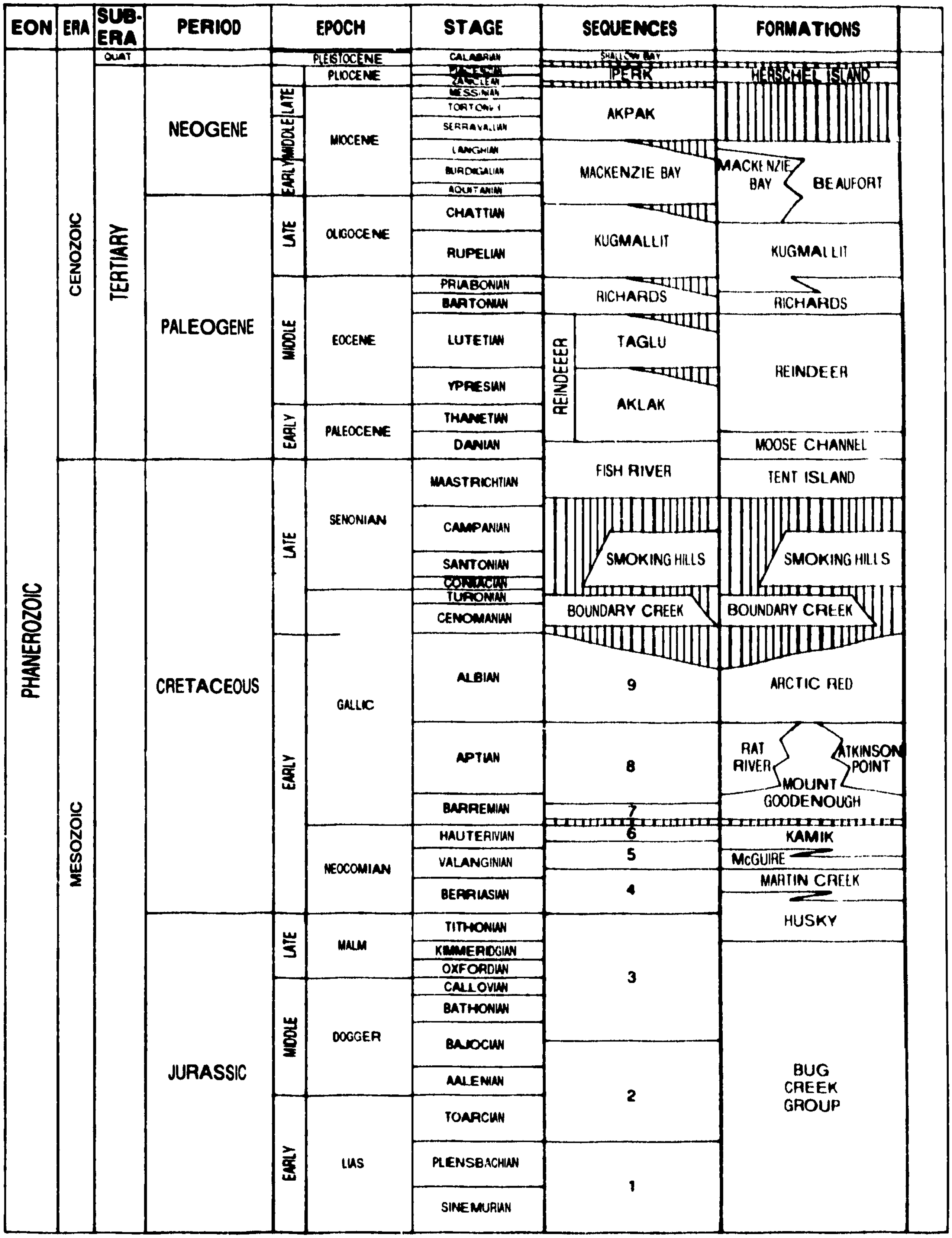
EON
ERA
SUB-ERA
PERIOD
EPOCH
STAGE
SEQUENCES
FORMATIONS
PHANEROZOIC
CENOZOIC
MESOZOIC
QUAT
TERTIARY
NEOGENE
PALEOGENE
CRETACEOUS
JURASSIC
PLEISTOCENE
PLIOCENE
LATE
MIDDLE
EARLY
MIOCENE
OLIGOCENE
EOCENE
PALEOCENE
SENONIAN
GALLIC
NEOCOMIAN
MALM
DOGGER
LIAS
CALABRIAN
PIACENZIAN
ZANCLEAN
MESSINIAN
TORTONIAN
SERRAVALLIAN
LANGHIAN
BURDIGALIAN
AQUITANIAN
CHATTIAN
RUPELIAN
PRIABONIAN
BARTONIAN
LUTETIAN
YPRESIAN
THANETIAN
DANIAN
MAASTRICHTIAN
CAMPANIAN
SANTONIAN
CONIACIAN
TURONIAN
CENOMANIAN
ALBIAN
APTIAN
BARREMIAN
HAUTERIVIAN
VALANGINIAN
BERRIASIAN
TITHONIAN
KIMMERIDGIAN
OXFORDIAN
CALLOVIAN
BATHONIAN
BAJOCIAN
AALENIAN
TOARCIAN
PLIENSBACHIAN
SINEMURIAN
SHALLOW BAY
IPERK
AKPAK
MACKENZIE BAY
KUGMALLIT
RICHARDS
REINDEER
TAGLU
AKLAK
FISH RIVER
SMOKING HILLS
BOUNDARY CREEK
9
8
7
6
5
4
3
2
1
HERSCHEL ISLAND
MACKENZIE BAY
BEAUFORT
KUGMALLIT
RICHARDS
REINDEER
MOOSE CHANNEL
TENT ISLAND
SMOKING HILLS
BOUNDARY CREEK
ARCTIC RED
RAT RIVER
ATKINSON POINT
MOUNT GOODENOUGH
KAMIK
McGUIRE
MARTIN CREEK
HUSKY
BUG CREEK GROUP

Fig. 2.3 Table of sequences (Dixon 1991; Dixon et al. 1992a) and corresponding formational terminology (Dixon 1982; Young and McNeil 1985) (modified from Dixon et al. 1992a).

of a thick accumulation of mud-dominated sediments of submarine-fan origin. The Upper Oligocene to Middle Miocene Mackenzie Bay Sequence is dominated by shale with minor beds of sandstone. Its depositional environment is considered to be prodelta/shelf, slope, and deep water. The Middle to Upper Miocene Akpak Sequence is predominantly composed of shale interbedded with thin siltstone and sandstone Sediments were deposited in a prodelta/shelf, slope and basinal environment. In the Middle to Late Miocene, uplift or lowered sea level resulted in significant erosion of the Tertiary deltaic sequences. The Pliocene to ?Lower Pleistocene Iperk Sequence was unconformably deposited on older sequences and is a thick, mildly deformed sequence of deep-water mudstone, unconsolidated sandstone and conglomerate It was deposited over a broad delta complex. The ?Pleistocene to Holocene Shallow Bay Sequence is the youngest sequence and consists of unconsolidated sediments comprised of mud, silt, sand and gravel.

2.4 Previous Petrographical and Mineralogical Studies

Previous petrographic studies of Maastrichtian to Oligocene strata revealed a relatively homogeneous mineralogical and textural composition of the mudstones, siltstones, sandstones and conglomerates of fluviodeltaic and perideltaic marine origin (Schmidt 1987) Sandstones are predominantly indurated arenites (quartz, feldspathic, lithic), and are compositionally similar in the Fish River, Aklak, Taglu, Richards and Kugmallit sequences, with the exception of lower volcanic contents in the latter two sequences (Nentwich and Yole 1982; Schmidt 1987, Nentwich 1989). Detrital mineralogy includes quartzose grains (monocrystalline and polycrystalline quartz, clear and black chert) ranging from 15 to 40 volume %, minor to moderate amounts (2-15%) of K-feldspar and plagioclase Volcanic, sedimentary and metamorphic rock fragments vary between 5 and 45%. K-feldspar and plagioclase, often occurring together with minor albite, have been preserved through to depths of 4400 m, with little alteration except for some replacement by carbonate minerals and albitization (Nentwich and Yole 1982; Schmidt 1987; Nentwich 1980, 1989). K-feldspar and albite range from 1 to 10% and plagioclase reaches a maximum of 6% X-ray diffraction studies indicate a total feldspar content of 5 to 30 %. Mica (muscovite and biotite) is present in minor to moderate amounts, to a maximum of 13 %. During burial, some dissolution of mica and chlorite occurred. The siltstones, sandstones and conglomerates are cemented by calcite and dolomite cements, whose precipitation was accompanied by dissolution of silica and aluminosilicate minerals. Minor cements include silica, illite, chlorite, montmorillonite, illite-smectite, feldspar and pyrite. The sandstones of the Richards and Kugmallit sequences are much less consolidated than the older sandstones of the Aklak and Taglu sequences (Schmidt 1987).

On QFL and QmFLt provenance-discrimination diagrams of Dickinson and Suczek (1979) the sandstone data for the Beaufort-Mackenzie Basin plot in the fields of recycled orogen and transitional and lithic recycled orogen, respectively. In LsLmLv and QpLsmLvm provenance-discrimination diagrams of Ingersoll and Suczek (1979), the sandstone data indicate a rifted continental-margin origin.

Mudstones and shales are dominated by fine quartz silt and clay minerals, with abundant silt-sized mica and feldspar. Authigenic minerals identified within these rocks include quartz and pyrite, with a notable absence of calcite which is present in adjacent sandstones. Mudstones and shales contain eogenetic siderite, and occasionally dolomite. Schmidt (1987) attributed the absence of calcite and scarcity of dolomite to dissolution and removal from the shales. Clay minerals comprise kaolinite, chlorite, illite and interstratified illite-smectite (Schmidt 1987; Nentwich 1989).

Powell et al. (1978) using cores from Reindeer D-27, Taglu C-42 and Taglu G-33 wells, observed mixed-layer minerals consisting of three minerals, smectite, vermiculite and illite in the <0.2-μm size fractions . If the amorphous inorganic material was not removed from the samples prior to analysis, a chlorite-like component was identified creating a pseudo-four component interstratified clay system. The authors suggested that with depth there is a progressive decrease in the expandable component in interstratified illite-smectite with a concomitant increase in the non-expandable component, but that the vermiculite-like content remained constant. The 0.2-2.0-μm clay fraction consisted of quartz, feldspar, kaolinite, chlorite, illite, 2:1 expandable and interstratified smectite-vermiculite-illite (Foscolos and Powell 1980).

The amorphous inorganic component initially increased with depth then decreased and is described as an unstructured fluffy material, which may have been derived from algae and bacteria and may have a composition similar to allophane. Foscolos and Powell (1980) suggested that the amorphous inorganic material resulted either from initial deposition or from silicate diagenesis. It cannot be completely removed with chemical treatments.

In the first in-depth study of the illite-smectite transition in the Beaufort-Mackenzie

Basin, Ko (1992) used the <0.1 μm fraction as the optimal size fraction to concentrate and characterize interstratified illite-smectite (I-S) minerals. The analyses included samples from 22 wells, both onshore and offshore in terms of XRD, geochemistry and oxygen isotopes. The progressive illitization of I/S with depth was identified as it proceeded continuously through four distinct interstratified I/S interlayer arrangements from: (1) a random I/S structure, through (2) a mixture of random and ordered I/S structures, (3) R1-ordered I/S structures, and to (4) a R>1-ordered I/S structure. The chemical composition of the I/S mixed-layers changed continuously together with increasing percent illite. Other minerals identified in the <0.1μm fraction include kaolinite, chlorite, and discrete illite. Ko (1992) and Ko and Hesse (1992) suggested that illitization is more advanced in offshore wells than onshore, as a consequence of higher geothermal gradients, as well as in geopressured shales compared to normally pressured horizons, due to higher water/solid ratios.

2.5 British American-Shell Oil-Imperial Oil Exploration Exploratory Well Reindeer D-27

The British American-Shell Oil-Imperial Oil Exploration (B.A.-Shell-I.O.E) Reindeer D-27 was the first exploration well drilled in the Beaufort-Mackenzie Basin. This wildcat well was spudded July 26, 1965 and completed November 24, 1965. Reindeer D-27 is located at latitude 69°06'05" N and longitude 134°36'54" W. The top kelly bushing elevation was 15.95 ft above sea level, and the well was drilled to a total depth of 12,668 ft (3862 m). Twenty-three cores were recovered for a total length of about 571 ft (174 m), which represents about 4% of the total depth drilled. The well was abandoned and plugged after showing only a hydrocarbon flow of gassy mud to the surface from the depth interval of 6,838 to 6,856 ft (2085-2090 m) (British American Oil Company 1966). Previous published research from this well includes biostratigraphy (Chamney, 1970), clay mineralogy (Bayliss and Levinson 1970, Powell et al. 1978; Foscolos and Powell 1980; Dean 1985; Ko 1992; Sears and Hesse 1992), geochemistry and stable isotopes (Ko 1992), K-Ar ages (Sears et al. 1993b).

The Reindeer D-27 well penetrated the normal downhole stratigraphic succession of Holocene to Albian age (Fig. 2.4). Sequences identified in the Beaufort-Mackenzie Basin but not present in the Mackenzie Delta area include: the Shallow Bay, Akpak, Mackenzie Bay, Smoking Hills and Boundary Creek sequences (Fig. 2.3). The well penetrated to the Barremian to Albian Mount Goodenough Formation of the Brooks-Mackenzie Basin (Hitchon et al. 1990;

Dixon et al. 1992a).

The first sequence encountered is the 16 ft (5 m) thick Iperk Sequence of Pliocene-?Early Pleistocene age. It consists principally of weakly consolidated to unconsolidated sandstone, conglomerate and interfingering with shale and siltstone deposited in a fluvio-deltaic environment. At its base is a basin-wide erosional unconformity. The Late Eocene or Early Oligocene Kugmallit Sequence is present to a depth of 440 ft (134 m) and consits of upper delta plain deposits predominantly of shale, siltstone and sandstone. The Kugmallit Sequences unconformably overlies the Middle Eocene to Late Eocene Richards Sequence, present to a depth of 1740 ft (531 m). It consists of prodelta deposits of shale and siltstone with some interbedded sandstone and conglomerate within the shale succession. The first coal beds are found at a depth of 825 ft (251 m). The sequence originally named Reindeer Sequence was subsequently raised to supersequence status and subdivided into the Aklak and Taglu sequences. The thick Early to Middle Eocene Taglu Sequence contains delta and prodelta shelf successions, with fluvial-dominant sediments present within the deltaic deposits. The sediments are predominantly shale with interbedded fine to very fine grained sandstone, siltstone and minor coal beds. Unconsolidated sands are present from 4,000 ft (1,220 m) to 4,760 ft (1,451 m) and conglomerates at 6,960 ft (2,129 m) and 8,884 ft (2,709 m). At a depth of 8898 ft (2717.7 m), an angular unconformity separates the overlying Taglu Sequence from the Late Paleocene to Early Eocene Aklak Sequence. The Aklak Sequence is present to a depth of 9544 ft (2909.7 m) and consists of shale with interbedded sandstone, siltstone. The Aklak Sequence unconformably overlies the Mid-toLate Maastrichtian to Early Paleocene Fish River Sequence. The Fish River Sequence is present to a depth of 10,727 ft (3270.5 m) and is interpreted as a shale-dominant shelf or possibly slope deposits with mudstone, claystone and interbedded siltstone (Dixon et al. 1992a). An erosional unconformity separates the Fish River Sequence from the underlying Barremian to Albian Mt. Goodenough Formation. The Reindeer D-27 well penetrates the Mt. Goodenough to a depth of 12668 ft (3862.2 m). It consists predominantly of shale with interbedded siltstone and sandstone. The first clean sandstone with glauconite is present from a depth of 11,098 to 11,440 ft (3,383-3,488 m). This is followed by a medium to dark grey, silty shale to a depth of 12,668 ft (3,862 m).

Vitrinite reflectance studies from the Reindeer D-27 show an initial increase of R_o of 0.3% at 1,000 ft to 0.5% at 4,100 ft, and then a fairly linear increase from 0.47% at 4,600 ft to 0.66 at 10,500 ft (Gunther 1975). However, the present day thermal gradient may not reflect

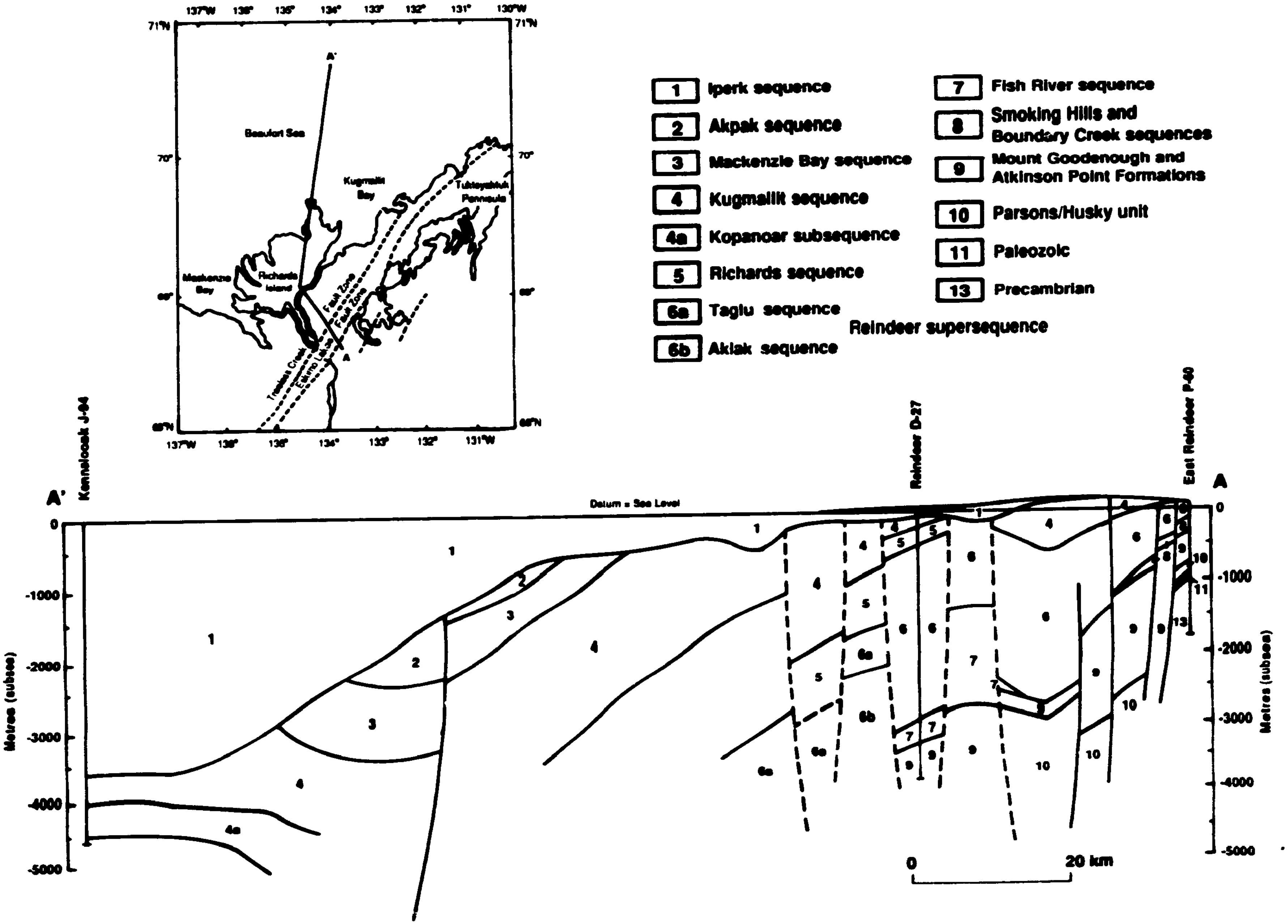
137°W
136°
135°
134°
133°
132°
131°
130°W
71°N
70°
69°
68°N
131°W
A'
A
Beaufort Sea
Kugmallit Bay
Tuktoyaktuk Peninsula
Mackenzie Bay
Richards Island
Treeless Creek Fault Zone
Eskimo Lakes Fault Zone
1 Iperk sequence
2 Akpak sequence
3 Mackenzie Bay sequence
4 Kugmallit sequence
4a Kopanoar subsequence
5 Richards sequence
6a Taglu sequence
6b Aklak sequence
Reindeer supersequence
7 Fish River sequence
8 Smoking Hills and Boundary Creek sequences
9 Mount Goodenough and Atkinson Point Formations
10 Parsons/Husky unit
11 Paleozoic
13 Precambrian
Kenalooak J-94
Reindeer D-27
East Reindeer P-60
Datum = Sea Level
0
-1000
-2000
-3000
-4000
-5000
Metres (subsea)
0
20 km

Fig. 2.4 Cross-section of the Beaufort-Mackenzie Basin through the Reindeer D-27 well (after Hitchon et al. 1990).

the paleothermal regime (Ko 1992). As there were at least two periods of uplift and erosion, continuous burial cannot be assumed. Majorowicz et al. (1988, 1989, 1990) concluded that the paleogeothermal gradient was no greater than the present geothermal gradient

The Reindeer D-27 well was drilled with weighted mud to control sloughing of unconsolidated sands. Various compounds used in drilling mud are often water soluble allowing liquid infiltration into well cuttings potentially causing contamination. Drilling mud used in the Reindeer D-27 well included: Aquagel, Baroid, Q Broxin, Lignite, Carbonox, Cellex Regular and bicarbonate of soda, with lesser amounts of other compounds (British American Oil Company 1966). These drilling muds contain abundant K^+ and are used under conditions of high pH (>11). Thus drilling mud may induce diagenetic alteration in well cuttings (Barefoot and Van Elsberg 1975; see also Dypvik 1981). This must be considered when performing any geochemical analyses.

CHAPTER 3.0 - ANALYTICAL METHODS

3.1 X-Ray Powder Diffraction Analysis

The precise characterization of clay minerals and especially mixed-layer illite-smectite (I/S) is difficult because of their fine-grained nature, poor crystallization and association with other crystalline and amorphous materials X-ray powder diffraction is the primary technique for routine investigation of oriented clay mineral specimens by determining the (00*l*) or basal diffraction series which is diagnostic for each discrete clay mineral. The crystallography of clay minerals is such, that the X-Y planes are similar and the average orientation of the crystallites are parallel to the mounting surface, whereas the Z direction has differing thickness.

3.1.1 Factors Influencing XRD Line Profiles

X-ray powder diffraction is probably the most widely used technique for obtaining qualitative and quantitative information on multiphase clay mineral mixtures. As there are many references describing the theoretical (and mathematical treatment) and practical aspects of XRD analysis for clay minerals (e.g. Klug and Alexander 1974; Cullity 1978; Moore and Reynolds 1989; Drits and Tchoubar 1990), I will not provide a detailed review.

Routine interpretation of mixed-layer I/S is essentially achieved through the visual inspection and study of one-dimensional diffraction profiles. There are many factors, however, which can influence the characteristics of XRD profiles and which may be divided into two groups (after correction for instrumental distortion) (1) crystallography-dependent factors, and (2) specimen-dependent factors Crystallography-dependent factors are: (1) particle size, (2) defect density, (3) particle quality, i.e., non-uniform and uniform strain; (4) chemical composition, and (5) mixed-layering (Jackson 1969; Reynolds 1989a, 1989b; Drits and Tchoubar 1990). Specimen-dependent factors include: (1) sample size, (2) sample thickness, (3) particle orientation, i.e. random versus oriented mounts, and (4) dilution by amorphous material (Cullity 1978; Moore and Reynolds 1989; Bish and Reynolds 1989; Reynolds 1989a). These parameters will be evaluated in diffraction profiles through changes in line shape, i.e. line broadening, or in the change in line shape with respect to the diffraction angle 2Θ, i.e. peak distortion resulting from increased background intensity at lower angles. They may include diminished peak intensity, peak broadening, peak shifting and the generation of irrational reflections (Reynolds 1989b). However, as peak heights are a function of N (number of layers) per particle and the peak breadth (ß) measured at half height, the integrated area under the peak remains constant and thus the intensity is independent of N (Reynolds 1989b)

3.1.1.1 Crystallographic-Dependent Factors

There have been many investigations of the effects of particle size Reynolds (1968) did this for illite, Ross (1968) for biotite, muscovite, montmorillonite, mixed-layer clays, graphite and periclase, Kodama et al. (1971) for muscovite, Tettenhorst and Roberson (1973) for ethylene-glycol solvated montmorillonite and Trunz (1976) for kaolinite Klug and Alexander (1974) asserted that to achieve a coherent scattering domain, crystallites in a powder or a single crystal must have a minimum of six unit cell translations in any single direction Thus depending on the unit cell size and the scattering power of the attendant atoms in the unit cell, coherent domains as small as 2 to 20 nm in diameter can be detected by XRD if present in sufficient quantities

Studies of monomineralic phases have shown, as particles become thinner, the principal reflections broaden, and the intensity varies in two respects (i) the reflections are displaced, generating an apparent series of irrational (or non-integral) reflections, and (ii) the reflections are less symmetrical. Trunz (1976) demonstrated for kaolinite that the reflections (001) (002), (004), and (006) are displaced to lower 2Θ angles (larger *d*-values), whereas (003) and (005) reflections are displaced to higher 2Θ angles (smaller *d*-values) The net result is a set of non-integral reflections

Ergun (1970) referred to defect density as randomly or irregularly distributed stacking defects in the Z direction which effectively divides a large crystal into an assemblage of smaller scattering domains These defects may affect (i) the layers themselves, (2) involve interlayer space, e g. the position of cations or solvated molecules, or (iii) stacking faults, e g the relative position and/or type of successive layers (Tchoubar 1984)

Ergun (1970) also referred to strain broadening, which is a consequence of random displacements of unit layers from their ideal positions, i e the separation between two unit layers (cells). Reynolds (1989a) demonstrated that strain broadening resulted in diffraction patterns displaying diminished intensities and increased broadness as a function of increasing unit layer separation.

Differing chemical composition of the silicate layers or interlayers of the same species and positions of the atoms in the unit cell may affect the intensities of reflections, but appears to have minor effect on the positions of these reflections (Reynolds 1989b; Drits and Tchoubar 1990)

Interstratified minerals such as mixed-layer I/S are common in weathering, sedimentary, diagenetic, hydrothermal and metamorphic environments However, in contrast to most minerals, I/S clays have X-ray particle thicknesses which are equal to or larger than the thickness of their constituent particles (Tettenhorst et al 1990). Mixed layering results in non-integral series of reflections and increased peak breadths which are a function of the endmember components The greater the separation, the broader the peaks.

3.1.1.2 Specimen-Dependent Factors

Conventional XRD requires a minimum of 10 mg of crystalline material in order to obtain measurable diffraction intensity. For quantitative analysis, sample length becomes especially important. At low diffraction angles the incident beam must not exceed sample length or diminished reflection intensity results (Bish and Reynolds 1989; Moore and Reynolds 1989). Samples that are "infinitely" thick at low angles may be too thin at higher angles for maximum diffraction effects, resulting in loss of reflection intensity at higher 2Θ angles. Homogeneity in sample mineralogy is also required for quantitative analysis. Whittig and Allardice (1986) suggested that aggregating and cementing minerals in a clay sample will result in deleterious effects in XRD studies and include. (i) the dilution of clay minerals which result in decreased diffraction intensity of crystalline phases; (ii) lack of ideal orientation of clay minerals; (iii) attenuation of the primary X-ray beam; (iv) an increase in the general level of scatter from the sample being analyzed by X-rays, and (v) amorphous material causing non-directional scatter of X-radiation from a sample which results in increased background radiation (see also Chapter 4).

3.1.2 Estimation of Layer Proportions in Mixed-Layer Illite-Smectite (I/S)

The routine analysis of mixed-layer I/S usually requires a determination of the nature and number of types of layers present, their proportions, and the presence or absence of order.

This may be achieved either through direct or indirect methods. Direct methods use information from peak positions and intensities of basal reflections (MacEwan 1956, 1958) whereas indirect methods apply structural models to calculate XRD patterns which are then compared to experimental patterns (Reynolds 1980; Reynolds and Hower 1970; Plançon 1981, Plançon et al. 1983, 1984; Corbató and Tettenhorst 1987; Tettenhorst et al 1990). The advantage of using indirect methods lies in the ability to study diffraction effects of individual parameters, e.g. types of interstratification, distribution of coherent domains, thicknesses of different layer types, etc. on the resultant XRD pattern (Drits 1987). It is important to note however, that the original structural model used for calculated profiles must be similar to the real mineral structure.

Identification of smectite illitization has been based principally on the interpretation of XRD patterns. Moore and Reynolds (1989) have summarized the methods used for the identification and interpretation of mixed-layer I/S from XRD profiles. An adequate method to determine the amount of the expandable (smectite-group) and non-expandable (illite) in mixed-layer I/S is to use both peak migration and $\Delta 2\Theta$ methods on ethylene-glycol solvated samples (Moore and Reynolds 1989). The $(002)_{10}/(003)_{17}$ reflection is the most sensitive to composition and the least sensitive to particle size, whereas lower 2Θ angle reflections are most sensitive to ordering type.

Ordering is defined by the term *Reichweite*, or R, which describes the probability of nearest neighbour arrangements. Reynolds (1980) described three types of mixed layering (or interstratification) apparent in diffraction patterns which include: (1) random (irregular or disordered), having no periodic alternation in the sequence of component layers (R0), (2) regularly ordered having a periodic alternation of component layers (R≥1), and (3) partially ordered, which is intermediate between random and ordered. In XRD, random mixed-layer clay minerals produce two distinct phenomena: (i) aperiodic or irrational (00*l*) diffraction series, and (ii) peak breadths which are broader than those of their pure component phases. Disordered mixed layering shows peak positions that are an average of the two minerals present and are dependent on the proportions and spacings of these components. Ordered mixed-layer clay minerals produce new reflections which contain components of a superstructure, or the sum of the *d*-spacing values of both layers. Ordering in mixed-layer I/S is determined by the position of the reflection between 5° and 9° 2Θ. Random ordering can be assumed if after ethylene glycol solvation a peak is present near 5.2° 2Θ; a reflection near 6.5° 2Θ indicates R1-ordering, with the peak diminishing and broadening as the composition becomes more illitic, and; a reflection at an angle greater than 7° 2Θ suggests long-range-ordering, or R>1, and the appearance of the $(001)_{10}/(004)_{17}$ peak is diagnostic.

3.2 Transmission Electron Microscopy (TEM)

There are numerous references that outline the principles and techniques of electron microscopy, including preparation techniques. For layer silicates, these include McLaren (1991), Buseck (1992), and Robards and Wilson (1993).

Allen (1992) states that mineralogical studies involving the TEM have basically focused on either mineral properties (i.e. structure and chemistry) or mineral behaviour (i.e. identification and relationships). The TEM can be used to facilitate mineral identification and the investigation of their textures, fabrics, intergrowths. replacements and other relations. Within the past two decades, much of the microstructural TEM studies have focused on rocks and minerals formed at relatively low surface and sub-surface temperatures. These are areas where conventional techniques have limited application because of the fine-grained nature of the minerals, which often are structurally and chemically disordered, heterogeneous and metastable (Allen 1992). Sedimentary rocks resulting from weathering, diagenesis, hydrothermal alteration or deposition, and low-grade metamorphism are ideal subjects for the TEM. A significant advantage of the TEM is that it allows direct observations of microstructure at a 2:1 layer scale. However, an important ancillary goal has been the attempt to reconcile TEM images of mixed-layer clay minerals with structures deduced by X-ray powder diffraction (Veblen et al. 1990; Środoń et al. 1990; Środoń et al. 1992).

HRTEM, as opposed to conventional transmission electron microscopy (CTEM), refers to the use of the TEM at higher resolutions to observe the layer structures of minerals as lattice fringes using bright-field illumination. As such, it is an imaging mode in which at least two beams pass through the objective lens, and the resultant lattice fringe image reflects the periodicity of the crystal (Veblen 1983). A distinct advantage of HRTEM is its ability to image crystalline and non-crystalline materials directly, in the case of clay minerals their individual layers, stacking sequences, ordering and coherency, at a scale at which they exist. This far exceeds the capability of conventional analytical techniques (e.g. X-ray diffraction or electron microprobe) which can only give information on average structural or chemical properties of a mineral specimen. HRTEM can investigate lattice or structural fringes of crystallites or small areas of larger crystals with a point-to-point resolution of at least 0.2-0.3 nm.

3.2.1 Sample Preparation

Sample preparation methods and techniques for the TEM are of fundamental importance, especially to studies concerning the nature and characterization of mixed layer I/S. Buseck (1992), Peacor (1992) and Robards and Wilson (1993) provide introductions to the common preparation techniques for the TEM, from which most of the following is summarized, except where otherwise noted. Buseck (1992) notes that to optimize data collection, prepared specimens require proper crystallographic orientation, appropriate thinness, and must be somewhat stable under vacuum and the electron beam. Lattice fringes can only be obtained and correlated with the layer sequences when the clay particles are oriented with the (00*l*) perpendicular to the electron beam. Sample thinness is a prerequisite to prevent significant refraction of the electron beam when passing through the sample and thus, minimizing sample and beam interaction. Four methods of sample preparation for clay minerals include: (i) grain mounts; (ii) beam milling; (iii) ultramicrotomy, and (iv) replica techniques.

3.2.1.1 Grain Mounts

Crushed or ground bulk samples and clay separates may be mounted directly on TEM grids supported by structureless film such as formvar or amorphous carbon by direct dispersal or evaporation of a fluid dispersed sample. The sample is usually projected over a hole in the support film (e.g. holey carbon) and a grain is located which has the proper orientation, or by tilting the stage until the critical zone axis is parallel to the optic axis of the TEM. The advantage of this technique is that specimens can be prepared quickly. Disadvantages include the long time generally required to find a properly oriented grain and the possible dehydration of hydrated clay minerals. During preparation, the original "in situ" spatial interrelationships, i.e. texture or fabric, may be destroyed as in the case of clay minerals, where the layer stacking sequences may be altered by plastic deformation (Buseck 1992). However, the sample may provide information on stacking sequences, crystal morphology and particle thickness (Peacor 1992) and the method provides a way checking for artifacts from beam-milling

3.2.1.2 Beam-Milling

Beam-milling (atom- or ion- beam) is the most common method of preparing mineral samples, polycrystalline materials and glasses (Barber 1970). A sample, usually a thin disk or piece of polished thin section, is placed in a beam mill and bombarded by a low angle stream of ions or atoms while the specimen rotates in its own plane. The surface is gently eroded until a hole is produced. The thinned edges around the hole are then examined by the high-resolution TEM. Beam-milling implants gas atoms and produces heating, and thus may produce artifacts in specimen preparation. This is apparent in the loss of interlayer water from expandable layer silicates and subsequent collapse of the interlayer, and other lattice damage. An advantage of this method is that, as thin sections may be used for the initial sample, the original mineral relationships and textures may be observed.

3.2.1.3 Ultramicrotomy

Numerous sample preparation procedures for ultramicrotomy and various epoxy resins for embedding clay powders have been outlined (Eberhart and Triki 1972; Tchoubar et al. 1973; Brown and Jackson 1973; Lee et al. 1975; McKee and Brown 1977; Tessier and Pédro 1982; Vali and Köster 1986; Laird et al. 1989b; Środoń et al. 1990). Spurr low-viscosity resin is the most often used embedding resin (Spurr 1969). The ideal resin must be stable under TEM conditions and impregnate the clay minerals without modifying the layer structure and creating artifacts (see Vali and Köster 1986; Laird et al. 1989). Peacor (1992) outlined a method whereby powdered and ground or crushed samples are sedimented in methanol onto a flat-surface of cured epoxy resin, followed by the addition of another layer of uncured resin, the sample is allowed to polymerize, and the block is trimmed and thin-sections cut with an ultramicrotome

Vali and Köster (1986) treated freezed-dried clay material once or twice with propylene oxide, then dispersed the material in Spurr low-viscosity resin twice at increased concentrations, allowing sufficient time for infiltration and impregnation. After curing, the block is trimmed and ultrathin sections, 50 to 100 nm thick are cut with an ultramicrotome. Laird et al. (1989b) outlined a similar procedure for sample preparation that allowed investigation of the same sample by both XRD and TEM using n-alkylammonium ions. Vali and Hesse (1990) demonstrated that ultrathin-sections could be treated with n-alkylammonium ions to stabilize expandable interlayers.

In an attempt to maintain the original sample texture and fabric, Srodon et al. (1990) employed a technique whereby bentonite rock chips were air-dried and subsequently rehydrated after having been coated with agar to ensure homogenous rehydration. The water was replaced with methanol which in turn was replaced by slow impregnation with L.R. White very-low viscosity resin Sections were then cut with an ultramicrotome.

3.2.1.4 Replica Techniques

Reference is made to this technique as it was used to determine the size fractions of the clays separated from cores and well cuttings and their purity. Replica techniques image the surface features or microtopography of clay minerals in conventional TEM. Correlations may be inferred between crystal morphology, growth mechanisms of basal faces and polytypism (Baronnet 1992).

Powdered, crushed or ground sample material is spread over a thin cover glass (Baronnet 1972, 1973) or mica flake (Nadeau 1985). The sample is coated with a 10-15 nm thick platinum-carbon layer and the layer coating the crystals and substrate is floated on dilute hydrofluoric acid. The substrate is removed by dissolution of the crystals and the platinum-carbon film is washed in deionized water, placed on standard EM grids and examined by CTEM.

Bassett (1958) and Sella et al. (1958) applied a gold-decoration technique to powdered, and crushed or ground samples after they were dispersed in deionized water and collected on a cover glass and air dried. The glass was subsequently heated to 300-350°C for one to two hours under vacuum, allowed to cool to 100-150°C, a gold decoration was flash evaporated, and followed by a 10 nm thick carbon coating. The remainder of the steps follows the procedure outlined for platinum-carbon coating.

Vali et al. (1991) used freeze-etch replicas to study the microtopography of 2:1 layer silicates. Clay mineral samples were dispersed into a dilute suspension of deionized water, sprayed with an air-brush into a cryomedium containing a mixture of propane-propylene at -196°C, and the droplets were instantaneously frozen without cryoartifacts. After evaporation of the propane-propylene mixture, the frozen droplets are mixed with one or two drops of ethyl benzene as a cryoglue and transferred to a gold specimen holder and placed in a freeze-etch unit. The droplet surface was fractured, etched by ice sublimation and Pt-C shadowed at an angle of 45° and coated with a 10 nm thick carbon layer. The replica was floated on deionized H_2O and dropped in dilute HF to dissolve adhering silicate particles. Freeze-dried images are prepared in a similar manner except the ice is removed through very low-temperature sublimation.

3.2.2 Identification of Clay Minerals from Lattice-Fringes

Before the advent of computer-image simulation, identification of layers of lattice-fringe images were based on intuitive interpretations. Values for $d_{(001)}$ of a pair of fringes were measured directly from the lattice-fringe image. At approximate Scherzer defocus, dark fringes overlie regions of relatively high-charge density, e.g. 2:1 layers, and bright fringes overlie regions of relatively low density, e.g. interlayers. Conventional interpretation, therefore, posited that dark layers that were 1.0-nm, 0.7-nm, and 0.5-nm, were 2:1, 1:1 and brucite-like sheets, respectively. However, the positions of dark and light lattice fringes are a function of operating instrumental characteristics such as accelerating voltage, beam divergence, spherical and chromatic aberration coefficients, objective aperture, size, as well as focus conditions, and crystal thickness, orientation to the electron beam, and the possible collapse of expandable layers when subjected to the high vacuum of the microscope or heating effects (Kohyama et al. 1982; Guthrie and Veblen 1989, 1990). In other words, lattice fringes change their shape and position as experimental imaging conditions change.

It has been inferred that untreated smectite-like layers in mixed-layer illite-smectite which have a basal spacing value of 1.4 nm determined from XRD, may collapse during ion-milling preparation technique or under high vacuum of the TEM (Lee et al. 1985; Klimentidis and Mackinnon 1986; Huff et al., 1988) giving a thickness of 1.0 nm (Page and Wenk 1979; Ahn and Peacor 1986a) and making it indistinguishable from illite.

Attempts to sustain expansion of the smectitic layers were made by intercalation of organic ions such as laurylamine (Yoshida 1973; Lee and Peacor 1986) and n-alkylammonium ions (Bell 1986, Vali and Köster 1986; Vali and Hesse 1990; Vali et al. 1991) which are relatively stable under TEM operating conditions. The use of these organic ions is limited to ground samples or clay separates as intercalation in whole rock samples causes a disruption of the original fabric, or the failure of smectite layers to swell after treatment (Ahn and Peacor 1986b).

3.2.2.1 Calculated Lattice Fringe Images

Guthrie and Veblen (1989) emphasized that dark fringes are not specific for 2:1 layers in the illite-smectite structure but rather are "lattice fringes", and the relationship between the position of the fringes to the crystal structure is a complex function of many parameters including operating conditions of the TEM. However, the periodicities of the lattice fringes reflect the periodicities of the real crystal structure. For reliable interpretation of the layer structure of clay minerals, it is essential to compare experimentally obtained images with simulated images generated by computer simulation (Guthrie and Veblen 1989, 1990, Veblen et al. 1990). Guthrie and Veblen (1989) concluded from image simulation that if expandable layers uniformly collapse in untreated mixed-layer I/S, the only difference between the two layers is composition. To obtain information regarding compositional differences for one-dimensional images, even when the specimens are not in perfect orientation, requires a change to "unconventional" overfocus conditions which displays the strongest contrast differences. It is inferred from a study of I/S that thick dark (intense) fringes overlie smectite-like interlayers and thin dark (less intense) fringes overlie illite-like interlayers for highly ordered I-S (Guthrie and Veblen 1989, 1990; Ahn and Peacor 1989).

3.3 Interlayer Complexes

As a result of the weak bonding between silicate layers, in contrast to the strong ionic-covalent bonding within and between tetrahedral and octahedral sheets, interlayer complexes can form as a result of the incorporation of inorganic and organic ions. The formation of interlayer complexes involves interaction of the three components which define the structure of 2:1 layer silicates. Ionic substitution within the octahedral and/or tetrahedral sheets in 2:1 layer silicates may result in an overall negative charge. This negative charge may be compensated by the introduction of exchangeable cations within the interlayers, and neutral molecules. Water is incorporated within the interlayers in the form of hydration shells of the cations and the layers. Naturally occurring interlayer cations, e.g., Mg^{2}, Ca^{2+}, Na^{+}, etc., may be exchanged by other inorganic cations or replaced by organic cations of varying complexity, i.e. methyl ammonium to long chain poly-functional cations (MacEwan and Wilson 1980). In terms of neutral molecules, water may be replaced in the interlayer by other neutral molecules, e.g., alcohols, glycols, glycerols, amines, ketones, sulphur compounds, or may even be replaced by inorganic salts (Bloch 1950).

3.3.1 Ethylene Glycol and Glycerol

There are a number of diagnostic tests used in XRD to identify and characterize soil and sediment clay minerals, to determine layer charge, and to facilitate an understanding of their physical and chemical properties. For 2:1 layer silicates, these tests include: the routine solvation with glycerol or ethylene glycol, which are used to characterize interstratified clay minerals with smectitic or vermiculitic components (Hower and Reynolds 1970; Środoń 1980), and (ii) the use of n-alkylammonium-ion exchange to deduce the magnitude and homogeneity (or heterogeneity) of the layer charge (e.g. Lagaly and Weiss 1969; Lagaly 1979; Laird et al. 1989; Vali et al. 1991).

Glycerol and ethylene glycol can only be used to distinguish expandable from non-expandable layers and gives no evidence of the amount or magnitude of the layer charge. Smectite-group minerals and vermiculites tend to show opposite behaviour with ethylene glycol and glycerol solvation Magnesium-saturated smectite-group minerals can form two-layer complexes with ethylene glycol resulting in a first order reflection in XRD of between 1.68 to 1.72 nm, depending on the exact layer charge and humidity conditions. High-charge smectite-group minerals or low-charge vermiculites will have a two-layer complex giving a first order reflection of 1.60 to 1 63 nm, whereas a high-charge vermiculite will form a one-layer complex having basal spacings of 1.43 nm (Brindley 1966; Suquet et al. 1975). However, with Mg^{2+}-saturation and glycerol solvation, smectite group minerals generally display a two-layer complex giving an increased basal spacing of between 1.77 to 1.80 nm. High-charge smectite-group minerals or vermiculite form a single layer complex with a spacing of between 1.40-1.43 nm (Brindley 1966; Suquet et al. 1975).

3.3.2 n-Alkylammonium Ion Exchange

The n-alkylammonium ion exchange technique (Lagaly and Weiss 1969; 1970) has been increasingly used as a technique to both characterize expandable 2:1 layer silicates in TEM (Ahn and Peacor 1986a; Bell 1986; Lee and Peacor 1985; Klimentidis and MacKinnon 1986; Vali and Köster 1986; Vali et al. 1990, 1991, 1992a; Sears and Hesse 1992) and to determine the layer charge density and estimate interlayer charge in XRD (Lagaly and Weiss 1969; Lagaly 1979; Laird et al. 1988, 1989a; Marcks et al. 1989; Ghabru et al 1989; Olis et al. 1990, Stanjek et al. 1992). Inorganic ions within the interlayer space of 2:1 layer silicates may be exchanged for the larger n-alkylammonium ions. The n-alkylammonium ion-exchange technique employs the quantitative relationship between layer charge density, shape and area (orientation) occupied by the organic molecules and their effects on the basal spacings of the clay-organic complex (Weiss 1963; Lagaly and Weiss 1969; 1970). If expandable layer silicates such as smectites and vermiculites are treated with aqueous solutions of n-alkylammonium hydrochloride of short and long alkyl chains (n_c=6 to n_c=18, with n_c being the number of carbon atoms per alkyl chain), the inorganic ions (e.g. Na^+, Ca^{2+}, Mg^{2+}) are usually exchanged within a few hours. When the clay-alkylammonium complexes are evaporated to dryness, there is a systematic arrangement of the large organic anisometric ions between the interlayers which results in a definitive increase in the basal layer spacings. Thus, the exchange technique is a diagnostic tool for the characterization of clay minerals.

The interlayer charge density refers to the number of interlayer cations per $O_{10}(OH)_2$, and is not necessarily equivalent to the layer charge, which is the negative charge of the layer per $O_{10}(OH)_2$. The arrangement and orientation of alkyl chains within the interlayer space is a function of the ratio of the area occupied by flat-lying n-alkylammonium ions (A_c), and the area available for each monovalent interlayer cation in the interlayer space, if the cations are thought to be arranged in a monolayer, and is referred to as the equivalent area (A_e) (Lagaly and Weiss 1969) (Fig. 3.1). The area required for the flat lying cation (A_c) is defined by the equation;

$$A_c = n_c(0.127)(0.45) + 1.4 \text{ nm}^2 \qquad (1)$$

where n_C is the number of carbon atoms in the alkyl chain, 0.127 nm is the increase in chain length per carbon atom in trans-trans configuration, 0.45 nm is the shortest distance between the chain axis estimated from the C-H distance and the van-der-Waals radii, and 1.4 nm^2 is the area occupied by the end groups. The equivalent area (A_e) is defined by the equation;

$$A_e = a_0 b_0/2(x+y+z) \qquad (2)$$

where a_0 and b_0 are the lattice constants (dimensions of the unit cell in a and b directions), and $(x+y+z)$ represents the charge density. When A_c is less than A_e, the alkylammonium ions between the interlayers are arranged in monolayers, but are not close-packed. For short alkyl chains ($n_c=6$ to $n_c=9$), the basal spacing is between 1.35 to 1.37 nm (Lagaly and Weiss 1969). With increasing alkyl-chain length, the area A_c of the ions increases and at A_c equal to A_e, the monolayers become closely packed If A_c is greater than A_e, the ends of the alkyl chain would extend beyond the monolayer. However, beyond the threshold of $A_c=A_e$ (i.e. longer chain lengths), a monolayer is rearranged into a bilayer (double layer) of flat lying alkylammonium ions giving basal spacings between 1.75 to 1.77 nm (Lagaly et al. 1976). If A_c is greater than $2A_e$, bilayers become unstable and because three layers of alkylammonium ions are energetically unstable as a result of electrical repulsion, further increases in alkyl-chain length causes the chain to assume a pseudotrimolecular structure, which belongs to the class of kink isomers, and gives a basal spacing of about 2.17 nm (Lagaly et al. 1976; Lagaly and Weiss 1975). It is defined as pseudotrimolecular because it has the basal spacing of three alkyl chains but it is not actually arranged in three layers. This relationship may be expressed as:

$$N_c(0.127)(0.45) + 1.4 = N(a_0)(b_0)/2(x+y+z) \qquad (3)$$

where N=1 for the monolayer-bilayer transition, and N=2 for the bilayer-pseudotrimolecular transition, and $(a_0)(b_0)$ is equal to 4.65 nm^2 for dioctahedral minerals and 4.9 nm^2 for trioctahedral minerals. When A_c is greater than $2A_e$, or if the charge density of the mineral is very high, the alkyl-chains form a "paraffin-type" structure (i.e. a tilting of the alkyl chain against the silicate layer structure) in the interlayer space (Brindley and Ray 1964; Brindley 1965; Johns and Sen Gupta 1967; Lagaly and Weiss 1969). The tilting angle is given by

$$\sin\Theta = \triangle d/1.26 \qquad (4)$$

where $\triangle d$ is the change of basal spacings with change in n_C and 0.126 nm is the change in length of chain per c-atom.

If the layer charge is homogenous then the interlayer cation density should be the same in each interlayer and the transition from monolayer to bilayer, and from bilayer to pseudotrimolecular spacing should occur sharply, i.e. at a critical chain length (n_C). However, smectites and low charge vermiculites do not show a sharp transition, which is indicative of a variable interlayer cation density. As a result of the variation of layer charge within and between interlayers (i.e. layer charge and chemical composition are heterogeneous; Lagaly and Weiss 1976; Lagaly 1982), the transitions occur over a certain range of alkylammonium ions of different chain length. This will result in the appearance of non-integral interstratified spacings on the XRD pattern (see Olis et al 1990).

The procedure for n-alkylammonium exchange has been revised several times to account for some discrepancies in the packing density of alkyl-chains in the interlayer space of 2:1 layer silicates. Studies have indicated that minor correction factors are required for the critical A_c for small particle sizes (< 80 nm in diameter) after expansion of the interlayer volume (Lagaly and Weiss 1970; Stuhl and Mortier 1974; Lagaly et al. 1976; Lagaly 1981) to reconcile small displacements of the interlayer cations as the interlayer cations bound near the edges of the silicate layers may not occupy an entire equivalent surface (A_c) of the layer. Thus, the consequence is a slightly increased interlayer spacing. Laird et al. (1989a) also suggested an empirical equation to reconcile differences in layer charges determined from the alkylammonium-ion exchange technique with those calculated from structural formulae.

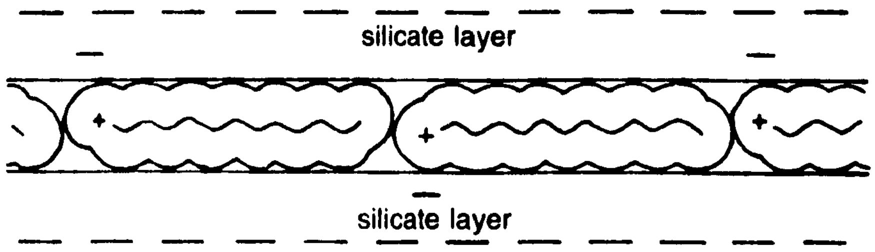

A - Monolayer

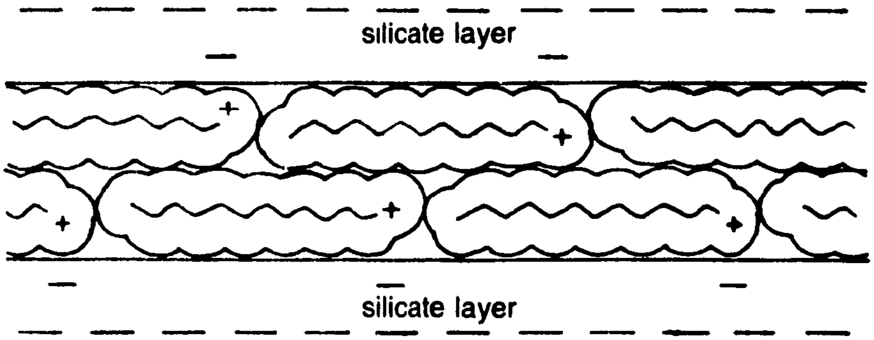

B - Double Layer

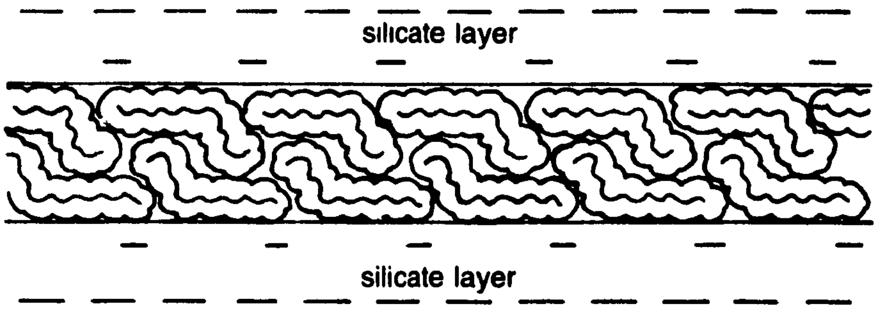

C - Pseudotrimolecular Layer

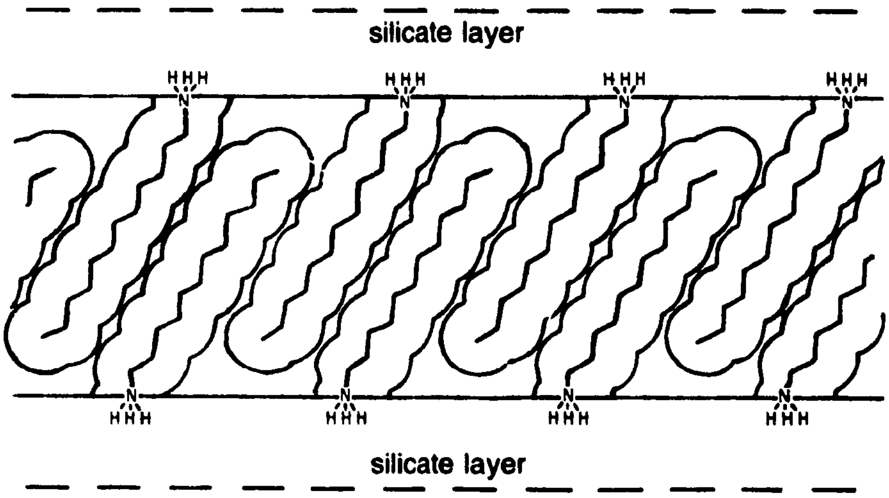

D - Paraffin Type Structure

Fig. 3.1 Arrangements of alkylammonium ions in 2:1 silicate interlayers (after Lagaly and Weiss 1969).

CHAPTER 4.0 - REVIEW OF CLAY PREPARATION TECHNIQUES

A prerequisite to the characterization of mixed-layer I/S is an understanding of artifacts produced during sample preparation. Various sample preparation procedures may account for some of the discrepancies observed between different clay mineral investigations (e.g. Ransom and Helgeson 1989). Chemical pretreatments, for example, have specific effects, and thus it is important to outline the changes in mineralogy that may result from their use, as well as the ramifications if pretreatments are avoided.

Numerous workers have emphasized the need for careful consideration of preparation and pretreatment of clay mineral samples for all types of analyses (e.g. Harward et al. 1962; Fenner 1966; Thorez 1975, 1985; Bish and Reynolds 1989). Whittig and Allardice (1986) stressed the need for continued research into possible modifications and alterations of clay minerals by mechanical and chemical treatments especially with respect to XRD and TEM studies. The kinds of problems encountered were stated by Whitehouse and Jeffrey (1955)·

> "An aqueous suspension of clay material is fundamentally different from a suspension of clay material in an electrolyte solution. After the addition of a chemical agent to an aqueous suspension of clay, the clay particle is no longer the same particle and the suspension is no longer the same system. These differences, chemical in essence, vary in degree if not in kind as the electrolyte and/or clay concentrations of the suspensions are varied".

4.1. Dispersion Methods for Clay Minerals (Particle Size Separation Procedures):

General procedures for clay mineralogical analyses may be found in Jackson (1969), Kunze and Dixon (1986), and specifically for XRD in Starkey et al. (1984), Wittig and Allardice (1986) and Moore and Reynolds (1989), and Nadeau and Bain (1986) for TEM.

The degree to which clay bearing samples must be physically and chemically treated prior to analysis is dependent upon: (i) the objectives of the study; (ii) the methods of analysis, (iii) the material being investigated; and (iv) instrument availability. Irrespective of the objectives, the gentlest procedure for dispersion which will limit compositional and structural changes should always be used.

To analyze clay minerals from soils, sediments and rock samples (i.e non-consolidated and consolidated or indurated samples), it is often necessary to isolate the clay minerals from other non-clay crystalline and non-crystalline (crypto-crystalline and amorphous) materials, i.e. quartz, feldspar, zeolites, carbonates, gypsum, pyrite, iron oxides, aluminum oxides, organic matter, and concentrate them. Although clay mineral separation and purification may be accomplished through centrifugation and chemical pretreatment, care is required during centrifugation and sample preparation to prevent contamination from coarser particles. Specific species of clay minerals may exist in well-defined size fractions or in a relatively wide range of particle sizes, and thus fractionation into various sizes is essential. Size fractionation also has the potential advantage of eliminating contaminant phases. In the past, this has been accomplished through physical and/or chemical procedures. Whereas contaminant phases may exist in concentrations below the detection limit of the XRD, the TEM may be used to assess the purity of individual fractions.

An important consideration is the degree and type of bonding between clay crystallites. In soils and sediments, cementation of clay minerals may be the result of crystal growth of carbonates or iron oxides, or clay aggregates may form from amorphous coatings of organic and inorganic material. Clay aggregates may also form as a result of high-layer charges with some non-ionic bonds between particles (Norrish and Tiller 1976) In argillaceous rocks, clay minerals can form bonds as a result of compaction and crystal growth Thus, the goal in separation is the complete disintegration of samples into their primary constituent particles. However, mineral separation procedures by their very nature destroy the primary sample fabric and texture and thus, in the end, may not represent an "in situ" or "natural clay system" (Brewster 1980).

4.2 Comminution

As a result of the increased difficulties in disaggregating indurated or lithified materials, Fenner (1966) argued that structural, genetic or diagenetic implications may be easily attributed to samples which do not warrant them. While there is no preferred method for the disintegration or crushing of soils and sediments, the ideal method for the isolation of diagenetic minerals is one that will not cause excessive abrasion or fragmentation of discrete particles. Ultrasonic vibration using high-powered ultrasonic probe or ultrasonic bath is the preferred method over crushing (i.e. mortar and pestle or percussion mortar), or rubbing and grinding (mechanical stirrer and automatic grinding, rolling or shaking machines)(see Bish and Reynolds 1989). There is broad consensus that mechanical disaggregation applying prolonged shaking does not result in true particle size distribution but rather an accumulation of mechanically abraded and fragmented clay-sized particles. Physical disaggregation is best achieved through impact rather than grinding methods. Crushing and/or grinding with pestle and mortar can break or alter the original clay particles. Excessive dry grinding may result in phase changes and crystal strain, and even in the production of X-ray amorphous material. Consequences of these actions may be line broadening of X-ray peaks and increased background-to-peak ratios (Moore and Reynolds 1989).

The energy released in ultrasonic vibration breaks the bonds between individual particles, causing dispersion (Adams and Stewart 1969). Ultrasonic vibration is effectively used for two purposes: disaggregation and dispersion. However, as Gee and Bauder (1986) have noted, no standard procedures for ultrasonic vibration have been adopted. Depending on the frequency, intensity and duration of ultrasonic treatment, and the concentration of suspensions, high-powered ultrasonic probes can rupture individual clay particles and may heat the clay suspension to undesired temperatures (Pusch 1966; Halma 1969). Gipson (1962) reported that ultrasonic vibration preferentially abraded cleavable minerals such as calcite and mica especially in the clay-size range. Šaly (1967) noted an increase in the amount of potassium released from hydromica (mixed-layer vermiculite-biotite) with exposure to ultrasonic vibration.

4.3 Chemical Pretreatment

According to Love and Woronow (1991), if a change was observed in the chemical composition or structure of the clay material resulting from chemical treatments, it may be either the result of (i) the removal of the accessory/contaminant material, (ii) the alteration of the clay material itself by the chemical treatment, or (iii) some unknown combination of these factors.

To aid in separation of the fine and ultrafine-particle size of the clay aggregates, chemical pretreatments and peptizers are often used to disaggregate clay particles, to remove coatings and cements, and to promote the stability of dispersions of constituent clay separates. Contaminant phases as coatings or films on clay minerals may act as a cementing agent binding individual clay particles together into larger aggregates. Thorez (1985) compared X-ray data of soil and clay minerals from weathering, diagenetic and marine environments prepared with distilled water and without chemical treatments and contrasted them with seventeen "conventional" chemical pretreatments. He concluded that there were three major modifications and/or alterations resulting from chemical pretreatment: (1) an increase in the amount of stable well-crystallized minerals, with the loss of labile and fragile mixed-layers, (2) the occurrence of new mineral phases such as vermiculite and/or smectite, and the transformation of some mixed-layer I/S into vermiculite or secondary chlorite, and (3) the increase in expandable layers in mixed-layer I/S and/or the transformation of smectite into a chloritic structure.

4.3.1 Organic Matter

Organic matter may be present as a coating or film on clay particles and may act as a cementing agent binding clay particles into aggregates. Initially this coating makes samples more difficult to disaggregate, but after the particles are in suspension it can increase the stability of the suspension (Emerson 1971). Organic matter may also be present in the interlayer space of expandable minerals and prevent expansion in solvation experiments. Organic matter may produce a high background/peak ratio in XRD by increasing the intensity of the Compton-modified scattering (Cullity 1978) resulting in broad diffraction peaks.

Oxidation and removal of organic matter can be achieved with the following treatments: hydrogen peroxide, hydrochloric acid, Na_2EDTA, sodium hypochlorite (Anderson 1963, Mikhail and Briner 1978), sodium permanganate-oxalic acid (Dümmler and Schroeder 1965), sodium hydroxide in methanol and benzene (Farrington and Quinn 1971), bromine and sodium carbonate (Mitchell and Smith 1974), sodium hypobromite (Troell 1976), carbon disulphide and ethanol (de Lange 1976) and low temperature ashing (Gluskoter 1965; Price and Jenkins 1980).

The most widely used among these treatments for organic-matter removal is still hydrogen peroxide. However, hydrogen peroxide has been shown to cause degradation or dissolution of lattice components in clay minerals and in Fe- and Mn-oxides (Laveulich and Wiens 1970; Thorez 1985). Other reported effects include, exfoliation (reduction in particle size) of mica or illite (Drosdoff and Miles 1938; Protz and St. Arnaud 1964), vermiculitization or smectitization of chlorite (Thorez 1985), modification of clay expandability (Perez-Rodriguez and Wilson 1969), the formation of calcium oxalate trihydrate or calcium oxalate monohydrate if calcium -bearing minerals are present (Martin 1954; Farmer and Mitchell 1963; Bourget and Tanner 1953; Jones and Beavers 1963), or alteration of amorphous material (Mitchell et al. 1964). Douglas and Fiessinger (1971) demonstrated that without the addition of a buffering agent, hydrogen peroxide treatment caused small degradation in peak intensity in vermiculite and bentonite phases. The use of HCl and Na_2EDTA would incompletely remove organic material from the interlayer spaces and prevent expansion with ethylene glycol or glycerol (Perez-Rodriguez and Wilson 1969). van Langeveld et al. (1978) compared the effectiveness of the various procedures for removing organic matter and suggested that all treatments alter or modify clay mineral expandability, but that even the most effective method left about 20% of the non-carbonate carbon.

4.3.2 Inorganic and Amorphous Material

Iron oxides and hydroxides occur in clay samples as coatings and discrete particles, including hematite, goethite and various iron-manganese compounds, which represent interlayered materials. Because these inorganic materials may act as cementing agents binding individual crystallites into larger aggregates, removal of inorganic matter, therefore may result in an increase in the smallest size fractions (Barberis et al. 1991). Iron oxides also may obscure XRD patterns because: (i) Fe absorbs Cu K_α radiation which in turn fluoresces and emits its own non-directional, characteristic X-radiation increasing the general background radiation (Brown and Brindley 1980); and (ii) Fe-oxides interfere with the orientation of clay minerals during specimen preparation (Hendricks and Alexander 1939). Townsend and Reed (1971) suggested that the removal of iron oxides uncovered peaks that had originally been obscured and intensified other peaks. Recently, graphite monochromators have been employed to separate K_α X-rays from fluorescent X-radiation, and this eliminates most of the background from Fe minerals.

The removal of Fe oxides aids in dispersion of the inorganic components which is often essential for effective particle size separation. Mehra and Jackson (1960) suggested a sodium dithionite citrate solution buffered with sodium bicarbonate (SDCSB) for the solubilization of Fe oxides (as well as calcite and phosphates) (Jackson 1969). Ferric iron is reduced with sodium dithionite and the ferrous iron is complexed with sodium citrate. Sodium dithionite citrate solutions dissolve some silicon and aluminum and may attack the clay mineral structure

(Newman and Brown 1987). SDCSB alters biotite to a vermiculite-like mineral as a result of the removal of K, Mg and Fe due to the chelating action of citrate (Douglas 1967; Sawhney 1960). This could result in the misidentification and overestimation of vermiculite in a sample. Other effects include increased expandability in mixed-layer 2:1 minerals and the extraction of iron from micas and nontronite (Thorez 1975; 1985).

The removal of carbonates aids in easier size fractionation. Retention of carbonates can prevent clay dispersion and create scatter in XRD resulting in poor diffraction profiles. Removal of carbonates can be achieved through the use of HCl, EDTA or heating with acetic acid buffered to pH 5 with sodium acetate (Grim et al. 1937; Jurik 1964; Ellinghoe and Wilson 1964). The use of HCl results not only in release of Ca and Mg which can be preferentially exchanged for interlayer cations in the clay minerals and which may interfere with cation exchange capacity and elemental analyses (Carroll 1959; Eslinger and Pevear 1988), but will also leach Al, Fe and Mg ions from the clay lattice structure (Mathers et al. 1955). Cook (1992) demonstrated that nontronite treated with NaOAc will extract exchangeable K from smectites. However, it should be noted that with these two treatments, differences in the XRD patterns were negligible, although peak intensity was diminished (Mathers et al. 1955; Cook 1992). Ethylene-dinitrilotetra-acetic acid (EDTA) is proposed as an alternative method to remove carbonates (Bodine and Fernald 1973). However, the EDTA anion can leach iron, barium, strontium and magnesium from the octahedral layers of chlorites and some smectite minerals, especially hectorite and saponite (Starkey et al. 1984). Jackson (1969) suggested, however, to use acetic acid with a sodium acetate buffer of pH=5.

Other chemical pretreatments include the use of alkaline solutions to remove amorphous compounds of silica, alumina and alumino-silicates from clay samples. Amorphous components in clay fractions can prevent the characterization of the layer silicates by XRD by acting as coatings and films on clay particles as well as cementing agents (Follet et al. 1965a, 1965b; Chichester et al. 1969). Dudas and Harward (1971) showed that the use of sodium hydroxide or potassium hydroxide resulted in the removal of interlayer compounds in clay minerals, and induced alteration of biotite. Acid ammonium oxalate solutions have been used to dissolve amorphous materials. Additional modifications include the increase of expandable layers in mixed-layer I/S and the vermiculitization of chlorite and mica (Thorez 1985). Other reagents include Na_2CO_3 (Follet et al. 1965b) which may be effective in dissolving free Si and Al compounds, but again may remove these elements from the clay lattice.

4.3.3 Peptizers and Dispersion

Clay minerals, dispersed in deionized water have colloidal dimensions and thus, may be treated as colloidal systems. The discussion of colloidal systems is limited to the effects of peptizers (or dispersants) on clay minerals because colloidal systems are not investigated in this study. The terminology used follows van Olphen (1977; 1987).

Aggregation describes the coalescence of several multilayer particles as well as the degree of layer stacking in a single particle. Flocculation (or coagulation) denotes particles which stick together upon collision in loose agglomerates (or flocs) and sediment under gravity. Van Olphen (1977) distinguished edge to face (EF) and edge to edge (EE) association as flocculation, and face to face (FF) association as aggregation. The reversal or restoration of the original dispersion of individual particles is referred to as deflocculation, peptization or stabilization. It is important to keep in mind that disaggregation and peptization are not concomitant phenomena (Juhász 1990).

Particle size separation can only be achieved if the individual components in a clay suspension are stable. The stability of a clay colloidal system is a function of the mineralogical, chemical, and concentration characteristics inherent in the system. Clay particles which are dispersed in deionized water are classified as lyophobic colloidal systems. In natural clay suspensions there is a tendency for clay particles to flocculate to minimize Gibbs' interfacial energy. Van Olphen (1977; 1987) explained that the stability of clay suspensions is a function of two opposing particle interaction forces: the electrical double layer which acts as a repulsive force between particles and the van der Waals'-London dispersion forces which represent the cumulative attractive force of all the atoms of one particle and all atoms of another particle. However, an additional complication for clay suspensions is a result of the distinct morphology of clay minerals which contain faces and edges. The electric double layer and the van der Waals' forces will be distinct for each exposed face. A reduction in the face charge or edge charge of clay particles decreases the range of their repulsive forces and promotes flocculation through van der Waal's attractive forces (for further details see van Olphen 1987).

The <2-µm size fraction of soils and sediments is frequently in a coagulated state which requires further dispersion, as particles smaller than 2 µm tend to agglomerate due to the adsorption of soluble salts and polyvalent cations. This is a consequence of surface charges (Halma 1969). Pusch (1966) argued that the size and distribution of particles determined from dispersed suspensions do not represent the real distribution in the sediment during formation in situ, regardless of the method of dispersion.

To achieve a stable clay suspension, excess electrolytes must be removed. This can be accomplished through washing, either by centrifugation, ultracentrifugation, ultrafiltration or dialysis (Jackson 1969; van Olphen 1977; Schramm and Kwak 1980). However, this procedure may not achieve the desired result as other factors play an important role, as noted in previous sections. The addition of a peptizer may also be required to promote dispersion (Jackson 1969; Moore and Reynolds 1989). The advantage of using peptizers to maintain suspension is the greater ease with which larger amounts of fine particle separates are obtained. It is possible to disperse clay minerals without removal of electrolytes by simply increasing the amount of the peptizer. Even after the removal of cementing agents and the addition of peptizers, complete dispersion may not be achieved if the pH of the suspension is either too acidic or basic (Protz and St. Arnaud 1964).

There are no universally accepted peptizers, as different octahedral cations are exposed and different cations adsorbed on the clay face, and the complexing ability of anions is dependent on the type of cation. Thus, the composition of the clay mineral determines the type of peptizer used. Generally, the peptizers suggested for dispersing clay minerals include: sodium pyrophosphate, sodium hexametaphosphate, and sodium carbonate (Jackson 1969).

To achieve a stable clay suspensions in which to separate different clay-size fractions, it is necessary to reverse the edge charge of the clay particles (van Olphen 1987). Anions of an appropriate peptizer are chemisorbed to broken clay particle edges where they form complexes with the exposed cations of the octahedral sheet. Reversal of the edge charges thus eliminates flocculation and creates a sufficient charge level to prevent attraction by van der Waals' forces. This eliminates EF and EE particle associations. The dispersive behaviour of peptizers, such as sodium hexametaphosphate and sodium pyrophosphate may result from their replacement of exchangeable cations and the formation of soluble undissociated complexes with the various cations (Tyner 1939; Hatch and Rice 1938).

As stated in previous sections, the addition of any chemical reagent changes the properties of the clay system, and peptizers such as sodium hexametaphosphate are not different in this respect. Sodium hexametaphosphate $(NaPO_3)_6$, will not disperse all clay minerals (e.g. kaolinite). There is still controversy over the use of "Calgon" as a peptizer (Yaalon 1976; Veneman 1977). Calgon is a polymer of 15-30 PO_3 groups, and in solution contains pyrophosphate and orthophosphate (Whitehouse and Jeffrey 1955). Treatment with Na-EDTA has been shown to result in the partial exchange of interlayer cations (Thorez 1985). Harward et al. (1962) demonstrated that there is an increase in the ability of expansion or collapse of 2:1 layer silicates after dispersion treatments. The phosphate ion may complex with saturating cations resulting in the appearance of additional XRD reflections (cf. Lindgreen and Hansen 1991). Omueti and Lavkulich (1988) demonstrated that for soils containing layer silicates, particularly chloritized montmorillonite, dispersion with sodium pyrophosphate resulted in XRD profiles with displaced reflections and the appearance of additional peaks not belonging to the original sample. Thus, it has been suggested that following the addition of a peptizer, agitation, centrifugation and washing be performed at least three times to remove excess phosphates (Nadeau and Tait 1987). In addition, peptizers such as sodium hexametaphosphate are chemisorbed on clay faces or edges and may result in erroneous interpretation in the SEM (Robert 1987 as cited by Malla 1987, p.35).

Thus, any operation, be it physical or chemical, which promotes disaggregation at low sodium concentration can have a beneficial effect on the dispersive quality of a clay suspension (Juhász 1990), but it is suggested that sodium pyrophosphate and sodium metaphosphate should only be used as a peptizer when performing particle size analyses, as was originally intended. These peptizers should not be used indiscriminately for dispersing clay minerals (Fenner 1966; Perez-Rodriguez 1969; Thorez 1975; 1985; Omueti and Lavkulich 1988).

CHAPTER 5.0 - Materials and Methods

5.1 Characteristics of Samples

Samples for this investigation were taken from drill core and well cuttings of the I.O.E.-Shell-B.A. Reindeer D-27 discovery well curated at the core repository of the Institute for Sedimentary and Petroleum Geology (I.S.P.G.) of the Geological Survey of Canada (G.S.C.), Calgary, Alberta. Composite samples from cuttings were combined by weight at 50-ft intervals (Ko 1992). Criteria for sample selection were: (1) the amount of sample material available for a given depth, (2) depth of the sample and (3) the closeness to sample depths for which bulk chemical analyses were available from Ko (1992). Initially, drill core samples were available from a depth of 2985 to 9561 ft and composite well cuttings from 6150-6200 ft to 12550-12600 ft, but as material was also being used for other investigations (Ko 1992), sample material from some depths became exhausted and no longer available for this project⁽¹⁾. As samples were prepared for multiple analytical purposes, but specifically for isotopic analyses (Rb-Sr, K-Ar), the overriding constraint on sample preparation and separation techniques was to minimize modification or alteration of the original material, especially to loss or gain of interlayer cations by sample pretreatment (see Chapter 4). Composite well cuttings were generally chosen at 1000 ft intervals from an initial depth of 6650-6700 to 12550-12600 ft, with two core samples located at 2945 and 4800 ft. Additional sample depths were chosen where abundant material was available, regardless of other criteria. Drill core samples had a characteristic greyish-brown colour, with a fairly uniform grain size. Most well cuttings consisted of claystone and mudstone, with a fairly uniform clay size fraction, although some samples were mudstones with clay and silt-size fractions. There were some problems in choosing composite samples from depths of 9250-9300 ft to 9750-9800 ft because of the high silt content of the shale material.

5.2 Sample Preparation

To eliminate other detrital minerals and contaminant phases, e.g quartz, feldspar, micas, kaolinite, chlorite, organic matter, etc., I/S mixed layers were isolated and concentrated by separation of the fine size fractions, where these minerals are most abundant (Johns and

---

(1) The original depths of the samples were delineated in feet, and are retained throughout this thesis to avoid artifacts that might be introduced by converting to meters.

Kurzweill 1979; Brewster 1980). Kittrick and Hope (1963) stated that X-ray diffraction (XRD) studies seldom reveal clay minerals in the <0.08-µm fraction that are not found in the 0.08-0.2 µm fraction. However, the hypothesis for the isotopic analyses originally planned for this study was that the ultrafine fractions may represent a neoformed component. The <0.1 µm and <0.05 µm size fractions were considered the ideal fractions to isolate mixed-layer I/S. In particular, it was thought that I/S of the <0.05-µm size fraction might be the neoformed component, whereas detrital I/S would occur in the coarser fractions (Morton 1985; Ko 1992; Sears and Hesse 1992; cf. Ohr et al. 1991).

5.2.1 Clay Separation and Centrifugation

Separation of clay minerals from composite shale well cuttings required approximately 100 g (90-120 g) of sample material. Composite samples were passed through 150 mm and 1.14 mm sieves to achieve a relatively uniform cutting size and to eliminate larger and finer cuttings which may give contamination from cavings or drilling mud (Ko pers. comm. 1990) These samples were then hand-picked to further remove extraneous material (i.e. drilling mud, iron-oxides, sulphides, carbonaceous material) and coarser-grained clastic sediments (e.g. silt- and sandstones) and other rock fragments (black and white chert). Following this procedure, well cuttings were thoroughly washed (three times) through agitation and decanting in deionized water in an attempt to remove contamination from drilling mud (see Dypvik 1981). In the process, samples were transferred to 250 mL centrifuge bottles and filled with approximately 150 mL fresh, deionized water. Deionized ultrapure water was produced by the Millipore™ Milli-Q water-purification system consisting of reverse osmosis, organic scavenging, and ion exchange cartridges in the McGill University Geochemical Laboratory. The drill core was scrubbed in deionized water to remove possible contamination from drilling mud, broken into smaller fragments to fit the opening of the 250 mL centrifuge bottles, which were filled with 150 mL of deionized water. Ideally, the central parts of the core should be sampled while avoiding material near the edges, in order to minimize drilling mud contamination (see Barefoot and Van Elsberg 1975; Ko 1992). However, due to the limited amount of core material available, this was not possible. The drill core and well cutting samples were disaggregated by placing the centrifuge bottles into a mechanical shaker (Red Devil Paint Shaker) and agitating them. At 15 min. intervals, the suspended contents were decanted and fresh deionized water added to the remaining cuttings. This procedure was repeated until most of the cuttings were reduced to their constituent particles (up to 2 hrs for more consolidated samples, i.e. usually deeper samples). The suspended material was transferred into 2 L bottles which were filled with additional deionized water. Alternatively, centrifuge bottles containing well cuttings were rolled gently on mechanical rollers overnight to disintegrate the cuttings to their constituent clay particles. Again, the material was then transferred to 2 L bottles which were filled with approximately 150 ml deionized water. If flocculation occurred after sediment agitation, the suspensions were cleaned of excess electrolytes either by washing through repeated centrifugation and washing or dialysis until effective particle dispersion was achieved. As there is still limited standardization between different clay laboratories, an attempt was made to minimize chemical pretreatment (see Chapter 4). Peptizers were not used to induce dispersion of clay-sized particles. Perusal of the available literature showed that conventional clay separation techniques often include chemical pretreatments and peptizers (e.g Jackson 1969, Moore and Reynolds 1989) for removal of Fe-oxides, organic material, carbonates, amorphous material, and dispersion, respectively. However, all of these pretreatments will modify the clay minerals, especially their expandability as shown by the work of Johns and Kurzweill (1979), Thorez (1985) and this study.

The <2.0 µm size fraction (equivalent spherical diameter or e.s.d) was collected by sedimentation in water using Stokes' law for the calculation of settling times (Jackson 1969). The procedure was repeated 3 to 5 times to ensure the complete collection of this fraction.

The 0.05-0.1 µm and <0.05 µm clay separates were obtained using a Sorval SS-3 table-top centrifuge with a fixed angle rotor and 250 mL centrifuge bottles (Dr. John Morton writ comm. 1990). Clay suspensions were decanted after each run into 2 L bottles, additional <2.0 µm clay suspension was added and resuspended through mechanical agitation. This procedure was performed from 6 to 8 times per sample to ensure the complete collection of these ultrafine clay separates. No ultrasonic vibration was used to resuspend sediments between centrifuge runs.

5.2.2 Chemical Pretreatment

To assess possible structural changes induced as artifacts in mixed-layer I/S as a consequence of chemical pretreatments, selected clay suspensions were split into halves (approx

50 g clay each), one dispersed in deionized water only, the other treated with a 10% sodium hexametaphosphate for improved dispersion (10 ml of 10% $[NaPO_3]_6$ per 2000 mL clay suspension) The clay fractions were then collected following the procedures outlined above.

5.3 Reduction of Water Volume

Fractionation of clay separates requires large volumes of water. To reduce these amounts of water and at the same time, to minimize the loss of ultrafine clays, many benign procedures were attempted before freeze drying. The first attempt was to use the Millipore membrane-filtration system, which is the same procedure as that for creating oriented XRD slides. As the smallest filter size available had a pore size of 0.1 μm, there was an initial large loss in the <0.1 μm fraction until the clay separates clogged the pore space. The procedure was also very time consuming to collect upwards of 300 mg of clay separates. The second procedure attempted was to freeze the clay suspensions and then allowed to thaw, which resulted in clay flocculation (Laird et al 1991). The excess water was decanted and the clay fraction collected and subsequently freeze-dried. However, often the finest fractions were lost. The third and most efficacious (although again very time consuming) method was to freeze-dry the large volume of very dilute solution as collected without intermediate water reduction steps. Dilute suspensions were lyophilized in a Labconco 6 L freeze-dryer, model 77530-01 at -55°C and a vacuum of between 10-20 microtorr. As the lyophilization process is dependent on the surface area and thickness of samples, the condenser temperature and vacuum, and the melting temperature and solute concentration of the clay suspension, approximately 2L of clay suspensions were divided into four 500 mL wide-mouth polyethylene containers. These samples required approximately 1-1/2 to 2 weeks to sublimate all the water. One disadvantage to this method is that it concentrates any remaining electrolytes which may be adsorbed to clay surfaces (see Chapter 4). This will have a deleterious effect on the lyophilized clay particles by increasing flocculation potential. Freeze-dried samples were stored in plastic vials with snap-lids under normal laboratory humidity conditions (50-60% R.H.).

5.4 Preparation of n-Alkylammonium Hydrochloride

Octylamine hydrochloride (n_c=8) and dodecylamine hydrochloride (N_C=12) were obtained from Dr. G. John Ross (Agriculture Canada, Ottawa) and were prepared and purified from their respective amines by the procedure outlined by Lagaly and Weiss (1969) and modified by Rühlicke and Kohler (1981). Additional octylamine hydrochloride (N_c =8) and octadecylamine hydrochloride (N_c =18) were chosen for characterizing the expandable components because of their commercial availability from Eastman Kodak Organic Chemicals, Rochester, New York; these chemicals are distributed by Fisher Scientific and need not be synthesized from their respective amines. They were used as received. However, as Olis et al (1990) noted, n_c=12 is preferrable to n_c=18 because of difficulties in the exchange reaction due to stearic hindrance in expanding the interlayer and difficulties in washing the samples.

Alkylammonium hydrochloride solutions were prepared as required and these solutions were stored at 65°C and renewed every 3-4 months. The concentrations for the respective alkylammonium hydrochlorides are given in Table 1 as calculated by Lagaly and Weiss (1969).

Table 1. Concentrations of Alkylammonium Hydrochloride

Chain Length ($C_nH_{2n+1}NH_3^+Cl^-$)	Molecular Weight	Molarity	Grams/100 mL
6	137.66	2	27.5
7	151.68	0.5	7.6
8	165.71	0.5	8.3
9	179.73	0.5	9.0
10	193.76	0.1	2.0
11	207.79	0.1	2.1
12	221.82	0.1	2.2
13	235.84	0.1	2.4
14	249.87	0.1	2.5
15	263.89	0.1	2.6
16	277.92	0.05	1.4
17	291.95	0.05	1.4
18	305.98	0.05	1.5

The concentrations of the organic salts were varied according to their solubility in water. Alkylammonium-ion solutions of the required molarity were prepared by dissolving a weighted amount of the n-alkylamonium hydrochloride in deionized water preheated to 65°C. Higher chain lengths are less soluble and were dissolved in water over a period of twenty-four hours in an oven at 65°C.

5.5 XRD Preparation (Post-Treatment)

Oriented samples for X-ray diffraction (XRD) analysis were prepared from 12-15 mg of freeze-dried clay separates in 5 mL of deionized water using a modified version of the membrane-filter transfer method of Drever (1973; modified by Pollastro 1982). The Millipore™ filter was retained and mounted on a glass slide with dilute white glue. Some samples containing highly expandable clays required up to 1 hr of vacuum-suction before all material was transferred to the filter (see Bish and Reynolds 1989). This approach is justified on the basis that the fine and ultra-fine particles of the clay separates are of fairly uniform size and thus there is limited particle-size segregation Filters were initially eluted with 5 ml deionized water to remove possible chemical contaminants from the manufacturing process and from possible subsequent contamination during handling. For samples exchanged with n-alkylammonium ions prior to embedding in Spurr VCD resin (see below), slides were made by dispersing the organic-clay complexes in an 85:15 ethanol:methanol mixture and evaporating them to dryness. Other selected samples were saturated with Mg^{2+} for determination of expandability following the method of Moore and Reynolds (1989). Following the transfer of the clay material to the Millipore™ filter, 5 mL of 0.1M MgCl was suctioned through the clay cake. This was followed by 5 mL of 50:50 mixture of 85:15 ethanol:methanol and deionized water to remove excess chloride anions All samples were air-dried and stored under humidity-controlled conditions (R H 50-60%) and solvated with ethylene glycol by the vapour pressure method at 60°C for 24 hrs, except for the samples exchanged with n-alkylammonium ions. Immediately following ethylene-glycol solvation, the samples were transferred to the X-ray diffractometer Selected samples were solvated with ethylene-glycol for 72 hrs to compare the result with specimens treated for 24 hr. No changes were apparent.

Glycerol solvation was performed by placing a few drops of glycerol on the Mg^{2+}-saturated clay cake and carefully smearing it over the entire clay surface. The slide was transferred to a desiccator containing glycerol which was placed in the oven at 60°C for 48 hrs. Before XRD, the mounts were allowed to equilibrate to room temperature and the excess glycerol removed by carefully placing a tissue over the clay surface.

5.6 n-Alkylammonium Exchange and Sample Preparation

Two preparation methods using n-alkylammonium ions were used on freeze-dried clay material. Clay samples were treated with n-alkylammonium ions (Vali and Köster 1986) (i) prior to XRD analysis and HRTEM imaging, and (ii) after embedding in a low-viscosity resin and ultrathin sectioning (Vali and Hesse 1990). Vali and Hesse (1992b) reported no visible differences in the layer structure of particles of phlogopite and vermiculite between the two preparation techniques

Selected clay samples were saturated with n-alkylammonium ions following the procedure of Rühlicke and Kohler (1981). Approximately 50 mg of freeze-dried clay separate were weighed and placed into 35 mL heavy-duty glass centrifuge test tubes with screw caps Approximately 5 mL of the appropriate n-alkylammonium ion ($n_c = 8$ and $n_c = 18$) was added to the tubes, closed and shaken vigorously for a few minutes to suspend the clay material Samples were incubated in an oven at 65°C for 48 hrs, and periodically agitated to resuspend the material. The suspensions were then transferred to polypropylene centrifuge tubes with snap caps and centrifuged for approximately 3 hrs at 10,000 rpm The supernatant was decanted and replaced with 5 mL of fresh aliquot of the appropriate alkylammonium solution, vigorously agitated and transferred back to the glass tubes. The samples were incubated at 65°C for an additional 48 hrs. Following the incubation, the samples were transferred to the polypropylene tubes and 1-2 mL of 85:15 ethanol:methanol was added The samples were again centrifuged for approximately 3-4 hrs, the supernatant decanted, then replaced with 5 ml of the ethanol:methanol mixture. This washing procedure was repeated 6 times to ensure the removal of excess alkylammonium chloride. After the final wash was performed, 1-2 mL of ethanol was added and the clay material resuspended by mechanical agitation The suspensions were transferred to 51 x 51 mm glass slides with disposable polyethylene pipettes and the ethanol was allowed to evaporate. After the samples were air dried, they were placed in a freeze-dryer and subjected to a high vacuum of between 10 to 20 microtorr for >12 hrs The slides were kept in vacuum until X-rayed

During test runs for this procedure, it was discovered that there may be an interaction between n-alkylammonium and the polypropylene microtest tubes Alkylammonium solutions stored in glass flasks with yellow polyethylene caps leached the colour from the caps. Subsequently, solutions were stored in glass flasks with glass stoppers and heavy-duty 50 mL glass test tubes with screw-caps, containing rubber insets were used. To minimize alteration of expandable layers in mixed-layer I/S, the procedure of Rühlicke and Kohler (1981) was modified to exclude Na-saturation. The interlayer cations of the clay material were exchanged with the appropriate n-alkylammonium-ion solution.

5.7 Embedding Procedures For HRTEM

Freeze-dried clay material was embedded in a low viscosity (60 centipoises) thermally-curing epoxy resin (Spurr 1969) following a modified procedure of Lee et al. (1975) and Vali and Köster (1986). Low viscosity is required for attaining complete impregnation, preventing the formation of gas vesicles and achieving parallel orientation of the layer silicates during sedimentation in the uncured resin (Marcks et al. 1989). In addition, strong bonding at the clay mineral/resin interface prevents their removal from the cured blocks during ultrathin-sectioning. Prisma Universal Bond (manufactured by Dentsply International, Milford, Delaware; available in Canada through Henry Schein Inc , 151 Carlingview Drive, Suite 5 Rexdale, Ontario M9W 5S4), a dentin/enamel bonding agent for dental applications, was used as an embedding medium. It is cured with high-intensity blue ultra-violet light.

The components for Spurr VCD resin are extremely toxic (mutanogenic and carcinogenic) and were carefully mixed under a fume hood using rubber gloves in the following mass quantities;

1 - Flexibilizer: Diglycidyl ether of polypropylene glycol
(DER 736: 6 units)

2 - Epoxy Resin: Vinylcyclohexene dioxide
(ERL 4206: 10 units)

3 - Hardener: Nonenyl succinic anhydride
(NSA: 26 units)

4 - Cure accelerator: Dimethylaminoethanol
(DMAE S-1: 0.4 units)

(The components for the Spurr VCD resin are manufactured by Polyscience, Inc. Warrington, Pennslyvania 18976-2590 and are available in Canada as a complete low viscosity resin kit from J.B. EM Services Inc., Mail: P.O. Box 693, Pointe-Claire-Dorval, Quebec, H9R 4S8 - Office: 4280 rue Serre, St. Laurent, Quebec H4T 1A6: Order No. JBS #052). The hardness of the embedding block is controlled by the amount of diglycedyl ether of propylene glycol. Lee et al. (1975) suggested 5 units mixed with the other reagents in the above proportions were optimal.

Two methods of impregnation and infiltration of the freeze-dried clay material with Spurr resin were tested. The first involved a five-day procedure involving slow infiltration and impregnation with intermediate solutions of Spurr resin (Vali and Koster 1986). The second was to immerse the clay material immediately in pure Spurr resin. The five day embedding method is a procedure allowing slow, complete dehydration, impregnation and infiltration of the clay material by the resin. Ten grams of clay separates were placed in 1.5 mL Eppendorf microtest tubes with snap caps and dehydrated by adding 1 mL propylene oxide (stored under refrigeration) equilibrated at room temperature under a fume hood. The caps were closed and test tubes were agitated by placing them in a mechanical rolling machine. Care must be taken to dehydrate the samples and to avoid excessive exposure to moisture as the embedding medium may not polymerize completely. Propylene oxide is also used as an intermediate solvent that allows rapid infiltration of the clay material by the Spurr resin. After two hours, the microtest tubes were centrifuged and the propylene oxide was decanted and fresh propylene oxide added and left for 24 hrs. On the second day, following the decanting of propylene oxide, 1 mL of a 20/80 mixture of epoxy resin and propylene oxide, respectively, was added to the microtest tubes, the caps closed and the microtest tubes shaken until all the clay material was dispersed. The samples were attached to a single-speed rotary shaker overnight. Day three, the microtest tubes were centrifuged and the 20/80 resin/propylene oxide mixture was removed and replaced by a 50/50 mixture. The same procedure was followed as outlined above. This was followed on days four and five by an 80/20 mixture and then the final infiltration of 100% epoxy resin, respectively. Prior to the addition of 100% resin and after centrifuging and decanting, the microtest tubes were put in the freeze-drier overnight to evaporate any remaining propylene oxide. The epoxy resin/clay mixtures were transferred to the silicone rubber flat embedding molds with an Eppendorf pipette or disposable polyethylene pipettes and polymerized in an oven at 70°C for 24 hrs. This slow curing allows the clays to orient themselves with their a-b plane parallel to the bottom of the cast. Generally, curing is complete within 8 hrs, but curing time can be reduced either by increasing the temperature or through additional accelerator (Spurr 1969).

The second method for embedding clay material using Spurr resin was to impregnate the samples in 100% resin immediately after treating with propylene oxide, without the intermediate steps of resin/propylene oxide infiltration. After immersing the clay material in the resin, the microtest tubes were agitated for 24 hrs on the mechanical roller to ensure complete dispersion and then transferred to the embedding molds and cured in oven for 8 hrs at 65°C. This method is preferable as it preserves the original texture produced for XRD specimens and is much less time-consuming.

The Prisma Universal Bond 3 is non-toxic and was used directly as received from the manufacturer. To test the efficacy of using the Prisma Bond as an embedding medium, 10 g of freeze-dried clay separates were placed in the microtest tubes and 1 mL of the Prisma Bond was added. The contents were attached to a single-speed rotary shaker for 24 hrs, then transferred to the embedding molds by pipette and covered with a transparent plastic cover slip. The mixture was cured by exposing the samples to high intensity blue ultraviolet light for 1 hr until the blocks hardened. As these blocks polymerize rapidly, the clays remain in a highly dispersed state and do not settle to the base of the blocks. Although the blocks after hardening remained sticky to the touch, this is not a serious problem and the bonding agent is an adequate alternative to embedding resins. The Prisma Universal Bond 3 is stable under the electron beam. A disadvantage is that not all the clay minerals may have proper orientation due to rapid curing.

5.8 Ultrathin-Section Preparation

From the embedded blocks of both untreated samples and samples treated with n-alkylammonium-ions, ultrathin sections were cut with an LKB Ultrotome III ultramicrotome equipped with either a Diatome diamond knife or a glass knife. The procedure is to trim the resin blocks with a razor blade normal to the a-b plane of the clay minerals in the approximate shape of a truncated pyramid with a side length of no more than 0.6 mm. The top face of the truncated pyramid was initially trimmed using a glass knife until very smooth and regular and then ultrathin sections were cut with the diamond knife. Ultrathin sections 70 to 100 nm thick are cut from this face, with the basal plane surface oriented perpendicular to the knife edge and to the cutting direction. Other orientations may result in distortion of the silicate layers. Selected sections were transferred onto the center of 300 mesh copper TEM grids by carefully touching the grids to the surface of the water on which the sections were floating. Samples requiring post-thin sectioning treatment with n-alkylammonium ions were transferred onto 300 mesh carbon or formvar substrate copper grids. The excess water was carefully removed with blotter paper.

5.9 Ultrathin-Section Treatment With n-Alkylammonium Ions

For clay separates not previously treated with n-alkylammonium ions, stable expansion of expandable layers was achieved by n-alkylammonium treatment of the ultrathin sections (Vali and Hesse 1990). For this purpose, the ultrathin sections on the center of copper electron microscope grids with formvar or carbon substrate were transferred to 1.5 mL Eppendorf microtest tubes containing 0.5 mL of an aqueous n-alkylammonium ion solution ($n_C=8$ and $n_C=18$) with 30-40% of the concentration suggested by Lagaly et al. (1976) The lids were closed and then placed in an oven at 60°C for 15 min. The microtest tubes were carefully shaken (to avoid loss of ultrathin sections) every five minutes to ensure complete exchange with n-alkylammonium ions. After removal from the microtest tubes, the grids were washed in deionized water. Washing was performed by turning the microtest tubes upside down until the grid settled to the cap. Then the microtest tube was carefully righted so the grid remained inside the cap. The cap was opened, preheated water (65°C) was dropped into the cap using a disposable pipette and the water carefully removed This procedure was performed a minimum of 6 times. The grid was held by needle-point tweezers and the excess mixture of n-alkylammonium solution and water remaining on the grids was removed by touching filter paper to the upper edge of the grid. It is important not to remove this excess water from underneath as the water may be suctioned through the ultrathin section, removing the embedded clay material.

This method requires extreme care. If the concentration of the alkylammonium ions/deionized-water solution is too high, precipitation on the ultrathin-sections results and prevents imaging of the layer silicates.

5.10 XRD: Data Acquisition, Reduction and Treatment

To facilitate comparisons between samples, diffraction conditions and clay specimen dimensions were kept constant to provide reproducible results. Sample length parallel to the

X-ray beam was about 25 mm. A specimen length of 25 mm ensures that the reflection position will not deviate more than 0.02° 2Θ over the length scanned. XRD analysis was performed on a Siemens D-5000 diffractometer (Cu K_α radiation with a Ni-filter) at 40 kV and 20 mA, equipped with a graphite-diffracted beam monochromator. The diffraction geometry consisted of two diffracted-beam Soller slits of 1° width each, and 1° beam- and 0.05° (or 0.15° for glycerol solvation) detector-slits. Samples were step-scanned by computer control from 2 to 40° 2Θ using a step-size of 0.01° 2Θ and a counting time of 1 sec per step. Data acquisition was controlled by the DIFFRAC/AT software program which incorporates a DACO-MP programming card (Socabim, 9 bis villa du Bel-Air, 71250 Paris, France). The experimental diffraction data were treated using the EVA2 graphics evaluation program which displays the unprocessed X-ray diffraction patterns and facilitates data treatment, i.e. graphic representation, smoothing, integration, fit, superimposition of scans, 2Θ peak determinations, background subtraction, etc. The diffractograms are reduced hardcopies displayed by EVA2 and printed using a Hewlett-Packard PaintJet. Layer proportions and ordering of mixed-layer I/S for the different depths were determined from Mg^{2+}-saturated, ethylene-glycol solvated samples. The percentage of expandable layers in mixed-layer I/S was resolved by the Δ2Θ method of Moore and Reynolds (1989), and ordering type (Reichweite) as defined by Reynolds and Hower (1970) and Reynolds (1980) and was confirmed using NEWMOD. Layer proportions were determined from the difference (Δ) in XRD peak positions for the $(001)_{10}/(002)_{17}$ and $(002)_{10}/(003)_{17}$ peaks. Additional information was acquired by comparing the experimental patterns with calculated patterns generated by NEWMOD (version 2; Reynolds 1985). The calculated patterns of NEWMOD were converted to DIFFRAC/AT files using the CVDAT utility program which enabled both the experimental and calculated profiles to be displayed by EVA2, facilitating direct comparisons (J. Ko pers. comm. 1993).

5.11 High-Resolution Transmission Electron Microscope (HRTEM) Data Acquisition

All ultramicrotomed samples were examined in bright field illumination at high-resolution with a JEOL JEM-100 CX II TEM at 100 kV and with a point-to-point resolution of 0.3 nm and a 40 μm objective aperture. The phase contrast of the lattice-fringe image taken in the Scherzer defocus depends on the structure of the specimen and instrumental conditions (Vali et al. 1991). The TEM is equipped with a side-entry sample stage which can be tilted to

30 or 60°. The magnification was between 20,000 to 100,000 to minimize beam damage to the samples. In addition, the negatives were enlarged 2 or 6 times, depending on the image.

CHAPTER 6.0 - RESULTS

X-ray powder diffraction (XRD) and transmission electron microscopy (TEM) were performed on 0.05-1.0 μm and <0.05 μm clay separates fractionated from shales with and without the addition of sodium hexametaphosphate as a peptizer, and either solvated with ethylene glycol or glycerol, or exchanged with an n-alkylammonium-ion solution. Comparison between XRD and TEM results is possible because analyses were performed on dispersed and size-fractionated materials, which is the conventional sample preparation procedure for XRD. Clay separates in ultrathin-sections and imaged in the HRTEM, however, do not display the original "in situ" texture or fabric.

6.1 Clay Mineral Separation

Ideally, any attempt to assess the smectite-to-illite (S-I) conversion as well as the layer structures or sequences of mixed-layer I/S requires an *a priori* knowledge of the composition of the precursor clay minerals deposited in a sedimentary basin. Detrital I/S may have undergone illitization during an earlier burial cycle. Pollastro (1990) noted that expandability and order type of I/S in a given sample may be heterogenous due to possible multiple origins of the clay material, such as multiple source areas, detrital versus neoformed origins, recycling, and weathering. XRD studies give average results for all grains of a given species, even though there may be multiple origins for different populations of the same material. In addition, well cuttings may introduce uncertainty in expandability measurements as contamination results from caved material at shallower depths in the well or from a smectite-group component in drilling mud.

The initial purpose for clay separation was to isolate the 0.05-0.1 μm and a <0.05μm clay fractions for isotopic analyses, i.e. Rb-Sr and K-Ar analyses (in preparation). The reason for collecting these particular size fractions was to concentrate the I/S component while reducing the amounts of other detrital and contaminant phases to minimum values. Implicit in this procedure is the assumption that separation of the ultrafine fractions isolates a neoformed clay (illite) from coarser-grained detrital illitic phases (Morton 1985; Ohr et al. 1991). To establish a burial-diagenetic trend in the S-I conversion, it is essential to eliminate the detrital material, otherwise any inherent diagenetic trends such as mineral alteration or neoformation may be overwhelmed by the detrital signal. This is an inherent problem with all size fractions > 0.1 μm.

The separation of a diagenetic component for isotopic analyses thus imposed a set of criteria or conditions on the clay fractionation procedures. The complete isolation of diagenetic and detrital components in shale clay separates is much more difficult than in sandstones, where diagenetic components are usually much finer-grained than the detrital material (e.g. Liewig et al. 1987). As a result of the size similarities between diagenetic and detrital clays, sample contamination remains a significant and consequential problem for determining burial diagenetic trends. An aim of the clay mineral fractionation process was to assess the efficacy of collecting a <0.05 μm fraction without aggressive chemical pretreatments, ultrasound or extensive mechanical agitation (Dr. Norbert Clauer, pers. comm. 1991; Dr. James Aronson, written comm. 1992). As outlined in Chapter 4, the effects of chemical and ultrasonic treatment on the chemistry and structure of clay minerals is not well understood, and published results are often contradictory.

Initial attempts at disaggregation and clay separation without chemical pretreatment began with 6 well cutting samples, each weighing approximately 20 gm. Samples were rolled in polypropylene bottles overnight, until the cuttings were reduced to their constituent particles. Dispersion was attempted by removing excess electrolytes through centrifugation, decanting of the supernatant and replacing with fresh deionized water. However, all 6 samples flocculated within a few hours. The pH of the deionized water was measured and found to be acidic Extensive dialysis was performed and dispersion was improved The < 2 μm fraction was sedimented by dispersing in large quantities of water. As a direct result of the difficulty in maintaining dispersion, additional samples were treated with a 1N Na-EDTA solution followed by dialysis. However, dispersion was not significantly improved.

An attempt was made to use the continuous-flow Sharples T-1 Supercentrifuge to collect and concentrate the <0.05-μm clay fraction and to remove contaminating phases, because it was thought that a conventional table-top centrifuge was insufficient to generate the acceleration required to sediment the <0.05-μm fraction from suspension. The supercentrifuge was chosen as the best and quickest means to achieve the separation of the ultrafine clay particles because of its high-speed operation (i.e. 50,000 rpm in contrast to a maximum of 8,000 to 10,000 rpm for the Sorvall SS-3 table-top centrifuge). Proper size fractionation is attained through the variation of flow rate and input nozzle diameter. However, the use of the supercentrifuge proved unsuccessful due to (i) a lack of adequate particle dispersion, and (ii) contamination resulting from coarser particles (e.g. quartz, feldspar) that was apparent from subsequent XRD analysis. The problem results from the initial small sample mass of less than 25 g. Other difficulties with the supercentrifuge included excessive amounts of water required for small sample sizes, with significant loss and/or contamination of clay material during transfer from the cellulose acetate clarifier bowl liner to the storage container. Chemical treatments are recommended with the supercentrifuge to achieve best results (Jackson 1969; Whittig and Allardice 1986). However, chemical pretreatment would have been counter-productive concerning the above stated objectives for viable clay analysis.

Following an earlier suggestion of Dr. John Morton (written comm. 1990), it was decided to attempt ultrafine clay separation using an IEC Centri-7 table-top centrifuge, but without the addition of chemical pretreatments. The IEC centrifuge had a maximum speed of approximately 2500 rpm. Clay separation was improved, resulting in minor quantities (10-40 mg) of clay separates dispersed in large quantities (2-4 L) of water.

An assessment of the clay separation procedure for shales from the Reindeer D-27 well and the associated results suggested that the separation of ultrafine material was possible without chemical pretreatments. However, the results implied that larger quantities of initial shale material were required to obtain satisfactory amounts of clay separates, i.e. 80-125 mg.

In addition, a Labconco freeze-dryer, a Sorvall SS-3 table-top centrifuge with an angle rotor and a top speed of 6500 to 8500 rpm and a Barnstead water deionizing system were acquired and installed. Following the procedure outlined in Chapter 5, sufficient quantities of 0.05-0.1 μm (100-200 mg) and <0.05-μm (125-300 mg) of clay separates were obtained principally for Rb-Sr and K-Ar analyses, and any remaining material was used in XRD and HRTEM in order to characterize the nature of the material.

6.1.1 Physical Nature of Clay Separates

Treatments to remove hydrocarbons from the clay-sized separates were not employed (e.g. Lindgreen and Hansen 1991). During the <0.05 μm clay mineral separation (but not during the 1.0-0.05 μm fractionation), organic material was released from the shale samples, which slowly coalesced and floated to the surface of the water. Thus the physical appearances of the clay separates included a change in colour of the finest fractions compared to the coarser ones. The 0.05-0.1 µm fractions were generally dark brown bec[illegible]e general retention of organic material, whereas the <0.05 µm fraction was tan to beige. The samples fractionated with the addition of a sodium hexametaphosphate solution were consistently lighter in colour than their untreated counterparts, usually being light beige to white. After freeze-drying, the untreated samples were fluffy whereas the treated samples were generally more powdery and compacted (see Section 6.4 for TEM description).

6.2 Terminology

The descriptive terms and clay mineral nomenclature used for the XRD results of this thesis generally follow Brown (1984), AIPEA recommendations (Bailey 1980, 1982; Bailey et al. 1982) and the classic mixed-layer terminology established by Reynolds and Hower (1970) and Reynolds (1980). However, the term "smectite" is avoided in preference to "smectite-group phase" (Vali et al. 1993b). Without accurate chemical composition of the expanded phase, accurate species identification is not possible. Both illite and smectite-group minerals are considered to have extensive variation in ionic substitutions and interlayer charges (Lagaly 1979; Nadeau and Bain 1986; Meunier and Velde 1989; Rosenberg et al. 1990; Aja et al. 1991a, 1991b; Vali and Hesse 1990; Vali et al. 1991).

6.3 XRD Analyses

Samples from 20 depth levels in the Reindeer D-27 well were analyzed by XRD for clay mineral composition, using the 0.05-0.1 µm and <0.05 µm size fractions that were subjected to various post-separation treatments, i.e. air-drying, ethylene glycol solvation, Mg^{2+}-saturation, glycerol solvation, and alkylammonium-ion exchange. As a result of the competing requirements for the various analytical methods and the limited amounts of clay material available, only between 12-15 mg of material could be assigned for XRD specimen mount. Oriented clay specimens prepared for diffraction were infinitely thick with respect to CuK$_\alpha$ radiation for the scanning range of 2°-40°2Θ, but were much shorter (25 mm) than the lateral spread of the incident beam on the specimen for diffraction angles of less than about 12°2Θ. At low diffraction angles, the spread of the incident beam is greater than the extent of the sample and resulted in loss of reflection intensity. Since all the samples were subject to the same conditions, no corrections were performed.

Figures 6.1a,b and 6.2a,b represent sets of one-dimensional XRD profiles for selected downhole depths from the Reindeer D-27 well. Figures 6.1a,b illustrate profiles of <0.05 µm and 0.05-1.0 µm size fractions separated without chemical pretreatment, whereas Figures 6.2a,b represent the same fractions separated with the addition of sodium hexametaphosphate as a peptizer. The four sets of patterns have been solvated with ethylene glycol to distinguish between expandable (smectite-group phase) and non-expandable (illite) components in mixed-layer I/S, and exhibit similar depth-dependent trends (see section 6.3.2).

The untreated 0.05-0.1 µm and <0.05 µm diffraction profiles indicate that mixed-layer I/S is the dominant mineral present in these size fractions, with illite increasing with depth. However, strong reflection intensities of approximately 0.98 nm and 0.49 nm in the 4800 ft and 7650-7700 ft depth samples of the 0.05-0.1 µm fraction are indicative of a component of discrete illite. Also present in this fraction are reflections of approximately 0.72 nm and 0.355 nm indicative of kaolinite or chlorite, depending on sample depth. Kaolinite was determined in samples above 10800 ft, whereas chlorite is indicated below 10800-10850 ft (Ko 1992). The minor, broad reflections of kaolinite or chlorite were not displaced with ethylene glycol solvation, and are fairly broad, which indicates they were not significantly interstratified with illite or smectite (Lindgreen and Hansen 1991). Chlorite was also imaged in HRTEM.

6.3.1 Particle-Size Effects

To eliminate or minimize the presence of the detrital and contaminant phases such as discrete illite, chlorite and kaolinite in the clay separates, a <0.05 µm fraction was separated from both the untreated and treated <0.1 µm fractions (Figs. 6.1a and 6.2a). Diffraction patterns for this <0.05 µm fraction (Fig. 6.1a) show that, even in this size fraction, it is not possible to completely eliminate these discrete mineral phases using only deionized water and a centrifuge. However, the amount of discrete illite has been significantly reduced, but as is evident in lattice fringe images this phase is never completely removed.

As a consequence of size fractionation, there are other distinct changes in the XRD patterns between the two untreated size fractions, which may only be partially explained by the particle size effect (Fig. 6.1a,b). Comparison between untreated 0.05-1.0 µm and <0.05 µm fractions reveals minor differences which include diminished peak intensity, increased peak

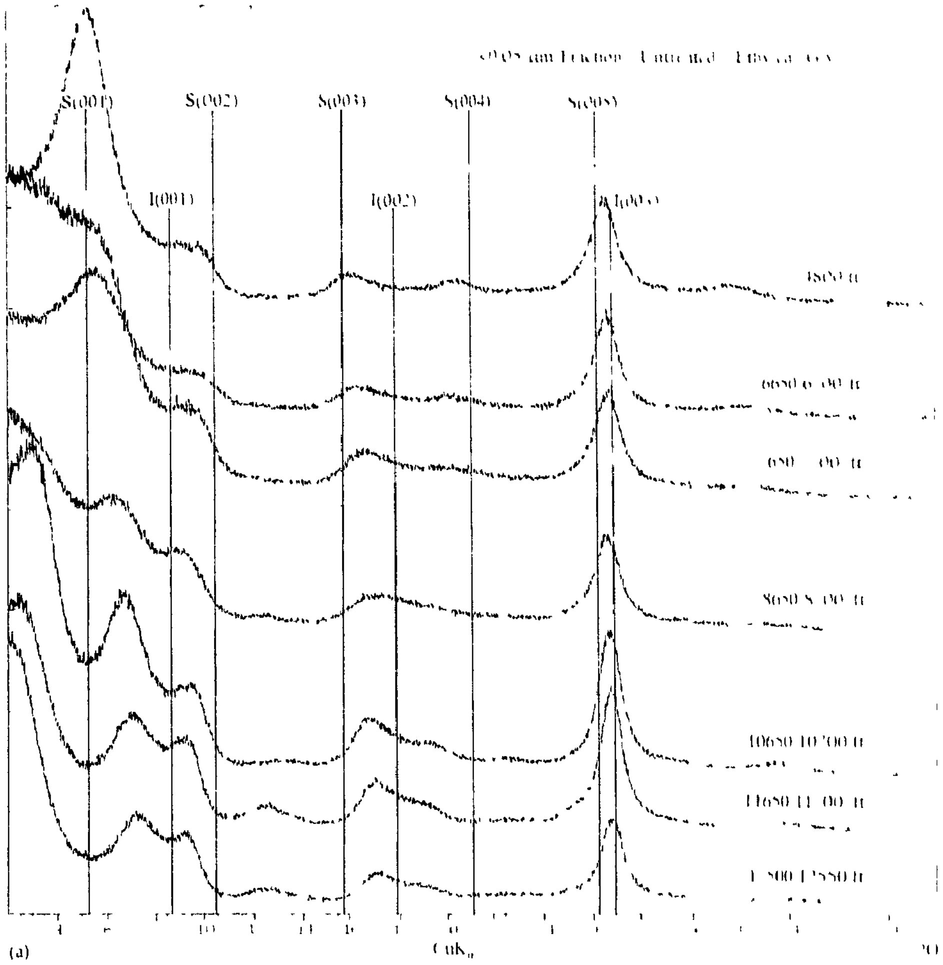
(a)
<0.05 µm Fraction Untreated Ethylene Glycol
S(001)
S(002)
S(003)
S(004)
S(005)
I(001)
I(002)
I(003)
4850 ft
6650-6700 ft
7650-7700 ft
8650-8700 ft
10650-10700 ft
11650-11700 ft
12500-12550 ft
CuKα
°2θ

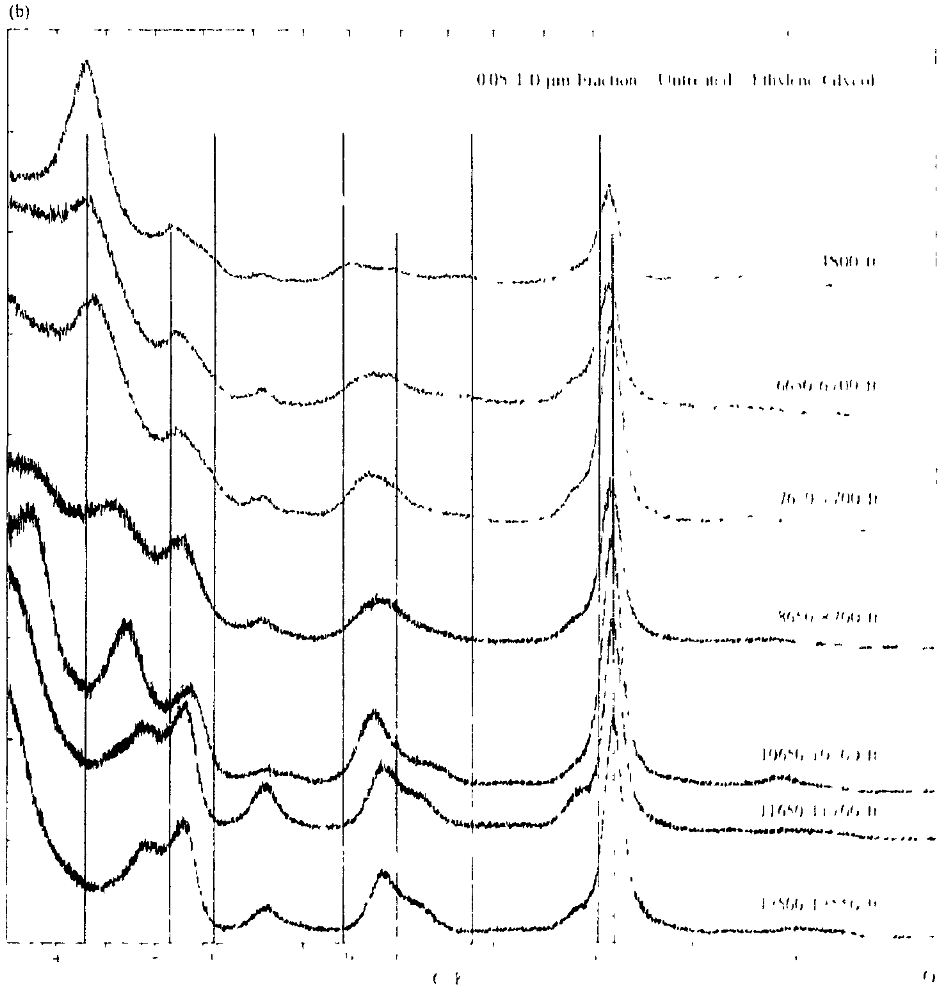
(b)
0.05-1.0 µm Fraction Untreated Ethylene Glycol
4800 ft
6650-6700 ft
7650-7700 ft
8650-8700 ft
10650-10700 ft
11650-11700 ft
12500-12550 ft
CuKα
°2θ

Fig 6.1 XRD patterns of untreated ethylene glycol-solvated samples: (a) <0.05, and (b) <0.05-0.1 μm size fractions. Lines designate the locations of the 00*l* reflections for pure smectite (long) and illite (short).

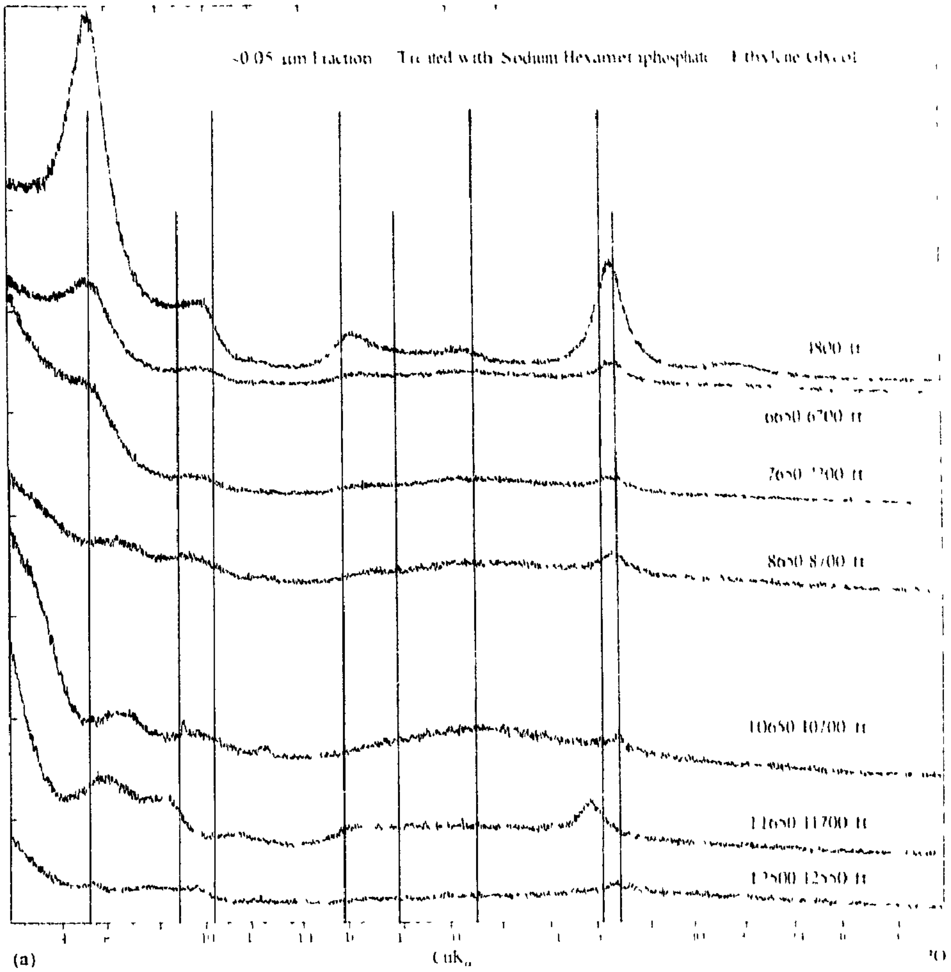
<0.05 µm Fraction Treated with Sodium Hexametaphosphate Ethylene Glycol
4800 ft
6650-6700 ft
7650-7700 ft
8650-8700 ft
10650-10700 ft
11650-11700 ft
12500-12550 ft
CuKα
30

(a)

(b)

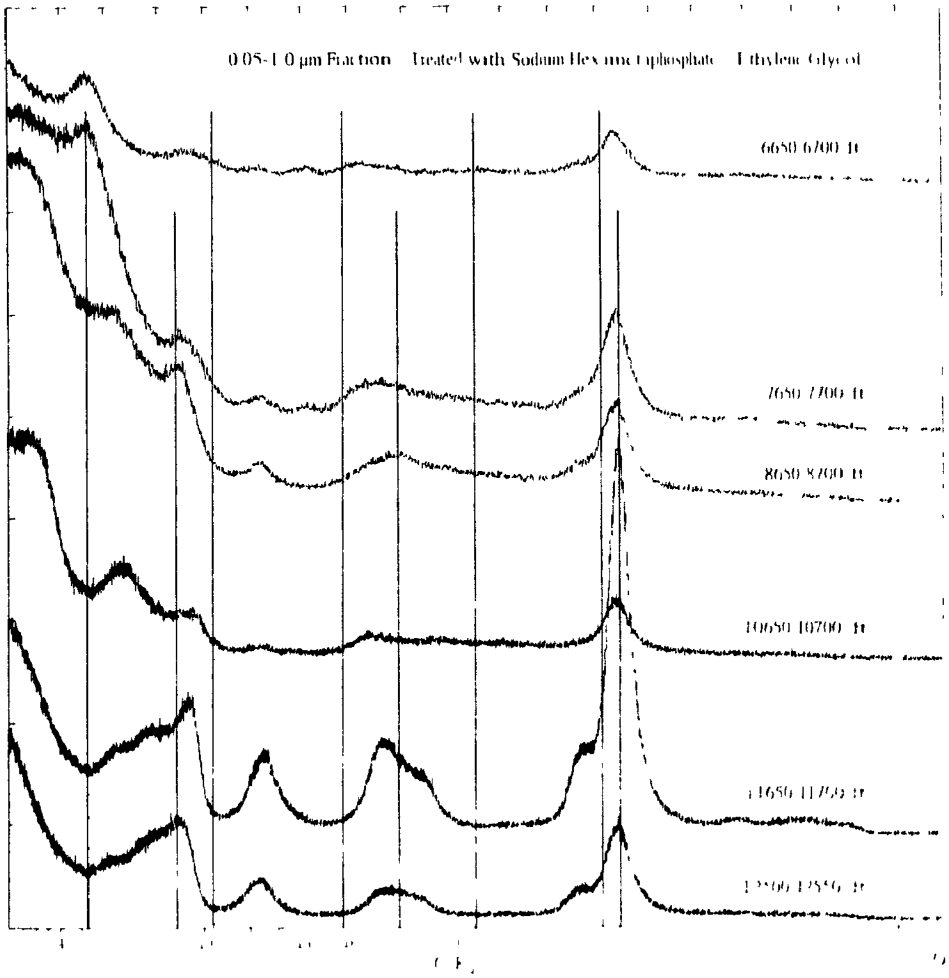
0.05-1.0 µm Fraction Treated with Sodium Hexametaphosphate Ethylene Glycol
6650-6700 ft
7650-7700 ft
8650-8700 ft
10650-10700 ft
11650-11700 ft
12500-12550 ft
CuKα

Fig. 6.2 XRD patterns of sodium hexametaphosphate-treated, ethylene glycol-solvated samples: (a) <0.05, and (b) <0.05-0.1 µm size fractions. Lines designate the locations of the 00*l* reflections for pure smectite (long) and illite (short).

breadths, and slight displacements of 2Θ angle peak positions in the finer fractions. However, background intensity remains approximately the same. The 4800 and 7650-7700 ft depth samples for example, exhibit diminished intensity of the $(001)_{1.0}/(002)_{1.7}$ peak indicating a significant reduction in the contribution from a discrete illite component (compare Figs. 6.1a and b). This reflection appears as a broad plateau that extends towards higher 2Θ angles when compared with profiles of the 0.05-1.0 µm fractions. In the deeper samples, the $(001)_{1.0}/(001)_{1.7}$ peak is generally stronger in this finer fraction. The $(002)_{1.0}/(003)_{1.7}$ and $(003)_{1.0}/(005)_{1.7}$ peaks have relatively the same position, but intensity in the finer fraction was diminished with increased broadening. An exception is the 12500-12550 ft depth sample, for which the 0.05-1.0 µm fraction exhibits diminished intensity, whereas the <0.05 µm fraction displays a totally degraded pattern (Fig. 6.1a,b).

In general, the effect of decreasing particle size in the untreated diffraction patterns is manifested by slight peak displacements, mainly the $(001)_{1.0}/(002)_{1.7}$ peak as a result of a decreased discrete illite component, with significant diminished intensity and increased peak broadness.

6.3.2 Effects of Sodium Hexametaphosphate Treatment

Although samples were prepared following identical procedures with the exception of the addition of sodium hexametaphosphate as a peptizer, comparison between the untreated and treated 0.05-1.0 µm size-fraction profiles are relatively congruent, such that nearly identical values for percent expandability (± 10%) and ordering could be obtained (cf. Figs. 6.1b and 6.2b). A treated 0.05-1.0 µm fraction for 4800 ft was unavailable. Replicate sample mounts gave identical results. Visible but inconsistent differences occur with reflections in the lower 2Θ angle regions which display slight displacements in 2Θ reflection position, peak broadening and diminished intensity. The most significant difference was the loss of the $(002)_{1.0}/(003)_{1.7}$ reflection, resulting in a broad peak of 0.50 nm.

Differences are more readily apparent when comparing the patterns for untreated (Fig. 6.1a) and treated (Fig. 6.2a) <0.05 µm fractions. With the exception of the 4800 ft depth sample, the intermediate and deep treated samples all show extensive displacements of the 2Θ reflections, and marked increase in peak breadths and diminished peak intensity. It is not possible to accurately assess the positions of the $(001)_{1.0}/(002)_{1.7}$ or the $(002)_{1.0}/(003)_{1.7}$ peaks in order to apply the $\triangle 2\Theta$ method to evaluate the amount of expandable component. However, with the possible exception of the 12500-12550 ft depth sample, it is still possible to determine the Reichweite values. The diffraction profile for the treated 12500-12550 ft sample is totally degraded.

Measured peak breadths for the $(002)_{10}/(003)_{17}$ reflection could not be made on the treated samples and crystallite thickness values cannot be determined. Some XRD patterns of the treated samples for the <0.05 µm fraction give the impression that layer silicate minerals are not present, e.g. Fig. 6.2a, 12500-12600 ft. However, this is a preparation artifact (bad orientation?) as abundant 2:1 layer silicates are observed in the HRTEM. It appears that the addition of sodium hexametaphosphate, especially to ultrafine fractions, produces artifacts on the 00*l* diffraction series of dispersed mixed-layer I/S, and that the minerals are not reconstituted into coherent X-ray scattering domains after air drying.

6.3.3 <0.05 µm Untreated, Mg^{2+}-Saturated and Ethylene-Glycol Solvated Fractions

The <0.05 µm size fractions were Mg^{2+}-saturated to achieve homoionic interlayer occupancy and subsequent uniform expansion of all expandable layers. They were then solvated with ethylene glycol to determine the percent expandable component and ordering. As a consequence of the apparent discrepancy between untreated and treated samples, the treated samples could not be used to determine the layer proportions.

The Mg^{2+}-saturated ethylene-glycol solvated profiles show that mixed-layer I/S is the dominant mineral with a systematic increase in the illite component with depth (Fig. 6.3). The non-expanded component increases from 24% at 4800 ft (core) to 43% at 6650-6700 ft (cuttings), and 53% at 7650-7700 ft, all with random (R0) interlayering. Samples from 8650-8700 ft and 9650-9700 ft have 65% and 71% non-expandable component, respectively, and show R1 ordering. The 10650-10700 ft sample displays an apparent decrease to 67% non-expandable material with R1-ordering. The 11650-11700 ft and 126550-12600 ft samples have slight increases in non-expandability to 78% and 82%, respectively, with R>1 ordering. Using a greater number of samples, Ko (1992) was able to recognize a significant discontinuity in the mineralogy between 9800 to 10800 ft, which is not as readily apparent from the 8 samples presented here. The overall trend, however, is one of a systematic decrease in expandability and a change from R0 to R1 to a depth of 9800 ft. Below this depth, a sudden increase in expandability occurs with R1 ordering, then the systematic decrease in expandability continues to about 20%, with R>1 ordering, in accordance with Ko (1992), which remains constant to 12500-12600 ft.

A determination of the expandable component was not made with air-dried specimens, as RH could not be strictly controlled. Eberl et al. (1987) demonstrated that air-dried Mg^{2+}-saturated samples gave different amounts of expandability as compared to their ethylene-glycol counterparts. However, results of Lindgreen and Hansen (1991) displayed better agreement between the two methods and suggested that RH was a dominant factor

6.3.4 Simulated Patterns

Layer proportions were determined using the Δ2Θ method, whereas the Reichweite or ordering value and the amount of detrital illite were obtained with the aid of the NEWMOD program. Figures 6.4 a,b,c represent three examples of the correlations between experimental and simulated patterns from different depths and Reichweite values Any sample could have been chosen, with the possible exception of the 8700-8750 ft sample which displayed slightly broader peaks. Simulated and experimental patterns exhibit apparent congruence, except for the intensity values, which are much stronger in the simulated profiles. Clearly the experimental and calculated ethylene-glycol solvated patterns indicate a two-component system From numerous studies which model X-ray diffraction patterns of mixed-layer I/S, Drits and Tchoubar (1990) assert that its not essential to obtain a perfect match between simulated and experimental values for the positions, profiles and relative intensities of the reflections because of the large number of parameters influencing the patterns. However, for a semi-quantitative estimate of the proportions of the expandable components, the results appear reliable. The simulated profiles suggest that the <0.05 μm clay fraction consisted almost entirely of I/S, with a minimal contribution from detrital mica. As well, the layer proportion values compare favourably to those estimated by Ko (1992) for the <0.1 μm size fraction using an alternative method for determining expandability.

6.3.5 <0.05 μm Untreated, Mg^{2+}-Saturated and Glycerol Solvated

Smectite-group layers in mixed-layer I/S were identified in untreated, Mg^{2+}-saturated

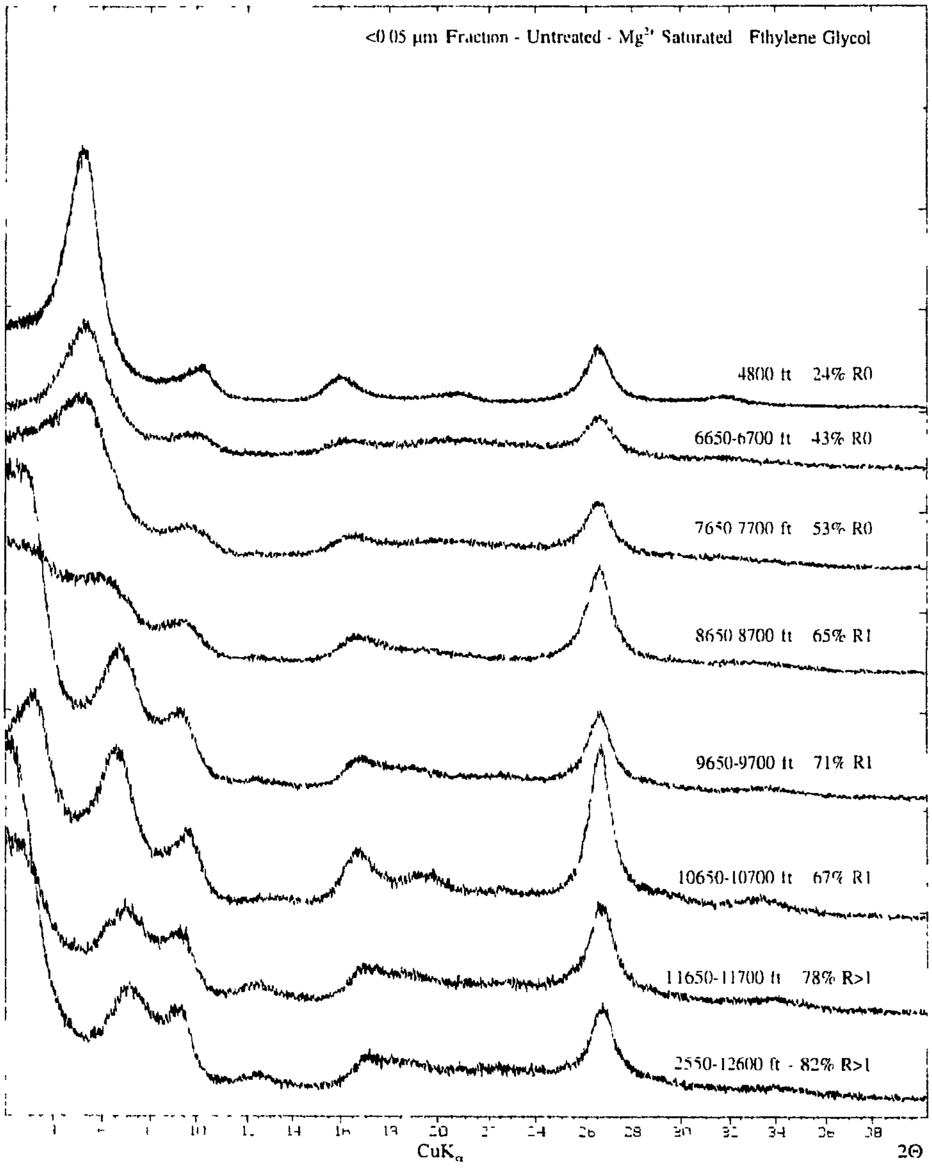
<0.05 µm Fraction - Untreated - Mg^{2+} Saturated Ethylene Glycol
4800 ft 24% R0
6650-6700 ft 43% R0
7650-7700 ft 53% R0
8650-8700 ft 65% R1
9650-9700 ft 71% R1
10650-10700 ft 67% R1
11650-11700 ft 78% R>1
2550-12600 ft - 82% R>1
4
6
8
10
12
14
16
18
20
22
24
26
28
30
32
34
36
38
CuK$_\alpha$
2Θ

Fig. 6.3 Experimental XRD patterns of Mg^{2+}-saturated ethylene-glycol solvated samples from the Reindeer D-27 well. Percentage values are for non-expandable component and ethylene-glycol solvated samples by $d_{(001)}$ spacings of 1.6-1.71 nm. It is apparent that some high-charge smectite group or vermiculite component may also expand to more than 1.6 nm on ethylene glycol solvation (MacEwan and Wilson 1980) resulting in misidentification of a smectite-group component. Ideally, after Mg^{2+}-saturation and glycerol solvation, a low-charged smectite will expand to about 1.8 nm, whereas a high-charged smectite-group mineral or vermiculite will expand to 1.4 nm (Brindley 1966). Thus, if only a low-charge-smectite group phase is present, the XRD profiles should compare favourably to the ethylene-glycol solvated profiles. If only a high-charge smectite-group phase or vermiculite is present, the XRD profiles will be similar to the air-dried diffraction patterns.

The diffraction patterns however show that the smectite-group mineral exhibits a two-layer complex with ethylene glycol solvation (Fig. 6.3), and may exhibit characterictics of a high-charge smectite-group or vermiculite-like component after glycerol solvation (Fig. 6.5). Overall, the diffraction patterns of glycerol solvated samples appear to have produced spacings characteristic of one- and two-layer complexes in the random I/S structures and predominantly as one-layer complexes in ordered I/S structures (cf. Bühmann 1992, figs. 3, 6, 7).

The XRD profiles of the glycerol solvated sample from 4800 ft clearly show a two-layer complex with glycerol having a *d*-spacing of 1.76-1.78 nm, indicating a low-charge smectite-group component (Fig. 6.5). The intermediate and deeper samples, however do not display such a regular response to glycerol. The 6650-6700 ft and 7650-7700 ft depth samples have a very broad reflection at about 5.2 2Θ and a series of broad overlapping reflections between 15° to 30° 2Θ. These broad reflections are characteristic of one- and two-layer complexes which may indicate an additional high-charge expandable component of 1.5-1.6 nm. However, Laird et al. (1991) showed XRD profiles for ultrafine fractions (<0 09 to <0.02 μm size fractions), which are inferred to be random mixed-layer I/S structures, but which failed to display reflections from an illite component (see their fig. 2), but the higher 2Θ angle reflections are very similar to the random patterns presented here.

The intermediate and deep Mg^{2+}-saturated, ethylene-glycol and glycerol solvated samples display similarities in the low angle peaks. The positions of the two reflections between 7° and 10° 2Θ are fairly coincident, suggesting a trend towards a one-layer glycerol complex and an increased abundance in the high-charged smectite-group or vermiculite component. The reflections at 7° 2Θ in the 11650-11700 ft and 12550-12600 ft are very broad and thus, the 0.98 nm component is more intense. It is important to note that the 0.98 nm illitic peak is more intense for all glycerol solvated samples than in ethylene-glycol solvated samples, although this may be the result of the weakening and broadening of the reflection at 7° 2Θ.

The reflections between 15° to 30° 2Θ for all R1 and R>1 mixed layers (as determined from ethylene-glycol solvated samples) are not congruent with a two-component I/S system for glycerol solvation. It was suggested by Lindgreen and Hansen (1991) that low-charge smectite-group layers could be simiIuated using *d*(001)=1.78 nm (*d*(001) of smectite-group layers in glycerol solvated samples) and ethylene glycol between the layers. It was concluded that the error in using ethylene glycol instead of glycerol in the simulation was assumed to be small, as the scattering ability of organic compounds is low compared to the scattering ability of the 2:1 silicate layer and the interlayer cations. This may be an incorrect assumption.

There were some similarities between the experimental and calculated profiles (not shown) for low 2Θ angle reflections but not for reflections between 15° to 30° 2Θ. This suggests that a high-charge expandable component is present in the mixed-layer I/S. The proportions of each component cannot be determined, however, without three-component modeling.

An additional complexity that must be commented on at this time is the presence of high-background from the possible adsorption of organic material on the clay material (Fig. 6.6) The organic material which was removed during the <0.05-μm clay separation procedure has a diffraction profile indicated by a broad reflection between 12° and 24° 2Θ. This broad reflection was not apparent in the diffraction patterns of the ethylene-glycol solvated samples but may influence the position of the reflections in the glycerol solvated samples. This broad reflection tends to overlap the reflections in the diffraction profiles of the glycerol solvated samples.

6.3.6 Alkylammonium-Ion (n_c=8 and n_c=18) Exchanged I/S

The alkylammonium-ion exchange technique has principally been used to determine the layer-charge density (and to deduce layer charge) of expandable clay minerals in soils and sediments. This has enabled the distinction between transitional 2:1 silicate layers such as low-charged smectite-group, high-charged smectite-group minerals and low-charged vermiculite (Senkayi et al. 1985; Malla and Douglas 1987b; Laird et al. 1988a; Ghabru et al. 1989; Stanjek et al. 1992). Recently, the method has been used to distinguish between high-charged vermiculite and expandable illite, and to determine the layer structure of rectorite minerals (Lagaly 1979; Laird et al. 1989a; Vali et al. 1991). As the method only measures the interlayer charge generated by adjacent layers, the proportions of differently charged interlayer spaces cannot be directly obtained by this technique (Lagaly 1979) Vali et al. (1991) also stressed that the true structure and composition of individual component 2:1 silicate layers of a mixed-layer I-S cannot be determined. However, the method can be used to qualitatively characterize the different expandable components in I/S as they change with burial depth.

The <0.05 μm size fraction from three sample depths, shallow (4800 ft, R0), intermediate (8700-8750 ft, R1) and deep (12500-12550 ft, R>1), fractionated without chemical treatment and treated with sodium hexametaphosphate solution were investigated. Each set of samples (untreated and treated) was exchanged with solutions of octylammonium (n_C=8) and octadecylammonium (n_C=18) ions, resulting in two sets of XRD patterns for each sample depth (Figs. 6 7a,b, 6.8a,b and 6.9 a,b). In addition, the air-dried and ethylene-glycol solvated patterns are shown to facilitate comparison with n_C=8 and n_C=18 profiles.

Ideally, octylammonium ions (n_C=8) have a monolayer arrangement in discrete low-charge smectite-group minerals (q < -0.46 per half unit cell) giving a basal spacing of 1.3-1.4 nm They have a bilayer arrangement in high-charge smectite-group minerals or vermiculite (q = -0.45 to -0 7 0 per half unit cell) with a basal spacing of 1.7-2.0 nm (Lagaly and Weiss 1969). Octylammonium ions will not expand very high-charged components (q > -0.8) such as illite or muscovite.

Ideally, octadecylammonium ions (n_C=18) would have a bilayer arrangement in a smectite-group mineral giving a basal spacing of 1.7-2.0 nm whereas high-charge smectite-group and low-charge vermiculite minerals would have a pseudotrimolecular or paraffin-type arrangement of octadecylammonium ions giving a basal spacing of 2.2-2.6 nm (Lagaly and Weiss 1969, Lagaly 1981, 1982; Senkayi et al. 1985). High-charge vermicilite and expandable illite would have a paraffin-type arrangement of the octadecylammonium ions for a layer charge of at least 0 75 per half unit cell giving a basal spacing of about 2.9-3.5 nm (MacIntosh et al. 1971; Lagaly 1982; Laird et al. 1987; Vali et al. 1991). High-charge vermiculite can be differentiated from expandable illite because it will expand with n_C=8, whereas expandable illite will not (Laird et al. 1989; Vali et al. 1991; Vali et al. 1992).

4800 ft depth sample

The untreated 4800 ft sample shows the predominance of a low-charge smectite-group component indicated by the presence of the 1.37 nm reflection after $n_c=8$ exchange (Fig. 6.7a). This broad peak may mask the presence of a discrete high-charge non-expanded component, i.e. analogous to the air-dried specimen. The reflection of 0.334-0.335 nm in the $n_c=8$ samples is almost coincident with the $(003)_{1.0}/(005)_{1.7}$ peak of the ethylene-glycol solvated samples and is present in the untreated samples of other depths (Figs 6.7a, 6.8a and 6.9a). This peak and the broad peak around 0.46-0.47 nm suggest a composite peak consisting of higher-order reflections of 1.8, 1.37, and 1.0 nm first-order reflections. The absence of a reflection at 1.8-2.1 nm indicates that either a discrete high-charge expandable component is not present or that it did not respond in a consistent manner to $n_c=8$.

The XRD pattern of the treated 4800 ft sample exchanged with $n_c=8$ is identical to the untreated sample with the addition of a nearly integral set of reflections of 2.4 nm and 0.84 nm (Fig. 6.7b). This suggests two possibilities; (i) an R1-ordered structure (double layers of two 2:1 silicate layers coordinated by a K interlayer with expandable interfaces) consisting of a 1.0 nm non-expandable component with a 1.4-1.5 nm low-charge expandable interface, or (ii) coherent domains of a high-charge smectite-group or vermiculite component with a pseudotrimolecular arrangement of the alkyl-chains in the interlayer space.

The diffraction pattern of the untreated 4800 ft sample exchanged with $n_c=18$ displays fairly broad peaks with the exception that some of the high-charge layers have expanded to 2.2-2.4 nm (Fig. 6.7a). A low-charge smectite-group component is indicated by an increase in the basal spacing to between 1.73-2.00 nm. A set of integral reflections of approximately 3.51/(1.75)/1.16 nm may be present, but due to overlapping reflections cannot be deciphered. The 1.0 nm peak characteristic of non-expanded illite is most likely contained within the broad plateau at 1.16 nm (Fig 6.7a). The reflection at 3.51 nm is unexpected at this depth and may correspond to one of two, or perhaps both, possibilities. (i) an R1-ordered structure consisting of a 1.0 nm non-expandable component and a 2.5 nm high-charged expandable component, giving rise to a 3.5 nm reflection. Lagaly (1979) demonstrated that an R1-ordered structure, i.e. rectorite, after exchange with $n_c=18$ had first-order reflections of between 3.3 to 3.4 nm (his fig. 3). (ii) The second possibility is the 3.51 nm reflection may be an R0-structure consisting of a non-expanded 1.0 nm component and an expanded 2.5 nm component with an intermediate interlayer charge density and a pseudoparaffin-type arrangement of octadecylammonium

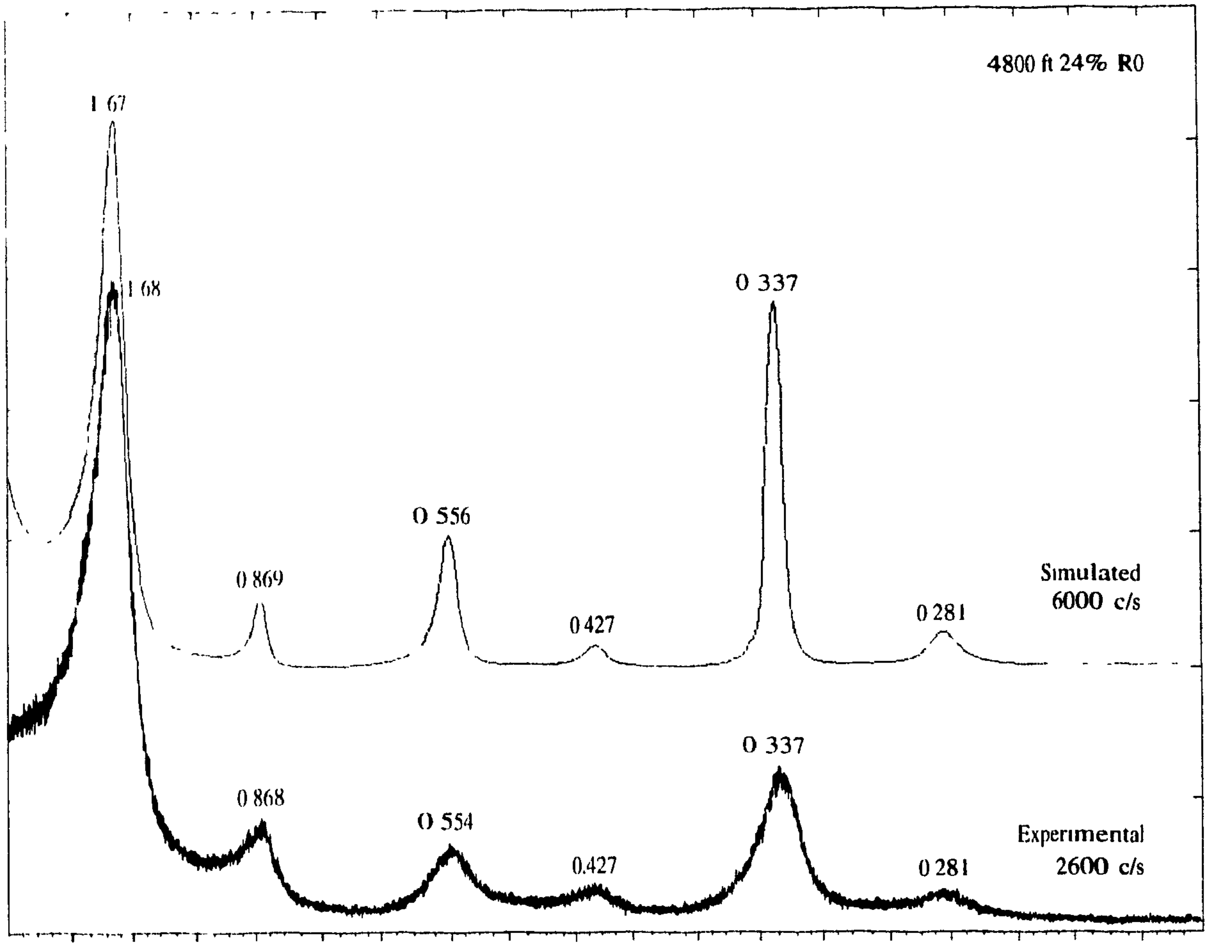
4800 ft 24% R0
1 67
1 68
0 337
0 556
0 869
0 427
0 281
Simulated
6000 c/s
0 337
0 868
0 554
0.427
0 281
Experimental
2600 c/s
4
6
8
10
12
14
16
18
20
22
24
26
28
30
32
34
36
38
CuKα
2Θ

(a)

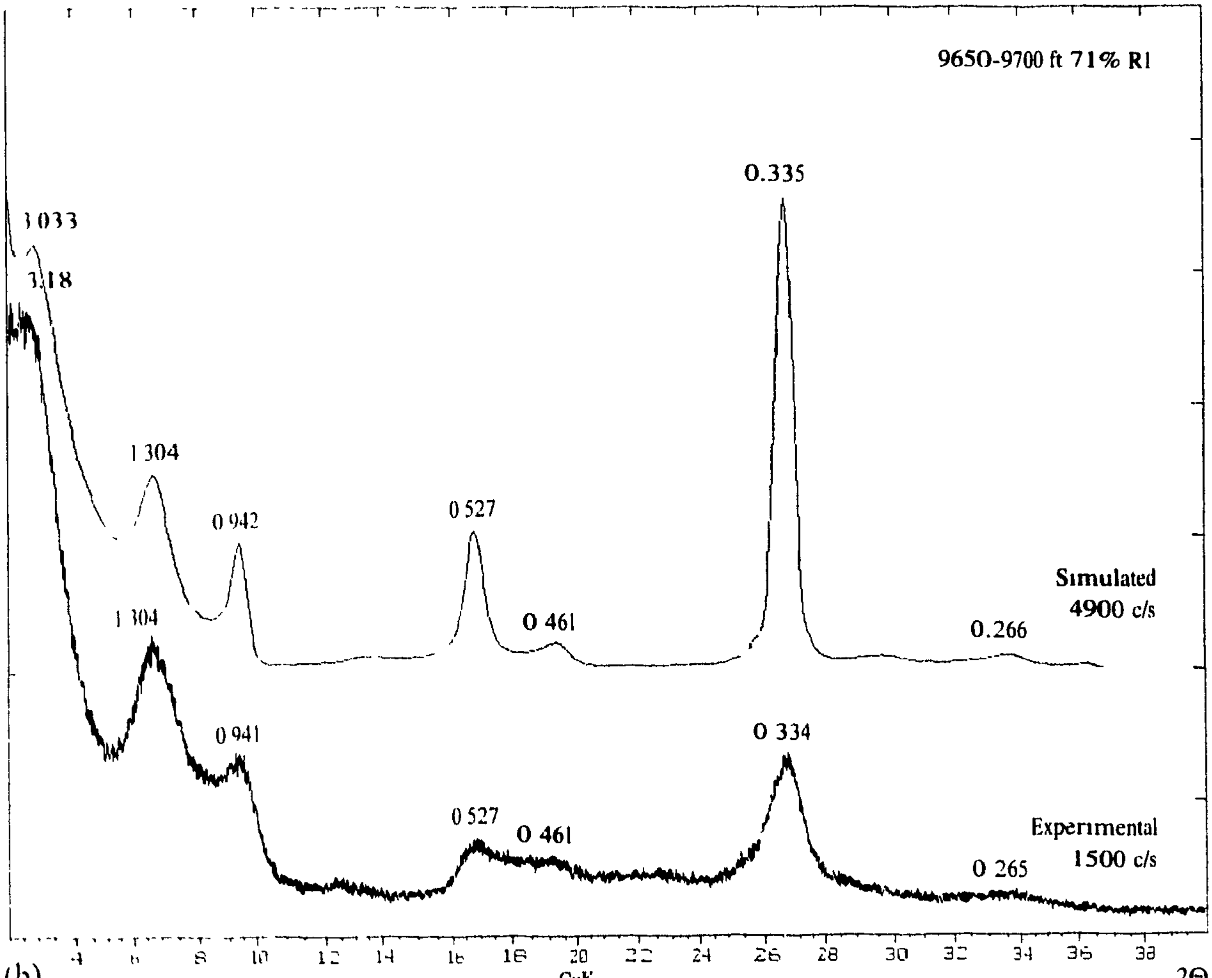
9650-9700 ft 71% R1
0.335
3 033
3.18
1 304
0 942
0 527
0 461
0.266
Simulated
4900 c/s
1 304
0 941
0 334
0 527
0 461
Experimental
1500 c/s
0 265
4
6
8
10
12
14
16
18
20
22
24
26
28
30
32
34
36
38
CuKα
2Θ

(b)

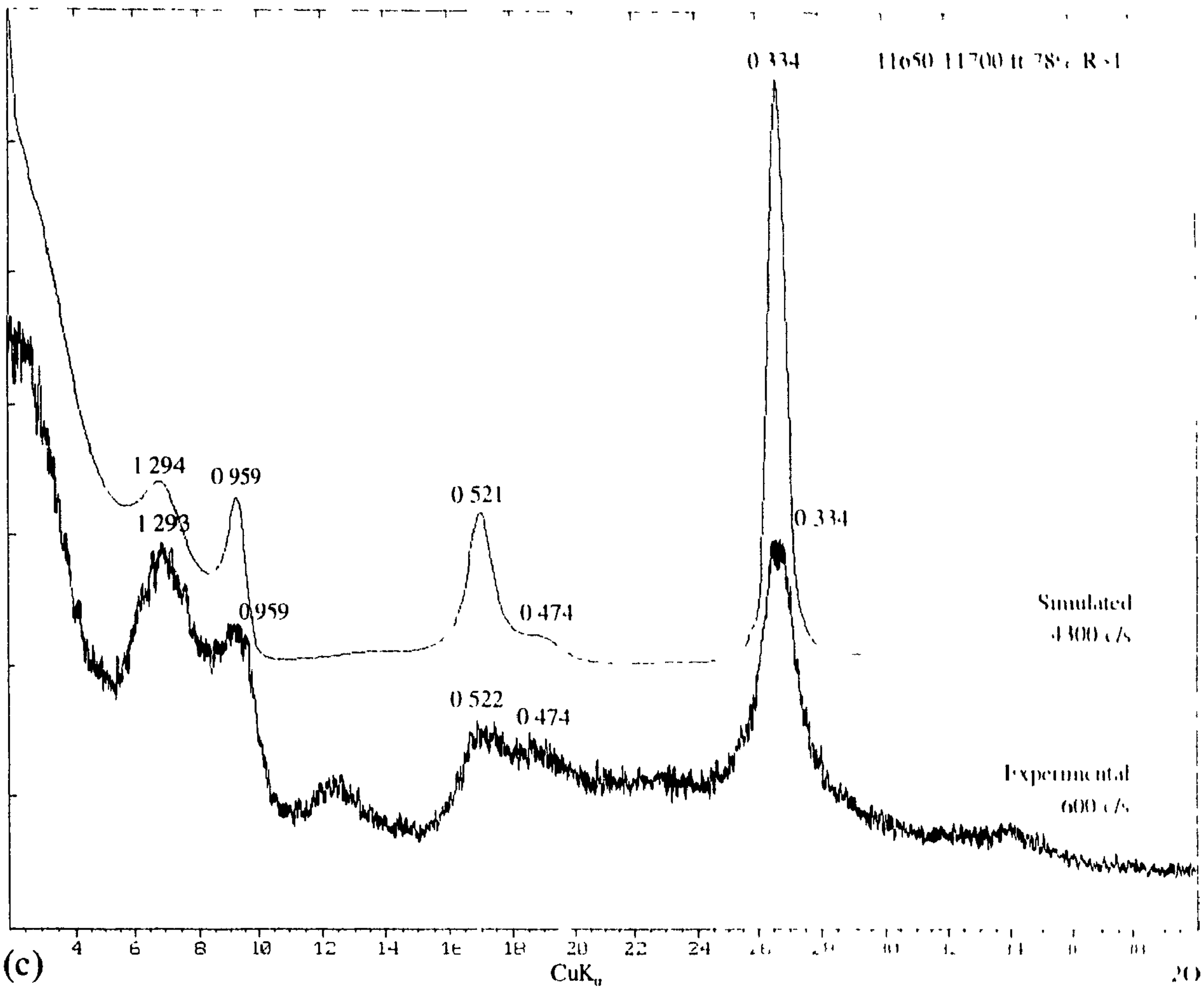
0 334
11650 11700 ft 78% R>1
1 294
0 959
0 521
1 293
0 334
0 959
0 474
Simulated
4300 c/s
0 522
0 474
Experimental
600 c/s
4
6
8
10
12
14
16
18
20
22
24
26
28
30
32
34
36
38
CuK$_\alpha$
2θ

(c)

Fig. 6.4 Simulated and experimental XRD patterns indicating percentage of the non-expandable component for: (a) 4800 ft, (b) 9650-9700 ft, and (c) 11650-11700 ft. (c/s = counts per second).

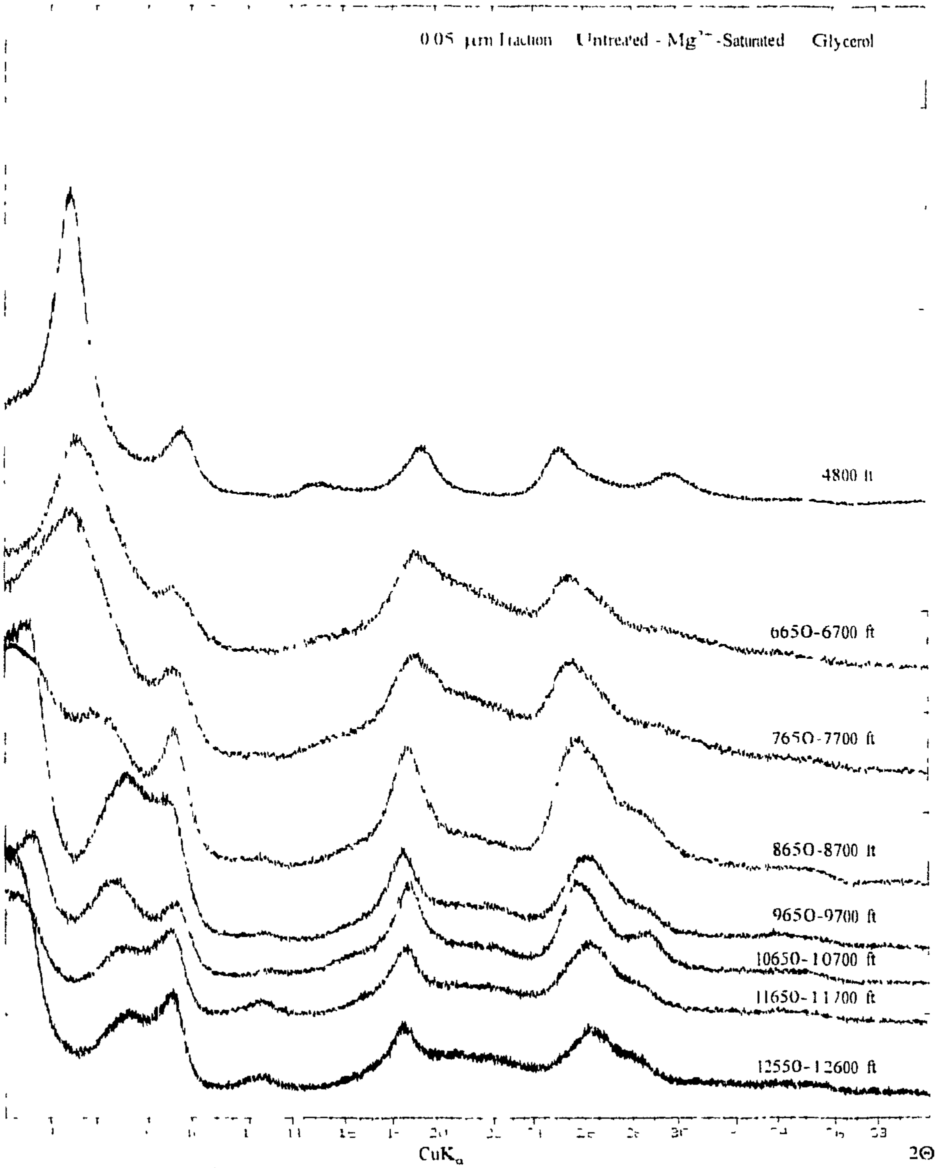
0.05 μm Fraction Untreated - Mg^{2+}-Saturated Glycerol
4800 ft
6650-6700 ft
7650-7700 ft
8650-8700 ft
9650-9700 ft
10650-10700 ft
11650-11700 ft
12550-12600 ft
20
30
CuK$_\alpha$
2Θ

Fig. 6.5 Experimental XRD patterns of Mg^{2+}-saturated glyercol solvated samples from the Reindeer D-27 well.

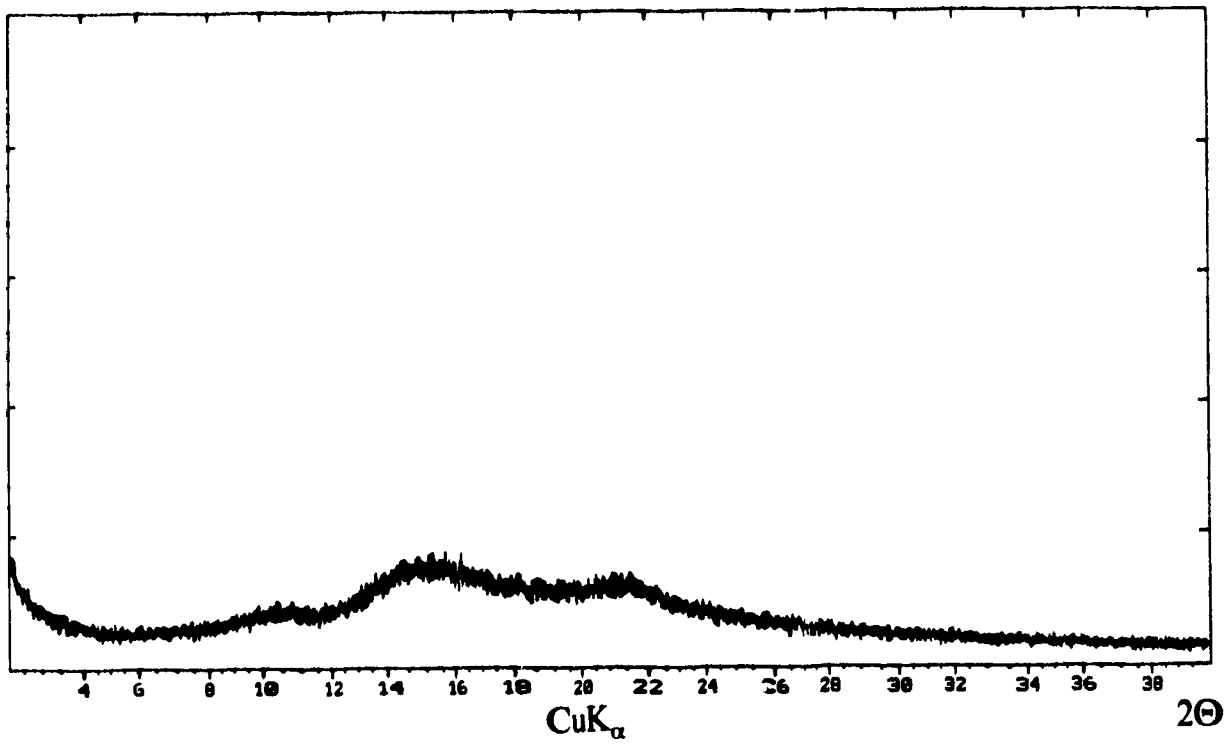
4
6
8
10
12
14
16
18
20
22
24
26
28
30
32
34
36
38
CuK$_\alpha$
2Θ

Fig. 6.6 Experimental XRD pattern from 9650-9700 ft of organic material removed from supernatant after the <0.05 μm fractionation.

ions. This may be an expandable illite of detrital origin.

The XRD patterns of the sodium hexametaphosphate treated 4800 ft sample exchanged with n_C 18 display additional peaks that are difficult to correlate because of low-angle scatter and peak overlap Reflections, however do not appear to be integral, but a number of peaks in the XRD pattern, e g 1.26, 1.12, 0.91, and 0 76 nm, are also present in deeper samples.

8700-8750 ft depth sample

The XRD pattern of the untreated 8700-8750 ft sample exchanged with n_C=8 is very similar to the 4800 ft sample, except the first-order reflection is shifted to slightly higher 2Θ angles (Fig. 6 8a). The 1.24 nm reflection indicates the presence of a low-charge smectite-group component and may mask a 1 0 nm non-expanded component of illite (e g. similar to air-dried I/S pattern) As no reflection at 1.7-2 0 nm was present in the diffraction pattern, a high-charge expandable component did not expand in a consistent manner with n_C=8 or the reflection is masked by low-angle scattering. The Mg^{2+}-saturated ethylene-glycol solvated pattern clearly showed an R1-ordered structure

The XRD patterns of the sodium hexametaphosphate-treated 8700-8750 and 12500-12550 ft samples exchanged with n_C=8 display the same series of integral reflections of approximately 2.5/1.25/0.843 nm (Figs. 6.8b and 6.9b) This integral series of reflections was also present in the 4800 ft sample, except the broad peak of 1.34 nm masks the second-order 1 25 nm peak. In contrast to the 4800 ft sample, the diffraction patterns of the intermediate and deep samples do not show reflections of their untreated counterparts. However, in the 8700-8750 ft sample, the second-order peak of 1.25 nm of the treated sample overlaps the first-order peak of 1 24 nm of the untreated sample. Additional samples (not shown), intermediate between 8700-8750 and 12500-12550 ft, also displayed approximately the same series of integral reflections

The XRD pattern of the untreated 8700-8750 ft sample exchanged with n_C=18 revealed two sets of approximately integral reflections: (i) 3.72/1 88/1.24/(0.93)/0.74/(0.62)/0.54 nm, and (ii) (51.9)/(25 9)/17 3/1 28/1.04/(0.87)/0.74 nm (bracketed reflections not observed) (Fig. 6.8a). These integral reflections are consistent with R1- and R3-ordered structures, respectively. The R1-ordered layer structure would consist of a non-expanded component of 1.0 nm and an expandable component of 2.7 nm having an intermediate to high interlayer charge density and a paraffin-type arrangement of octadecylammonium ions. This would result in a total thickness of 3.72 nm, and the 1.88, 1.24, 0.74 nm reflections would be the second-, third- and fifth-order reflections of such a structure. The second series of integral reflections, which was also present in the 12500-12550 ft sample, suggests reflections from an R3-ordered superstructure with a first-order reflection of 5.19 nm. This sequence would consist of three non-expanded layers of 3.0 nm and an expanded layer with a thickness of 2.1-2.2 nm which may correspond to an intermediate interlayer charge density with a pseudoparaffin-like arrangement of the octadecylammonium ions. The 1.73, 1.28 and 1.04 nm reflections would be the third-, fourth-, and fifth-order reflections of such a superstructure. It is important to note, that in diffraction patterns of samples intermediate (not shown) between 8700-8750 ft and 12500-12550 ft, the first set of integral peaks diminishes with depth.

The XRD pattern of the sodium hexametaphosphate treated 8700-8750 ft sample exchanged with n_c=18 reveals increased complexities (Fig. 6.8b) due to peak overlap. It appears however, that two sets of approximately integral reflections are present (i) 4.04/(2.03)/1.36/1.02/0.81 nm, and (ii) (4.46)/(2.23)/1.46/1.12/0.91/0.76/0.65 nm (bracketed reflections are not observed) (Fig. 6.8b). Inaccuracies are probably due to peak overlap. These assumptions can be made because two sets of integral reflections are present in the untreated sample, and the second set of reflections is also displayed in the 12500-12550 ft sample as very sharp, non-overlapping integral reflections. The first set of reflections may be the R1-ordered structure of the untreated sample which has been displaced in the treated sample. The first-order reflection of 3.72 nm of the untreated sample is displaced to a lower 2θ angle in the treated sample giving a first-order reflection of 4.05 nm. The second set of reflections may correspond to the R3-ordered structure of the untreated sample. The first-order reflection of approximately 5.2 nm in the untreated sample has been displaced to a higher 2θ angle in the treated sample giving a first-order reflection of approximately 4.46 nm.

12500-12550 ft depth sample

The XRD diffraction pattern of the 12500-12550 ft sample exchanged with n_c 8 is characterized by a broad peak of 1.14 nm, which is close to the 1.0 nm peak of illite (again similar to the air-dried sample) (Fig. 6.9a). The diffraction pattern is similar to the 4800 and 8700-8750 ft samples with the first-order reflection shifting to higher 2θ angles with depth. There is no indication of a high-charge expandable component of 1.7-1.8 nm in the XRD pattern.

The diffraction pattern of the treated 12500-12550 ft sample (Fig 6.9b) was discussed with the treated 8700-8750 ft sample

The diffraction pattern of the untreated 12500-12550 ft sample exchanged with n_c=18 (Fig 6 9a) showed a simpler pattern than the 8700-8750 ft sample (Fig. 6.8a). It displayed only two relatively sharp peaks at 1 73 and 1.04 nm, which are similar to the second set of integral reflections displayed in the 8700-8750 ft sample and would be the third- and fifth-order reflections of an R3-ordered structure (this structure has been explained with the 8700-8750 ft sample) It is suggested that the intermediate and deep samples consist of similar components. There is no indication of a strong component from domains containing expandable illite, which would give a first-order reflection at 2 9-3 1 nm after n_c=18 exchange (Laird et al. 1989a; Vali et al. 1991) (Fig 6 9a)

The XRD pattern of the sodium hexametaphospate-treated 12500-12550 ft sample exchanged with n_c-18 has a series of integral peaks with a first-order reflection of 4.46 nm. This integral series is (4 46)/2 23/1.49/1.12/0 89/0.75/0.64 nm (bracketed values not observed) (Fig. 6.9b) Comparison between the untreated (Fig 6 9a) and the treated (Fig 6 9b) samples reveals few similarities The small 0.45 nm peak is present in both samples, but the strong 1.73 and 1 04 nm peaks of the untreated sample are not present in the treated sample. It is apparent that the series of integral peaks with a first-order reflection of 5.19 nm in the untreated sample has been displaced to a higher 2Θ angle with a first-order reflection of 4.46 nm in the treated sample

6.4 TEM of Freeze-Etch and Freeze-Dried Replicas

Freeze-etch replicas can be used to view the surface microtopography of the clay minerals as well as to determine particle dimensions. Figure 6.10 is an HRTEM freeze-etch replica of an untreated <0.05 μm size fraction from 11650-11700 ft depth. This untreated sample displays distinct aggregation of all the particles which makes individual particles difficult to discern The crystallites appear to be randomly superposed over one another, resulting in loss of detail and the appearance of irregular grain shapes. However, the majority of the grains in this size fraction appear to be subhedral to anhedral equant particles with minor amounts of irregularly shaped particles The anhedral nature of the particles may result from particle fragmentation, which most likely occurred during disaggregation.

Figure 6.11 is an HRTEM image of a freeze-dried sample. An alternative technique was attempted to better isolate individual crystallites in order to observe the nature of the grain morphology and dimensions. The sample has been Pt-C shadowed at at an angle of 45°, and the darker areas represent the shadows of the crystallites. The crystallites exist in a randomly connected 3-dimensional network and consequently not all crystals are ideally oriented. Similar to the freeze-etch replica however, there is a tendency for untreated < 0.05 µm separates to aggregate during sample preparation. Sharp-edged lath-like and equant particles are visible (Fig. 6.11, solid arrows). However, similar to the freeze-etch image, crystallites are superposed over one another sometimes giving the appearance of irregular particle shapes.

It is difficult to measure particle dimensions in these images, but HRTEM lattice-fringe images (next section) generally suggest that the grain sizes are within the range predicted by the modified Stoke's equation for centrifugal gravity settling.

6.4.1 Lattice-Fringe Images

Samples from the same depths investigated by XRD were also imaged using HRTEM. Although only a limited number of images have been selected for this study, results are based on hundreds of images taken and are representative of commonly observed features. It is important to emphasize the difficulty in attempting to investigate and image ultrafine clay mineral fractions such as those studied here. It was exacerbated by the limited quantity of material, which prevented replicate analyses. Sample reproducibilty is difficult to achieve as the large surface area of the ultrafine-clay size particles make them chemically reactive and very fragile (when compared to the <0.1 µm size fractions). In addition, the ultrafine size makes measurement of the interlayer spacings imprecise, as the domains do not react consistently with alkylammonium ions, and thus some assumptions had to be incorporated from previous work (Vali et al. 1991; Vali et al. 1992b) on coarser fractions.

6.4.1.1 Terminology

For the description of the layers or interlayers within clay particles observed in the HRTEM after n-alkylammonium ion exchange, the nomenclature of Vali et al. (1991) is followed here. Particle is a general term applied to all coherent units occurring in ultrathin-section. Identification and characterization of clay particles was based on the response of the interlayers to alkylammonium ions of different chain lengths. The smallest clay particles viewed in ultrathin section consisted of a single layer, whereas the largest particles in the Beaufort-Mackenzie material consisted of about eight to ten 2:1 silicate layers. It is misleading however, to refer to the thickness of a single layer. As a result of many factors such as variability in TEM operating and imaging conditions as well as adsorption of inorganic and organic material, single layers have variable thickness. Only sequences of layers with uniform layer spacing can be measured.

The term packet is used to describe a uniform sequence of parallel 2:1 silicate layers which may have expandable or nonexpandable interlayers, or both. Thin coherent sequences of non-expanded interlayers, consisting of three or more 2:1 layers after treatment with n_C=18 are considered as illite. Expandable "illite" refers to coherent sequences of uniform layers with interlayers that expanded with n_C=18 but not with n_C=8 (Vali et al 1993b). This distinguishes them from high-charged smectite-group or vermiculite phases which expand with both n_C=8 and n_C=18. Low-charge smectite-group phases may appear as single isolated 2:1 layer silicates or as sequences with irregular layer spacing. High-charge smectite-group or vermiculite phases appear as coherent sequences with uniform layer spacing.

6.4.1.2 Focus Conditions

A continuing debate regarding HRTEM imaging concerns the conditions of focus i.e. structural (underfocus) versus compositional (overfocus) imaging. This has significant implications not only for the differentiation of smectite-group and illite layers or interlayers, but also for the existence of ordered mixed-layer I/S (e.g. Guthrie and Veblen 1989; Veblen et al. 1990, Ahn and Buseck 1990; Vali et al. 1991). Figures 6.12 and 6.13 are two lattice fringe images of untreated, n_C=18-exchanged clay samples from 4800 ft depth imaged under exactly the same TEM operating conditions, except for a change in focus from underfocus (Scherzer defocus) (Fig. 6.12) to overfocus (Fig. 6.13). The images were taken within seconds of each other.

Comparison between the two images reveals striking, fundamental differences in the morphology and composition of the 2:1 layers present. As the 4800 ft depth specimen was originally dispersed and separated from a moderately indurated shale, the expectation is that

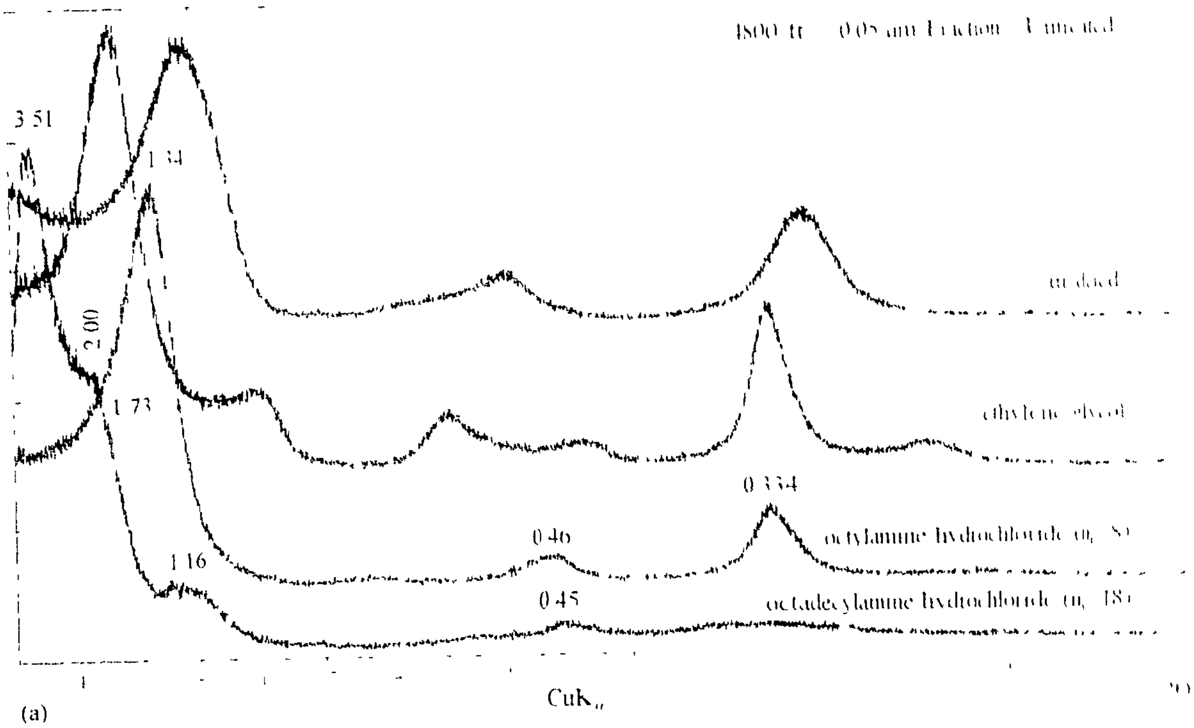
1800 ft - <0.05 μm Fraction - Untreated
3.51
1.34
2.00
1.73
air dried
ethylene glycol
0.334
0.46
octylamine hydrochloride (n_c 8)
1.16
0.45
octadecylamine hydrochloride (n_c 18)
CuK_α

(a)

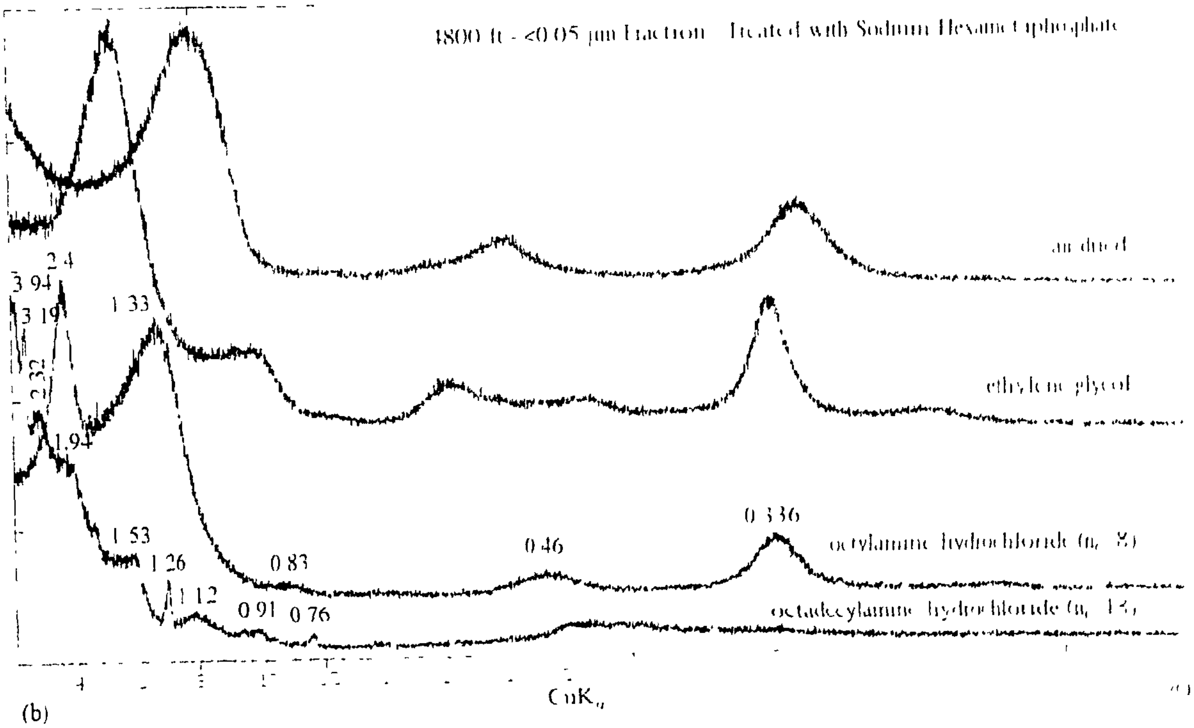
1800 ft - <0.05 μm Fraction - Treated with Sodium Hexametaphosphate
air dried
3.94
2.4
3.19
1.33
ethylene glycol
1.94
0.336
1.53
0.83
0.46
octylamine hydrochloride (n_c 8)
1.26
1.12
0.91
0.76
octadecylamine hydrochloride (n_c 18)
4
CuK_α

(b)

Fig. 6.7 Experimental XRD patterns from 4800 ft of air-dried, ethylene glycol solvated, octylammonium-ion ($n_c=8$) exchanged and octadecylammonium-ion ($n_c=18$) exchanged: (a) untreated, and (b) treated with sodium hexametaphosphate.

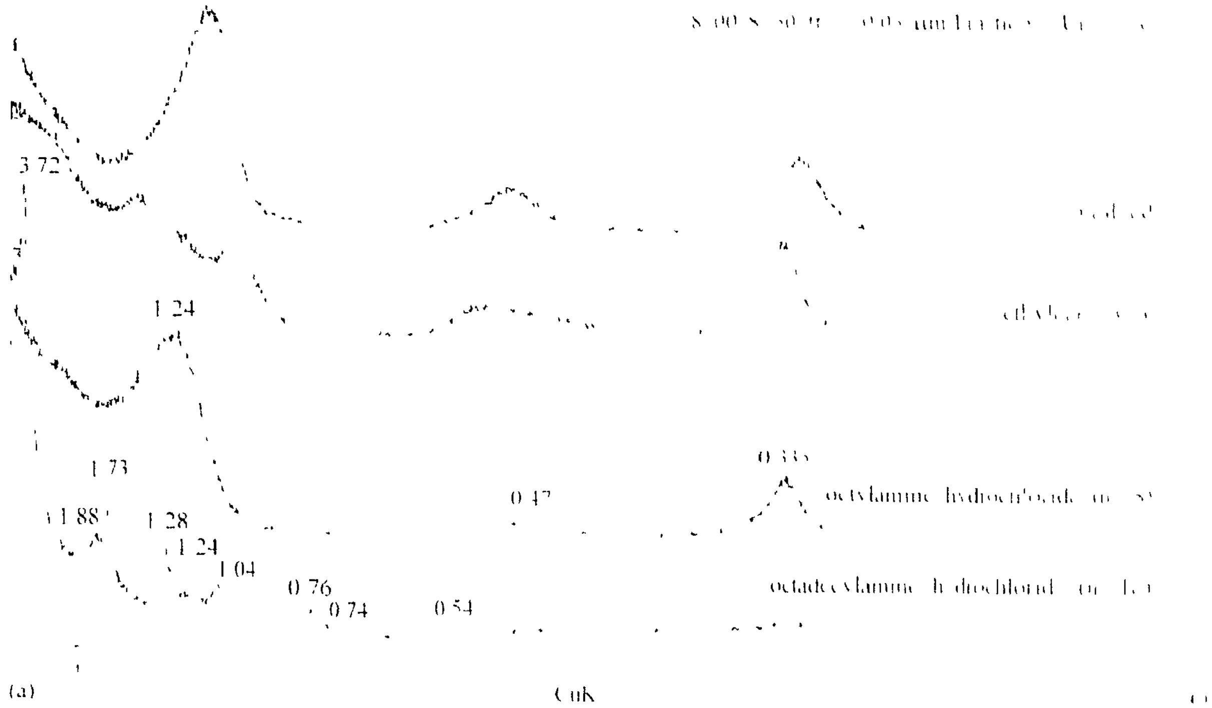
8700-8750 ft <0.05 µm Fraction
air dried
ethylene glycol
3.72
1.24
1.73
1.88
1.28
1.24
1.04
0.76
0.74
0.54
0.47
0.335
octylamine hydrochloride
octadecylamine hydrochloride
(a)
CuK

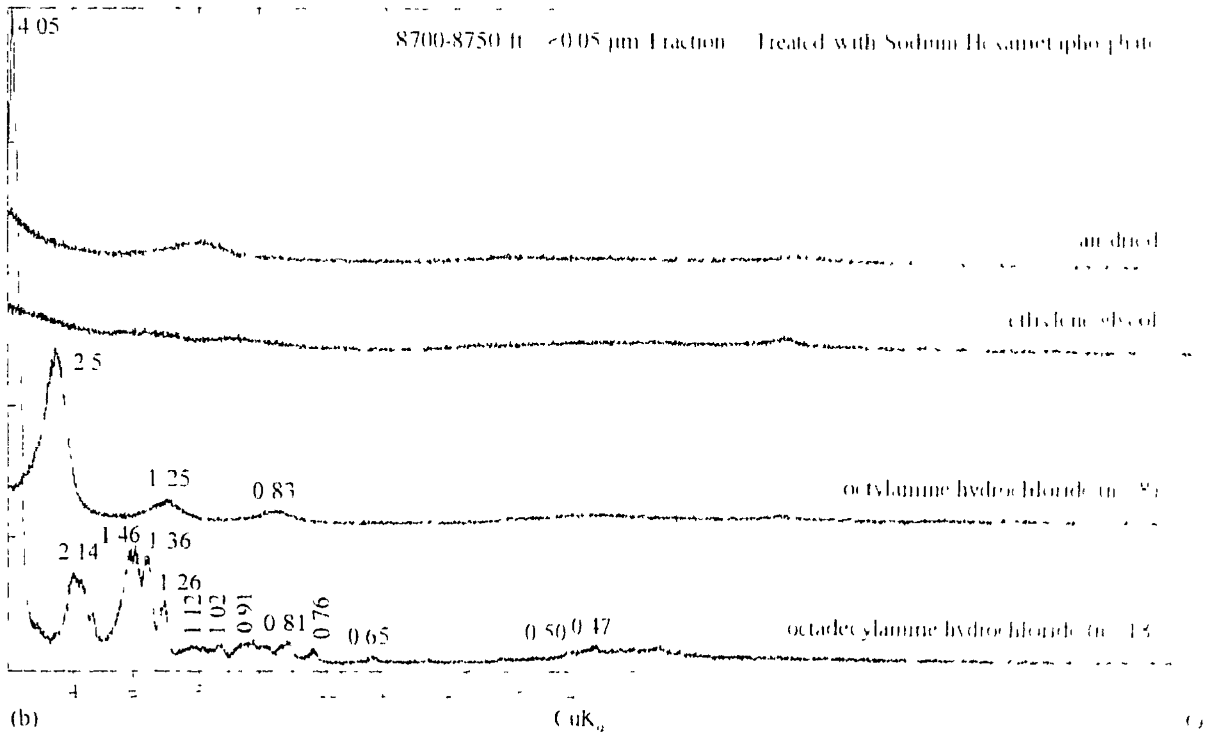
4.05
8700-8750 ft <0.05 µm Fraction Treated with Sodium Hexametaphosphate
air dried
ethylene glycol
2.5
1.25
0.83
octylamine hydrochloride
2.14
1.46
1.36
1.26
1.12
1.02
0.91
0.81
0.76
0.65
0.50
0.47
octadecylamine hydrochloride
4
(b)
CuKα

Fig. 6.8 Experimental XRD patterns from 8700-8750 ft of air-dried, ethylene-glycol solvated, octylammonium-ion (n_C=8) exchanged and octadecylammonium-ion (n_C=18) exchanged: (a) untreated, and (b) treated with sodium hexametaphosphate.

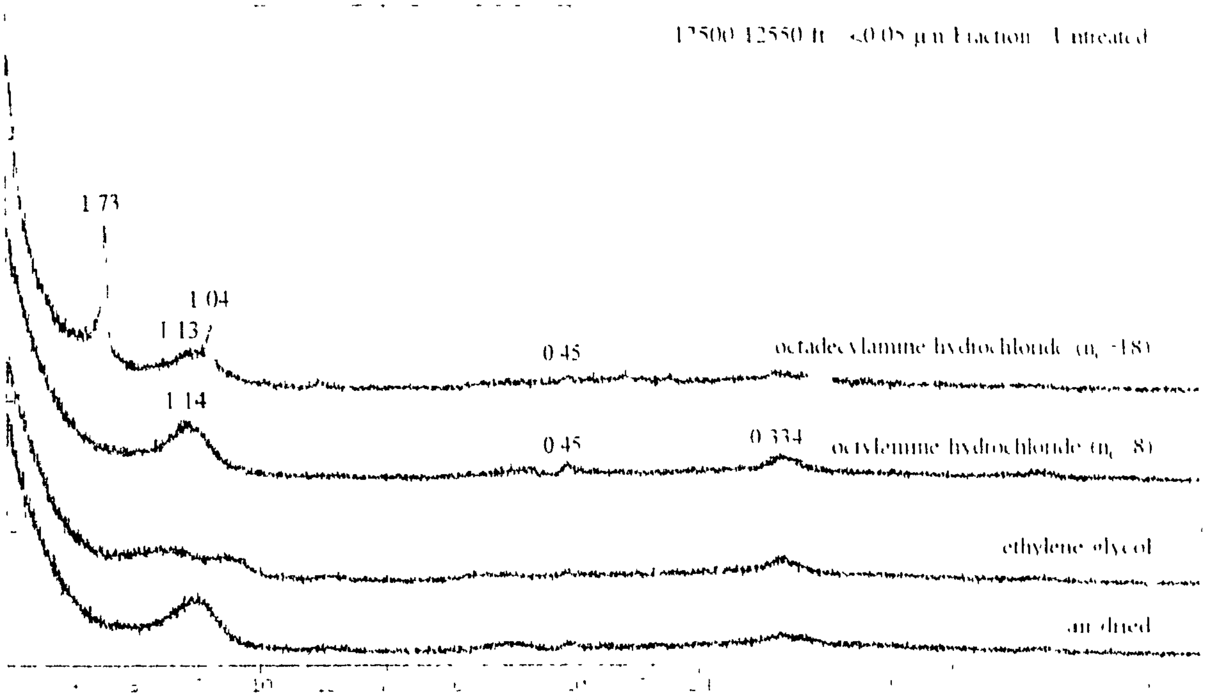
12500-12550 ft - <0.05 µm Fraction - Untreated
1.73
1.04
1.13
0.45
octadecylamine hydrochloride (n_c =18)
1.14
0.45
0.334
octylamine hydrochloride (n_c = 8)
ethylene glycol
air dried
10
20
CuKα
°2Θ

(a)

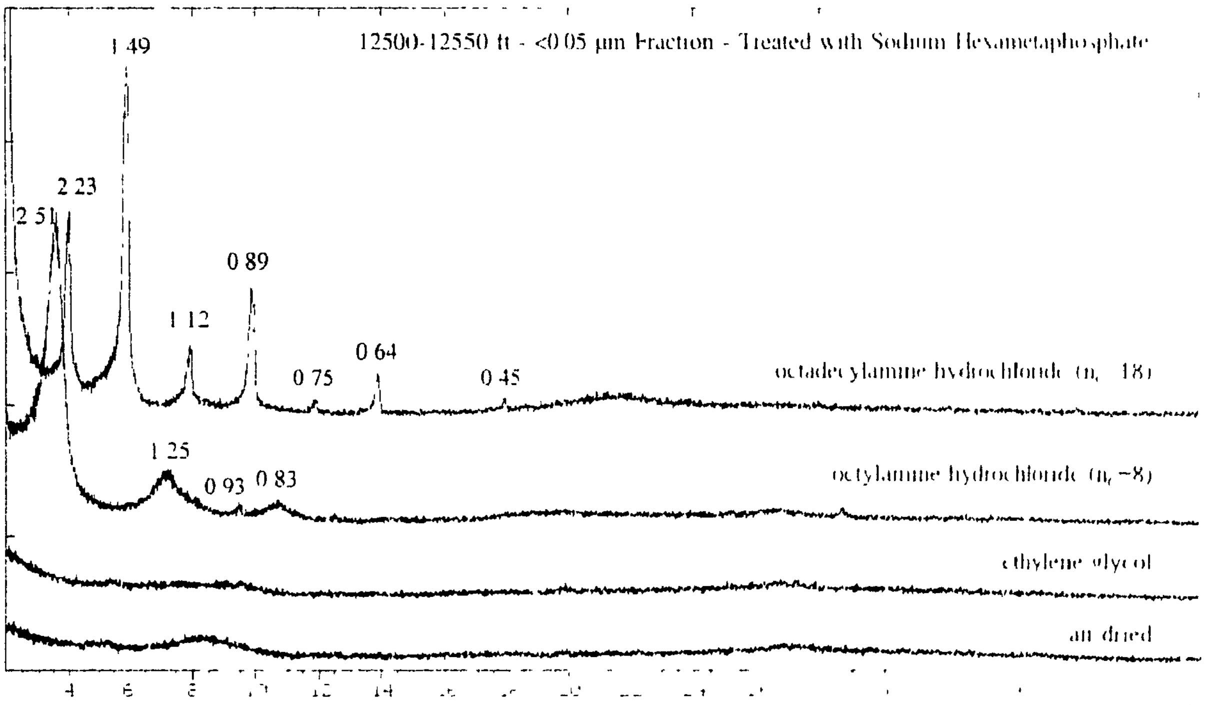
12500-12550 ft - <0.05 µm Fraction - Treated with Sodium Hexametaphosphate
1.49
2.23
2.51
0.89
1.12
0.64
0.75
0.45
octadecylamine hydrochloride (n_c = 18)
1.25
0.93
0.83
octylamine hydrochloride (n_c =8)
ethylene glycol
air dried
4
6
8
10
12
14
CuKα
°2Θ

(b)

Fig. 6.9 Experimental XRD patterns from 12500-12550 ft of air-dried, ethylene glycol solvated, octylammonium-ion (n_C=8) exchanged and octadecylammonium-ion (n_C=18) exchanged: (a) untreated, and (b) treated with sodium hexametaphosphate.

single layers of smectite will be present and observed. At approximate Scherzer defocus, dark fringes overlie regions of relatively high-charge density, e.g. 2:1 layers, and bright fringes overlie regions of relatively low density, e.g. interlayers. The underfocus lattice-fringe image (Fig. 6.12) reveals the presence of predominantly single curved and wavy 2:1 layers characteristic of smectite-group phases (black arrows), isolated non-expanded double layers (solid triangles) and packets of three 2:1 silicate layers with non-expanded interlayers characteristic of illite (solid diamonds). The overfocus micrograph (Fig. 6.13), however, reveals the predominance of two 2:1 silicate layers with thicker packets of 2:1 silicate layers with non-expanded interlayers. The single layers observed in underfocus are replaced by two layers in overfocus (white arrows). It is important to reiterate that single layers are never observed in any sample at overfocus conditions. As single layers of smectite-group phases are expected to be present at certain depths (e.g. shallow depths) and since single layers are observed only at the Scherzer defocus, it is concluded that this is the proper and correct imaging condition to study smectite-group and illite layers. Lattice fringe images in overfocus conditions do not represent "real" layer images. The underfocus condition is in direct contrast to Guthrie and Veblen (1989a, 1990) and Veblen et al. (1990) who used overfocus conditions to discern compositional differences between smectite-group and illite interlayers. In addition, their approach required the generation and use of calculated images to correctly interpret ordered mixed-layer I/S.

These two images are evidence that the Scherzer defocus in conjunction with alkylammonium-ion exchange techniques enables a distinction to be made between smectite-group phases and illitic material strictly on the basis of interlayer expansion and without the need of employing image simulation.

6.4.1.3 Sample Impurities

XRD of untreated and treated 0.05-1.0 μm ethylene-glycol solvated separates suggested the presence of a significant discrete illite (or mica) component in addition to mixed-layer I/S. This was also investigated using the HRTEM. The presence of discrete packets of micaceous material was clearly evident in the 0.05-1.0 μm fractions of shallow depth samples. Micaceous material usually occurred as thick packets containing 10s of non-expanded interlayers.

Figures 6.14 and 6.15 are lattice fringe images from 4800 ft depth of the 0.05-1.0 μm


20 µm

Fig. 6.10 TEM image of freeze-etch replica from 11650-11700 ft (see text for discussion).


20μm

Fig. 6.11 TEM image of freeze-dried replica from 11650-11700 ft. The shadowing is from the bottom right corner to the upper left corner of the photograph (see text for discussion).

20 nm

Fig. 6.12 Lattice-fringe image from 4800 ft at Scherzer defocus or underfocus conditions (see text for discussion).


20µm

Fig. 6.13 Same image as Fig. 6.12 except at overfocus conditions (see text for discussion) size fraction, untreated and exchanged with $n_c=18$. Figure 6.14 represents a lattice-fringe image showing aggregated particles which exhibit coherent sequences of 2:1 layer silicates with non-expanded interlayers, and coherent sequences of $n_c=18$ expanded interlayers having a uniform spacing of approximately 2.4-2.5 nm thickness. Originally deposited detrital particles must have consisted of thick sequences of non-expanded interlayers and thus, are here considered to be micaceous. It is very unlikely that neoformed illite would attain such thicknesses at this shallow depth. The solid arrow indicates an area characterized by frayed and wispy layers at the termination of a micaceous particle that appears to display dissolution of some of the layers (Fig. 6.14). If this interpretation is true, this observation may have significant consequences for the Beaufort-Mackenzie Basin, as the dissolution of detrital micaceous minerals would provide a source (perhaps the only one) of K^+ for illite neoformation at depth. Figure 6.15 provides additional evidence of the presence and apparent alteration of detrital mica. This image exhibits coherent sequences of packets of expanded and non-expanded interlayers, similar to the previous image. In addition, in the lower center of the image is a large single particle consisting of a core of a thick sequence of non-expanded interlayers with expanded interlayers at the outer margins (Fig. 6.15, white arrows). This detrital micaceous particle is apparently undergoing diagenetic alteration of the interlayers similar to weathering (Vali et al. 1992). Also present are the frayed and wispy layers at the termination of the micaceous particle (Fig. 6.15, black arrow) indicative of layer dissolution that was present in the previous image. These different kinds of alteration of detrital micaceous particles at shallow depths make it difficult to distinguish in XRD analysis between diagenetic processes of alteration, dissolution and crystallization or neoformation of illite and thus would be perceived as a random ordered (RO) structures

6.4.2 Untreated and Treated Samples

As the <0.05 µm size fraction is expected to contain the least amount of impurities and detrital material and the maximum amount of homogeneous neoformed material, it was used to investigate the effects of the addition of sodium hexametaphosphate as a peptizer on the arrangement of layers in I/S.

4800 ft sample depth

Ultrathin sections of clay separates from shallow depths display subtle but obvious differences between samples without treatment and with the addition of sodium hexametaphosphate (treated sample). The principal differences between the untreated and treated samples is the presence of aggregation and irregular orientation of the 2:1 silicates layers and packets in the untreated samples, especially the aggregation of some packets of non-expanded micaceous particles. The treated sample tends to display better dispersion, showing better orientation of the smectite-group layers with less random or irregular variation in layer spacing. In addition, there are more coherent sequences with uniform spacing, increases in the abundance of double layers and generally thinner packets of 2:1 silicate layers with nonexpanded interlayers. Figures 6.16, 6.17 and 6.18 are lattice fringe images of clay material from 4800 ft which have been exchanged with octylammonium ions (n_c 8). They are typical images for shallow depths. Figure 6.16 was fractionated without treatment, whereas Figures 6.17 and 6.18 represent images of samples fractionated with a sodium hexametaphosphate solution. All three images are similar in appearance, and are characterized by domains of smectite and illite: (i) areas of bent and wavy low-charged smectite-group minerals appear as single layers or as clusters or sequences of layers with variable or irregular layer spacing (1.3 to 3.0 nm) (short arrows), (ii) areas of coherent sequences of expanded high-charged smectite or vermiculite layers (2.0-2.4 nm) with a more uniform interlayer spacing (long arrows), (iii) isolated double layers (solid triangles), and (iv) packets of four to five 2:1 layer silicates with non-expanded interlayers and packets with more than six 2:1 silicate layers with non-expanded interlayers characteristic of detrital micaceous minerals (solid diamonds). Figure 6.16 displays abundant non-oriented single layers (small arrows), coherent wavy and curved sequences of expanded interlayers (long arrows), minor isolated double layers (solid triangles) and packets of four to five 2:1 layers with non-expanded interlayers (solid diamonds). Figure 6.17 is an overview of a treated sample that displays the relative wavy and curved orientation of the single layers and coherent expandable sequences of low- and high-charged smectites (or vermiculites), respectively. Figure 6.18 is a close-up of Figure 6.17, which demonstrates that the thin packets of three to four 2:1 silicate layers with non-expanded interlayers (solid diamonds) are more parallel and straighter as compared to the wavy, single and packets with expanded interlayers (long arrows). Double layers are rarely seen. Also visible is an aggregate of three non-expanded interlayer packets with non-expanded basal surfaces or a single very thick micaceous particle (A). This interpretation could not be confirmed without n_c 18 exchange (see below). As these are size-fractionated samples, it is not possible to characterize the interrelationship between the smectite-group minerals and the non-expandable packets as they would exist in situ, but appear as random mixtures in fractionated samples.

Samples from the same depth exchanged with octadecylammonium ions ($n_c=18$) display similar features as the $n_c=8$-exchanged samples. However, it is not possible to distinguish between expanded vermiculite and expanded illite at this depth, without examining the same particles before and after treatment. As with the $n_c=8$ exchanged samples, the treated sample tends to show better dispersion and orientation of all the 2:1 silicate layers and packets, with generally thinner packets of non-expanded interlayers. The high-charge smectite-group minerals or vermiculite tend to have a slightly greater interlayer spacing at about 2.4-2.6 nm, but this remains an approximation because of the very fine particle size and small coherent domain size. In addition, treated samples display more coherent sequences of expanded interlayers with uniform spacing in contrast to the untreated samples. Differences are more readily apparent in XRD.

Figures 6.19, 6.20 and 6.21 are another set of lattice fringe images from 4800 ft depth exchanged with $n_c=18$. Figure 6.19 is an untreated sample and Figures 6.20 and 6.21 are treated with sodium hexametaphosphate. Generally all three images display abundant, wavy and overlapping single layers of smectite-group minerals (short arrows), some coherent sequences of uniform spacing of high-charged smectite-group (or low-charged vermiculite) (long arrows), and packets of three to five 2:1 layers with non-expanded interlayers characteristic of illite (solid diamonds) and packets containing large numbers of non-expanded interlayers (>8 layers). Illite interlayers will not expand with $n_c=8$, whereas high-charge smectite-group or vermiulite interlayers will expand. Packets which do not expand with $n_c=18$ are considered to be non-expanded illite, whereas high-charge vermiculite and high-charge illite will expand giving a uniform spacing of approximately 2.4-2.6 nm. In Figure 6.20, a single particle displays expanded layers surrounding a core of 2 non-expanded interlayers (B) which is typical of particles in the coarser fractions(Fig. 6.15) Figure 6.21 is a lattice-fringe image of a treated and $n_c=18$ exchanged sample which displays thicker packets of non-expanded interlayers that are considered detrital. Also visible is a small sequence of double layers (open triangles) with an expanded interface of about 1.7-1.9 nm. Also present are expanded layers of high-charge smectite-group or vermiculite minerals with a thickness of about 2.4-2.6 nm, evidence for the predominance of the coherently expanded interlayer sequences (hollow diamonds).

Thick packets (8-10 layers) of non-expanded interlayers are considered detrital micaceous


20 µm

Fig. 6.14 Lattice-fringe image from 4800 ft of untreated 0.05-0.1 μm size fraction after octadecylammonium-ion ($n_C=18$) exchange (see text for discussion).

20 µm

Fig. 6.15 Lattice-fringe image from 4800 ft of untreated 0.05-0.1 μm size fraction after octadecylammonium-ion ($n_C=18$) exchange (see text for discussion).


20 µm

Fig. 6.16 Lattice-fringe image from 4800 ft of untreated <0.05 μm size fraction after octylammonium-ion (n_c=8) exchange (see text for discussion).


50 μm

Fig. 6.17 Low magnification lattice-fringe image from 4800 ft of treated <0.05 μm size fraction after octylammonium-ion (n_C=8) exchange (see text for discussion).


A
20μm

Fig 6.18 Close-up of Fig. 6.17 (see text for discussion).

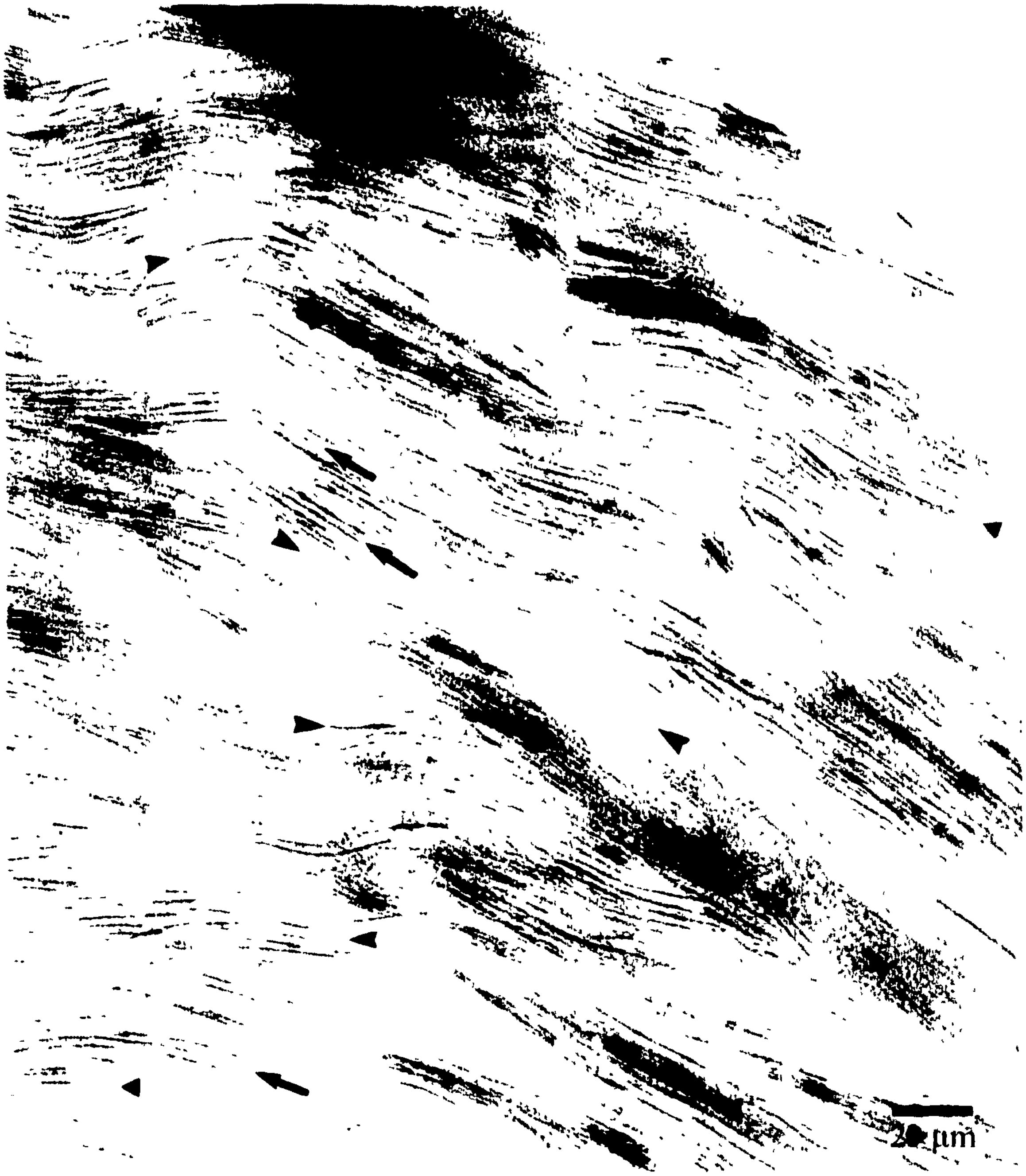
20 µm

Fig. 6.19 Lattice-fringe image from 4800 ft of untreated <0.05 μm size fraction after octadecylammonium-ion ($n_C=18$) exchange (see text for discussion).


B
20μm

Fig. 6.20 Lattice-fringe image from 4800 ft of treated <0.05 μm size fraction after octadecylammonium-ion ($n_C=18$) exchange (see text for discussion).


20 µm

Fig. 6.21 Lattice-fringe image from 4800 ft of treated <0.05 μm size fraction after octadecylammonium-ion ($n_C=18$) exchange (see text for discussion).

particles.

12500-12550 ft depth sample

Untreated samples from 12500-12550 ft generally exhibit more compaction and aggregation of the non-expanded packets, whereas the treated sample tends to show better dispersion of the non-expanded packets with the packets containing fewer layers

Figures 6.23 and 6.24 represent typical lattice fringe images of deep samples for untreated and treated samples, respectively, exchanged with n_C=8. Both images are characterized by abundant packets of 2:1 layers with non-expanded interlayers. Figure 6.23 displays packets of three to six 2:1 silicate layers with non-expanded interlayers (solid diamonds) and some isolated double layers (solid triangles) and sequences of doubles layers (hollow triangles). Figure 6.24 is a treated sample which displays packets of three to five 2:1 silicate layers with non-expanded interlayers (solid diamonds) and abundant double layers (solid triangles), but sequences of double layers are less apparent (hollow triangles) Generally, the most significant difference between untreated and treated samples are packets of non-expanded illite which are thinner than in the untreated samples.

Comparison between untreated and treated samples from the same depth, exchanged with n_C=18 shows signficant differences. The samples are similar in orientation to the previous untreated and treated samples exchanged with n_C=8, except the treated samples show abundant packets of 2:1 silicate layers with expanded interlayers of 2.3-2.6 nm thickness Figure 6.25 represents a low-magnification HRTEM image showing an overview of the typical layer structures of illitic material of deep samples as prepared for an XRD mount. The predominant features are the random distribution of relatively thin packets of nonexpanded interlayers (solid diamonds), with minor amounts of packets containing expanded interlayers having a uniform interlayer spacing of approximately 2.3-2.6 nm (hollow diamonds). The individual non-expanded packets of illite show slight differences in orientation and spacings with respect to other packets. A few packets appear as larger aggregated units. Some of the packets of non-expanded illite have uniform expanded basal surfaces (C) Also present are sequences of double layers with 1.7-1.8 nm expanded interfaces (hollow triangles). The close-up (Fig 6.26) of the untreated sample shows the random distribution of thin packets of relatively straight three to six 2:1 silicate layers with non-expanded interlayers (solid diamonds) and some isolated double layers (solid triangles). In the upper right corner of the image is a coherent sequence of double layers (hollow triangles). Some of the oriented packets display uniform expansion between packets (D). Figure 6.27 is another untreated sample exhibiting features similar to the previous image; minor amounts of packets of expanded interlayers with uniform expansion (hollow diamonds) can be seen as well as sequences of double layers (hollow triangles) and isolated double layers (solid triangles) Also apparent is a coherent sequence consisting of three non-expanded packets and one double layer with relatively uniform expanded interfaces, which may behave as a single particle (E). These particles are never seen in treated samples. Figure 6.28 represents an overview of the sample from the same depth as Figures 6.26 and 6.27 treated with a dilute solution of sodium hexametaphosphate. The lattice-fringe image displays similar features as the untreated sample, with one very obvious difference. The treated sample reveals abundant packets of 2.1 silicate layers with expanded interlayers (hollow diamonds). Isolated double layers are present, but sequences of double layers are less apparent. Figure 6.29 is a close-up of the previous image, displaying the predominance of packets of coherent expanded interlayers of uniform spacing (2.3-2.6 nm) characteristic of expanded illite (hollow diamonds). Non-expanded packets of illite are also present (solid diamonds). As well, in the center of the micrograph, is an apparent large chlorite particle (F) contiguous with a non-expanded illite packet.

6.4.3 TEM Characterization of the Layer Structures with Depth in the <0.05 μm Fraction of the the Reindeer D-27 Well

As evidenced from the description of the layer structures observed in the lattice fringe images from the 4800 ft and 12500-12550 ft sample depths, there has been a drastic change in the layer structures with depth. However, as there are also differences in the layer structures between untreated and chemically-treated samples in the <0.05 μm fraction, I will confine myself to describing the changes in the untreated samples. It is important to note that the layer structure sequences are much more homogeneous in the <0.05 μm fraction than in the 0.05-1.0 μm fraction (cf. Fig. 6.14 vs. Fig. 6.16).

The obvious difference between the 12500-12550 ft sample depth and the 4800 ft sample depth is the complete absence of single layers or irregular sequences of low-charged smectite group minerals characteristic of shallow depths. The single layers of discrete smectite particles (fundamental smectite particles of Nadeau et al. 1984a, 1984b, 1984c) can only be


20 μm

Fig. 6.22 Lattice-fringe image from 8700-8750 ft of untreated <0.05 μm size fraction after octylammonium-ion ($n_c=8$) exchange (see text for discussion).


20 μm

Fig 6.23 Lattice-fringe image from 12500-12550 ft of untreated <0.05 µm size fraction after octylammonium-ion (n_c=8) exchange (see text for discussion).


20 µ

Fig. 6.24 Lattice-fringe image from 12500-12550 ft of treated <0.05 μm size fraction after octylammonium-ion (n_C=8) exchange (see text for discussion).


c

Fig. 6.25 Low magnification lattice-fringe image from 12500-12550 ft of untreated <0.05 μm size fraction after octadecylammonium-ion (n_C=18) exchange (see text for discussion).

Fig. 6.26 Close-up of Fig. 6.25 (see text for discussion).

Fig. 6.27 Lattice-fringe image from 12500-12550 ft of untreated <0.05 μm size fraction after octadecylammonium-ion (n_c=18) exchange (see text for discussion).


0 μm

Fig. 6.28 Low magnification lattice-fringe image from 12500-12550 ft of treated <0.05 μm size fraction after octadecylammonium-ion ($n_c=18$) exchange (see text for discussion).


F
20µm

Fig. 6.29 Close-up of Fig. 6.28 (see text for discussion).

found in abundance at shallow depths. There are no mixed-layer I/S structures visible in any of the < 0.05 μm alkylammonium-ion exchanged samples and no smectite-group phase was associated with ordered 2:1 mixed-layer structures. Smectite-group and illitic material was observed as separate, discrete phases. However, packets of non-expanded interlayers of illitic (or micaceous) material were present at all depths. Shallow samples exchanged with n_c 18 consisted predominantly of single isolated curved layers of a smectite-group phase, minor amounts of double layers and packets of three 2:1 layers with non-expanded interlayers (Fig 6.30).

Ultrathin-sections from intermediate depths treated with n_c =8 consisted predominantly of sequences of double layers with expanded interfaces forming R1-ordered structures, minor amounts of isolated double layers layers, coherent sequences of uniform spacing of a high-charge smectite-group or vermiculite phase and packets of non-expanded interlayers containing three or four 2:1 silicate layers (Fig. 6.31)

Deeper samples, when treated with n_c=18 consist predominantly of packets of non-expanded interlayers consisting of three to six 2:1 illite layers, packets of expanded interlayers of illite, sequences of double layers with expanded interfaces (R1-ordered structures) and isolated double layers (Fig. 6.32).

Whereas lattice fringe images can provide direct evidence of layer structures, they can only give indirect evidence for the S-I conversion. Freeze-etch replicas exhibit the surface microtopography of clay minerals and may show the original texture or morphology of individual particles or aggregates occurring in a sample. Figures 6.33 and 6.34 represent freeze-etch replicas of untreated <1% dispersions from a depth of 11650-11700 ft and display the surface structures of some particles. These images show single crystals having a euhedral lath-like morphology overgrown on the surface of larger particles (Figs. 6.33 and 6.34, short arrows). The crystals exhibit well developed and parallel stepped edges within an aggregate of very fine particles with irregular outlines. Dissolution and growth features can often be observed in the same particle. Dissolution appears as irregular embayments on the edges of the single thin particles on the surface of larger particles (Figs 6.33 and 6.34, short arrows) However, evidence of crystal growth is more readily suggested in images of freeze-dried samples of the <0.05 μm fraction (e.g. Fig. 6.11, short arrows) which display sharp-edged euhedral lath-like crystallites.


50 µm

Fig. 6.30 Lattice-fringe image from 4800 ft of untreated <0.05 μm size fraction after octadecylammonium-ion (n_c=18) exchange (see text for discussion).

20 µm

Fig. 6.31 Lattice-fringe image from 8700-8750 ft of an untreated <0.05 μm size fraction after octylammonium-ion ($n_c=8$) exchange (see text for discussion).


20 µm

Fig. 6.32 Lattice-fringe image from 12500-12550 ft of untreated <0.05 µm size fraction after octadecylammonium-ion ($n_c = 18$) exchange (see text for discussion).


50 µm

Fig. 6.33 TEM image of freeze-etch replica from 11650-11700 ft (see text for discussion).

Fig. 6.34 TEM image of freeze-etch replica from 11650-11700 ft (see text for discussion).

CHAPTER 7.0 - DISCUSSION

The alkylammonium-ion exchange technique is usually applied to deduce the layer charge and charge heterogeneity of expandable clay minerals in soils and sediments (Malla and Douglas 1987b, 1987c; Laird et al. 1987, 1988, 1989a; Marcks et al. 1989; Ghabru et al. 1989; Chen et al. 1989; Stanjek et al. 1992). In this study, the alkylammonium-ion exchange-technique was used to characterize the structural and compositional changes in I/S on the basis of interlayer-charge densities with depth of burial and to facilitate comparisons between XRD and TEM results.

One focus of this study was an investigation of the effects of sodium hexametaphosphate on the measurement of expandability in mixed-layer I/S. A significant difference to the earlier work is that in the previous study by Sears and Hesse (1992) the clay minerals were characterized in XRD with the aid of ethylene-glycol solvation. Ethylene glycol and glycerol, however, evaporate in the vacuum of the TEM, resulting in the collapse of expandable interlayers. Stable expansion of expandable clay minerals in TEM can only be achieved by exchanging the inorganic cations for the large anisometric alkylammonium ions. Although the conclusions of the earlier XRD study are still valid, TEM observations revealed the presence of more than one type of expandable component in alkylammonium-ion exchanged I/S. This was an observation that could not be obtained with XRD using ethylene glycol, which can only be used to characterize the expandable component in untreated I/S.

7.1 Physical Properties

The ultrafine clay particles obtained from shales during size fractionation may be the result of particles formed during: (i) precipitation in the pore space (Ahn and Peacor 1986a), (ii) transformation of pre-existing particles (Bell 1986), or (iii) overgrowths on detrital particles broken off during sample comminution (Morton, written comm. 1990). The abundance of subhedral illite and the minimal amounts of detrital phases strongly suggested that the <0.05 μm fraction approximates a mineral separate and not a size separate of indeterminant composition. The presence of sharp-edged lath-like crystallites in the freeze-dried replicas evinces neoformation (Fig. 6.11). However, anhedral or irregular shaped particles in aggregated freeze-etch replicas (Fig. 6.10) may imply overgrowths which broke off from detrital nuclei during sample disaggregation. The small lath-like particles on larger particles and irregular edges exhibited in freeze-etch replicas imply crystal growth and dissolution, respectively (Figs. 6.33 and 6.34). The lack of feldspar grains, or fragments of feldspar suggests that the separation procedure employed in this study was complete.

Comparison between untreated and treated samples from the same depth in lattice-fringe images generally reveals that the clay separates are of similar thickness and composition for a given depth (e.g., compare Figs. 6.24 and 6.25). The separation of the <0.05 µm fraction from the <0.1 µm fraction using the addition of sodium hexametaphosphate, however, resulted in thinner packets of non-expandable illite (e.g., Fig. 6.25).

7.2 Mineralogical Properties

Comparison between the <0.1 µm fraction collected by Ko (1992) who performed an in-depth investigation of the minerological changes of the <0.1 µm size fraction in the Beaufort-Mackenzie Basin and the 0.05-1.0 µm and <0.05 µm fractions obtained for this investigation showed significant differences. Although procedures for physical disaggregation and clay fractionation were similar, Ko (1992) used chemical pretreatment. Clay mineral separates in this study were not subjected to any aggressive chemical pretreatments (except with sodium hexametaphopshate for comparative purposes). Ko (1992), for his XRD analysis, followed the procedure of Jackson (1969) for isolating clay minerals from soil samples and included chemical treatments for removal of carbonates, Fe-oxides, organic material, and peptizers for increased dispersion. This resulted in better peak intensity (see chapter 4). Further XRD analysis was warranted when the initial XRD results of this study were compared with results obtained by Ko (1992) who had investigated the S-I transition in the same area.

The amounts of the expandable component determined from XRD in this study are systematically smaller by 5%-10% compared with Ko (1992), but are well within his margin of error (± 10%), although different methods for determining layer proportions were employed. The diffraction profiles of samples in this study exhibited anomalously broad peaks and diminished peak intensity characteristic of small particle size. As previously noted, poor 00*l* intensity may result from small sample mass, short sample length, poor orientation, or from the clay material itself. Ko's (1992) XRD profiles showed generally much higher peak intensities, especially in the low 2Θ angle regions, whereas higher 2Θ angle reflections displayed diminished intensity. This may have resulted from specimens having small sample mass, i.e. thin samples (Dr. David Pevear 1993, personal comm.). This made it difficult for Ko to use the $(002)_{10}/(003)_{17}$ reflection to calculate expandability (see Figs 6.1a and 6.2a of this study). In this study, low 2Θ angle reflections had diminished intensities (likely the result of short samples with small mass) but exhibited more pronounced $(002)_{10}/(003)_{17}$ reflections which enabled layer proportions to be calculated using the concepts of Reynolds and Hower (1970), Reynolds (1980) and Moore and Reynolds (1989).

Further comparisons with Ko (1992) revealed similarity in mineralogy between comparable size fractions. Additional peaks, i.e. shoulders on low-angle peaks, and differences in ordering were revealed in intermediate samples of Ko (1992) that were not observed in this study (see Ko's fig. III-1). For example, Ko (1992) was able to describe a mixture of random and ordered I/S in most samples from between 6700-6750 to 8300-8350 ft (see Ko's fig, III-1B), which was not apparent in samples of comparable depths in this study. These profiles are described here as random (R0) structures. In addition, Ko (1992) referred to a "reversed glycol effect" whereby ethylene glycol solvation on I/S induced a more pronounced reflection to the lower-angle side of the 0.50 nm peak rather than to the higher-angle side as would be expected. This was attributed to the effect of a 1.4 nm component in mixed-layer I/S. However, the close correspondance between experimental and calculated diffraction profiles for untreated ethylene-glycol solvated samples in this study suggests this may be an artifact from sample treatment (see below). Although, glycerol solvated samples clearly indicate a high-charge expandable component is present as well as a low-charge smectite-group mineral in mixed-layer I/S from the Reindeer D-27 well, it is not apparent in ethylene-glycol solvated samples.

Differences between XRD profiles of ethylene-glycol solvated samples from this study and Ko (1992) must be considered in terms of chemical pretreatments, which produce additional vermiculite-like or high-charge smectite-group-like reflections. Harward et al. (1962) demonstrated that diffraction patterns of a 0.2-2.0 μm fraction of Ca^{2+}-saturated samples dispersed in water were the same as samples treated with sodium hexametaphosphate (Calgon). However, differences were observed in the amount of expandable components when the same samples were solvated with ethylene glycol. In addition, Calgon resulted in additional shoulders on low-angle reflections. Thorez (1985) discussed the effects of chemical pretreatments and concluded that not only are expanded components increased, frequently new phases appear having $d_{(001)}$ values equivalent to vermiculite and smectite. In addition, one may infer that the loss of the $(002)_{10}/(003)_{17}$ peak in chemically pretreated samples is the direct result of the harshness of chemical pretreatments on very fine fractions (<0.1 µm). This may be related to the charge heterogeneity of the expandable component, or due to the hydrolysis and removal of interlayer aluminum during H_2O_2 and SCBD treatments, causing the degradation of the clay minerals (Brewster 1980). However, sodium hexametaphosphate may produce Na-exchange resulting in a three-component mixed-layer I/S, i.e. illite/2-glycol smectite/1-glycol smectite (Dr. David Pevear 1993, personal comm.). If this is true, the $(002)_{10}/(003)_{17}$ is broadened by the addition of a 1-glycol layer 1.4 nm component smectite-group peak

Thus, the XRD results of this study are considered as more closely reflecting the mineralogy as it exists in the geological environment, for the fine fractions. However, as Brewster (1980) emphasized, carbonate and Fe-oxide bonding, and masking by amorphous materials, may prevent the characterization of the "natural clay system" by XRD It is apparent that ethylene glycol is not sensitive enough to indicate the presence of a high-charge smectite-group or vermiculite-component in an untreated sample from the Reindeer D-27 well. Although glycerol solvation in this study indicated the presence of more than one expandable component in mixed layers, it was not possible to determine the $d_{(001)}$ of the respective expandable components due to overlapping reflections.

7.2.1 Anomalous Profiles of the Reindeer D-27 Well

The diffraction patterns of samples from the Reindeer D-27 well are, in general, analogous to patterns derived from soil clays. These are characterized as being of "lesser" quality due to diminished intensity, unusual broadness and overlapping reflections, with displacement of reflection maxima and changes in peak shape resulting from increased background intensity (Stanjek et al. 1992).

There are many possibilities as to why the profiles from samples from the Reindeer D-27 well yield anomalously broad and diminished peaks as discussed in Chapters 3 and 4. Weir and Rayner (1974) investigated a <0.04 µm clay size fraction almost completely free of impurities from a soil profile and determined a two-component interstratified I/S. They attempted to determine the amount of expandable and non-expandable components using an early version of NEWMOD. Diffraction broadening and particle size were investigated by changing mean crystallite thicknesses from 7-13 to 3-7, 2-6, or 1-5 layers, and they were able to improve the agreement between experimental and calculated patterns. Changes in Fe and K values made negligible differences to the calculated patterns. The measured diffraction broadening suggested that the patterns observed are consistent with very thin diffracting domains consisting of four to five 2:1 silicate layers.

NEWMOD was used in this study to isolate the most important variables influencing anomalously broad peaks and diminished intensities of the experimental profiles. However, it is difficult to use the calculated patterns to accurately model the ultrafine particle size of the <0.05-μm clay fraction and achieve congruency with experimental patterns (Figs. 6.4a,b,c). In addition, NEWMOD is a program that is theoretically based on MacEwan crystallites, or a two-component system (whereas lattice-fringe images of this study suggested the presence of a multi-component system). NEWMOD 3C, which can model three-component systems, was not available to the author during the research.

To simulate two-component diffraction patterns with NEWMOD, a number of variables can be manipulated. In this instance, the most acceptable results were obtained using most of the default parameters of the program. The assigned parameters included: a step scan of 0.04° (the experimental step-scan was 0.01°), crystallite thicknesses of 7-14 layers in equal proportions, Mg^{2+} as saturating cation, 0.8 K atoms per illite half unit-cell, 0 Fe atoms per I-S half unit-cell, and smectite-group and illite thicknesses of 1.69 and 0.98 nm, respectively. The results were adequate in terms of reflection positions and in similarity of line shape (Figs. 6.4 a,b,c), but inadequate with respect to reflection intensity. Peak shape and position can be modeled using the parameters of LowN and HighN, (the largest and smallest crystallites present) or by the defect-broadening option δ which requires a value for the defect-free distance and N, the largest particle thickness. Agreement between experimental and calculated profiles was not improved by recalculating the patterns using a smaller mean crystallite thickness to achieve better results with respect to peak broadness, as reflections in the lower-angle region are unacceptably displaced to lower 2Θ angles. For example, to model the effects of small particle size (i.e. thin particles), layer thickness values for LowN and HighN of 2 and 5, respectively were assigned. The resulting calculated pattern exhibited a similar $(002)_{1.0}/(003)_{1.7}$ reflection with respect to the default parameter profile, but the $(001)_{1.0}/(002)_{1.7}$ reflection was displaced to lower 2Θ values. This was also true for the defect broadening option, as well as for increasing the amount of Fe or K atoms per I-S half unit-cell. A change in one parameter resulted in changes to the simulated profile that bore no relationship to the experimental results.

There was no way to manipulate the calculated pattern to achieve verisimilitude with the observed intensity and broad peaks of the experimental pattern.

As modeling of the XRD profiles suggested that particle thinness and stacking defects had marginal impact in controlling the diffraction profiles of the experimental patterns, the effect of strain broadening has been proposed as the dominant factor in controlling line shape, and especially for the samples treated with sodium hexametaphosphate. Reynolds (1989a) discussed strain broadening using the model of Warren and Averbach (1950), wherein the integrity of the unit cell is maintained, and distortions between unit cells are the result of random displacements. The effect of increasing random displacements between unit cells creates a diffraction profile with increased peak broadening and diminished intensity with minimal displacement in reflection position with respect to 2Θ (Reynolds 1992, his fig. 13). Strain broadening principally effects higher 2Θ angle reflections and to such a degree that they merge with the baseline. Increasing displacements between unit layers destroys long-range ordering and ultimately short-range ordering as well, until the profile resembles that of glass, and the only remaining peaks are at low angles. However, the effect of strain broadening on calculated diffraction profiles of I/S cannot be assessed using NEWMOD.

A partial explanation to the anomalous diffraction profiles may lie in the Mg^{2+}-saturated ethylene glycol and glycerol solvated diffraction patterns. Reynolds (1989a) predicted that a smectite-group mineral with variable interlayer thickness after ethylene glycol solvation is analogous to the displacement of unit layers in strain broadening. Ko (1992) suggested that the anomalous broadness and diminished intensities of the I-S reflections manifested in the Reindeer D-27 samples are due to varying thickness of the glycol complex within the interlayers resulting from the addition of a minor amount of high-charge expandable layers, or from possible ethylene glycol evaporation from thin samples. He suggested that some layers may form single layer complexes with ethylene glycol.

Recently, minerals with compositions and charges intermediate between end-member vermiculite and smectite have been described from soils and sediments, e.g. smectite-group phases with a vermiculite layer-charge range (April et al. 1986; Senkayi et al. 1983; 1985; Douglas 1982). These seemingly intermediate minerals have been variously described as low-charged vermiculites, high-charged smectites, and beidellites. Güven (1988) suggested that a low-charge vermiculite and a high-charge smectite (layer charge of -0.5 to -0.7 per $O_{10}(OH)_2$) may have the same layer charge but different expansion behavior. Generally, the experimental

XRD patterns reveal that the expandable component behaves like a low-charge smectite-group mineral when solvated with ethylene glycol (Fig. 6.3), but behaves like a mixture of low-charge smectite-group and high-charge smectite-group or vermiculite minerals when solvated with glycerol (Fig. 6.5). The Mg^{2+}-saturated glycerol solvated patterns (Fig. 6.5) indicate that the I/S response changed with type of ordering i.e. one- and two-layer comlexes with R0 and single complexes with R1 and R>1. It is apparent that deeper samples have a greater abundance of higher charge expandable layers as indicated by the almost identical reflection positions for glycerol and ethylene-glycol solvation at low 2Θ angles (but not for higher 2Θ angle reflections). This suggests that there is an increasing high-charge smectite-group or vermiculite component and a decreasing low-charge expandable component with depth. This is consistent with Ko's (1992) K-saturation results. It also confirms the results of Powell et al. (1978) and Foscolos and Powell (1980) who reported a vermiculite-like component in the Reindeer D-27 well. It was concluded that a three-component mixed-layer system was produced, and that smectite-group minerals were converted to illite through an intermediate vermiculite.

Without three-component modeling however, neither the proportions of each component can be deduced, nor can the nature of the interstratification be detailed.

7.3 Effects of Sodium Hexametaphosphate on Layer Structure

7.3.1 Ethylene Glycol-Solvated Samples

Strain broadening is applicable to other types of disorder that involve displacements between scattering domains (e.g. unit layers). Reynolds (1989a) demonstrated that, if there is minimal displacement or separation between scattering domains, the individual domains form an X-ray coherent relationship or array. If, however, there is a relatively large separation between scattering domains, the scattering relationship is incoherent. For intermediate cases between these two extremes, the unit layers form a scattering array that is termed partially coherent. With the exception of the 4800 ft depth sample, comparing the $(001)_{10}/(001)_{17}$ peak of the <0.05 μm fractions of the untreated and treated samples (Fig. 6.1a and 6.2a) reveals, as best as can be estimated by visual inspection, that reflection displacement with respect to 2Θ, while apparent, is not as profound as the effects of peak broadening and diminished intensity. It is difficult to evaluate peak shape for these fine fractions. Breadths of the $(002)_{10}/(003)_{17}$ reflection of the treated sample cannot be measured to determine crystallite thicknesses. Even in the 0.05-0.1 μm fractions, modifications of the diffraction pr[illegible] evident (Fig. 6.1b and 6.2b). However, the 4800 ft sample exhibits a diffraction pattern that is very similar for both untreated and treated samples. The $(00l)$ diffraction series remain relatively sharp because they represent diffraction from an entire stack of layers (Reynolds 1989b). Treated samples with increased amounts of a non-expandable component tend to display increasing loss of longer-range ordering between unit layers, without decreasing significantly the thickness of the particles as compared to the untreated samples. As different specimen mounts were attempted for XRD analysis, all giving the same results, the only conclusion is that the treated dispersed particles did not reconstitute into large X-ray coherent stacking sequences compared to the untreated sample.

This phenomenon can best be explained by strain broadening, which suggests that peak width increases and intensity diminishes, especially in higher angle reflections, without significant 2Θ peak displacement, as a consequence of increasing distance between X-ray coherent unit layers (Reynolds 1989a) Eberl et al (1987) demonstrated that decreasing grain size produced a sharper rise in background at smaller 2Θ angles and a more intense background band between 22° and 33° 2Θ. This is evident in the treated samples From computer simulation of pure clay mineral phases, Drits et al. (1984) demonstrated that this band resulted from rotational stacking faults (+60° or +120°). Eberl et al (1987) concluded that the density of rotational faults increases in the finer fractions of sericites However, it is important to note that the presence of X-ray amorphous material will also yield high background intensities between 20° to 45° 2Θ, which is present in the clay material collected in this study (Fig 6 6)

The addition of a peptizer such as sodium hexametaphosphate changes the chemistry of the clay suspension as well as chemically modifying or altering the surface characteristics and interlayers of the primary clay particles (Whitehouse and Jeffries 1955, see also Chapter 4). The chemical reaction with the peptizer may have irreversible effects on the clay structure The dispersive ability of sodium hexametaphophate results from the reversal of edge charges of the clay particles (van Olphen 1977; 1987). Phosphate anions are chemisorbed to the broken clay particle edges forming complexes with the exposed cations of the octahedral sheet. Reversal of the edge charges eliminates mutual flocculation and creates a sufficient charge level to prevent attraction by van der Waals' forces An additional effect is the replacement of exchangeable interlayer cations by Na^+, which may expand the interlayer distances of the dispersed units. Thus artifacts are probably indeed induced by chemical pretreatment.

Structural artifacts are intimately related to chemical changes. XRD analysis of this investigation suggested that when the <0.05 µm size fractions were prepared for XRD mounts, the adsorbed phosphate ions on the clay edges, the Na^+-exchanged interlayer cations and the exchanged cations on the clay surfaces interfered with the subsequent rearticulation of the original ultrafine clay particles during air drying. This resulted not only in differences in the amounts of the measured expandable components between untreated and treated samples, but because the original particles did not rearticulate, thinner layer sequences consisting of smaller X-ray coherent scattering domains were generated. Division of a crystal into smaller X-ray coherent scattering domains results in decreased reflection intensity (Drits and Tchoubar 1990).

Results presented here contradict some of the results in the published literature. It has been shown that Na-montmorillonite can be easily dispersed by osmotic swelling and, after air drying, will reassemble into X-ray coherent scattering domains (Norrish 1954). Reynolds (1992) also demonstrated in XRD patterns obtained from rock fragments, and from <1 µm random and oriented K-bentonite samples treated with sodium pyrophosphate, that laboratory preparation procedures did not induce structural artifacts. The conclusion is that the original samples either did not disaggregate into fundamental particles, or if they did, the fundamental particles rearticulated duplicating the one-dimensional structures of the original, untreated rock. Results from this study indicate that the ultrafine clay-size fractions from the Beaufort-Mackenzie Basin are far more sensitive to chemical pretreatments than coarser fractions. Clay material of this study dispersed with sodium hexametaphopshate clearly produced structural artifacts Not only are the reflection intensities significantly diminished but are displaced and broadened This would result in inaccurate estimates of expandability, if the reflections could be measured. Consequently, the peptizer not only altered the arrangement of layers or the stacking sequences, but modified the interlayers as well. Structural artifacts are induced in ultrafine size fractions during sample preparation.

It is important to note that the effects of sodium hexametaphosphate may be different for smectite-group-rich I/S and illite-rich I/S. It is suggested that if separation of mixed-layer I/S occurred along smectitic interlayers, the layers could rearticulate preferentially along the same faces during drying, resulting in little change in the one-dimensional XRD pattern (Ahn and Peacor 1986b; Ahn and Peacor 1989). The creation of structural artifacts however is evident with decreasing size fractions, but these artifacts may also be dependent on composition. The 4800 ft depth sample displays little difference between untreated and treated samples. Yet these differences are more significant in deeper samples which have an increasing illite content

7.3.2 n-Alkylammonium-Ion Exchanged Samples

Exchanging the samples with octylammonium ions ($n_c = 8$) should produce diffraction patterns with a first order basal reflection at 1.8-2.1 nm for high-charged smectite-group or vermiculite components and a 1.3-1.4 nm peak for a low-charge smectite-group component (Lagaly and Weiss 1969, 1970; Lagaly 1981, Ghabru et al 1989). A first-order 1.0 nm reflection for illite should also be present and not be affected by the $n_c = 8$ exchange. After exchange with octadecylammonium ions ($n_c = 18$), a first-order reflection would be expected at 2.2-2.6 nm if a high-charge smectite-group or vermiculite component is present, and a first-order reflection at 1.8-2.1 nm for a low-charge smectite-group component. In addition, a first-order reflection of 9.8-1.0 nm for a non-expandable component of illite, and a first-order reflection of 2.8-3.1 nm for expandable illite may be apparent. These reflections would only be present if individual components are present in coherent sequences and the material does not contain impurities or sample contamination. However, the investigation of the diagenetic mixed-layer I/S from the Reindeer D-27 well did not give expected diffraction results. Since there is no detailed information available in the literature, an attempt is made to discuss the discrepancies between theoretical and experimental results. Simply stated, n-alkylammonium-ion exchange of untreated samples generated unforseen results in the XRD analysis, and thus it is even more difficult to assess the changes manifested in the treated samples.

7.3.2.1 n-Alkylammonium-Ion Interaction

The question arises as to why n-alkylammonium-ion exchange gives anomalous results with diagenetic mixed-layer I/S in the Reindeer D-27 well. Clay-organic interactions are not easy to understand nor to decipher (Malberg et al. 1989). It has been suggested that the application of alkylammonium-ion exchange may produce inconsistent results due to variations in the washing and drying procedures (Johns and Sen Gupta 1967; Walker 1967). Weiss (1963) concluded that the determination of *d*-values is dependent on sample preparation and pretreatment, such as washing with water or alcohol, temperature of drying, and grinding of samples. To achieve acceptable results, it is necessary to use an excess of alkylammonium ions over the exchange capacity of the clay minerals. However, the degree of exchange is also affected by the magnitude and distribution of layer charge of the minerals present, the particle size, the temperature of treatment, pH, type of interlayer cation, type of clay mineral, the degree of dispersion, the use of chemical pretreatment, the presence of electrolytes and the alkyl chain-length and solution concentration (Walker 1967, Lagaly 1982). There are few published data specifying the individual effects of each factor on the *d*-spacing values. There may be incomplete or variable penetration of the alkyl chains with insufficient solution concentration, whereas concentrated solutions may cause exfoliation of the crystallites, especially with longer chains and higher temperatures. This may be a problem in ultrafine clay minerals, which have a large surface area and are thus, chemically very reactive. The rate of drying must be sufficient to allow the alkyl chains to move over one another, otherwise the chains may stick and interfere, and subsequent kinking interferes with the interpenetration of the chains into interlayer space (Lagaly 1976). However, procedures employing alkylammonium ions used in this study have been used effectively by Vali and coworkers and are fairly standardized (see bibliography). Thus the explanation for the variability in the basal spacings between experimental and theoretical values must lie with the compositions of the clay material itself.

It is important to note that the clay materials investigated in this study are not pure materials nor were chemical pretreatments employed to increase their purity (see Chapter 4). The clay minerals therefore contain various organic, inorganic and amorphous materials both adsorbed on the clay surfaces and as interlayer materials. Barefoot and Van Elsberg (1975) recognized two adsorbed layers in clays from the Beaufort-Mackenzie Basin: (1) an outer, poorly structured layer consisting of water, and possibly organic and inorganic complexes, and (2) an inner, more structured layer containing silanol groups, organic compounds and metals (e.g. Fe, Mn, Pb, Zn).

Lagaly (1981) reported that organic molecules adsorbed at the edges of clay material may partially penetrate the interlayer during alkylammonium exchange resulting in increased interlayer spacing. Hydrocarbons were present in these samples during separation and can react with the alkylammonium ions during the exchange processes (Malberg et al. 1989). Polar molecules such as ethanol which are used for washing can aggregate and cluster between alkyl chains within the interlayers of some vermiculite and smectite-group minerals and can cause additional expansion (Lagaly 1981). Vali and Hesse (1992) suggested that this may be the cause of increased basal spacings in XRD patterns for fine-grained particles. In addition, erroneous values for basal spacings from a paraffin-type structure may be generated due to less-than-perfect, paraffin-type, chain packing (Malla and Douglas 1987).

Direct imaging of the layer structures of alkylammonium-ion exchanged I/S in HRTEM enables the determination of the structures present in the sample. However, discrepancies are encountered here as well. Low-charge smectite-group layers often were observed as dispersed layers rather than as coherent sequences with a uniform spacing of 1.3-1.4 nm after $n_c = 8$ exchange or with a uniform spacing of 1.8-2.1 nm after exchange with $n_c = 18$. Malberg et al. (1989) concluded that when montmorillonites are immersed in ethanol in order to remove excess alkylammonium ions, not only dispersion and curling of the layers occurred, but some packets also broke apart. In addition, some of the interlayer spacings of the layer structures did not display consistent expansion, especially if compared to coarser size fractions. Stanjek et al. (1992) demonstrated that fine clay minerals (<0.1 µm) from soils did not completely exchange the alkyl-chains and resulted in incomplete expansion of the interlayers.

The lack of some expected reflections in XRD, especially first-order reflections of a high-charge smectite-group or vermiculite component after $n_c = 8$ exchange, indicated that some layer structures did not occur as coherent sequences, as was visible in HRTEM. In addition, diffuse reflections of some low-angle peaks in $n_c = 18$ exchanged samples (e.g., 12500-12550 ft, Fig. 6.9a) may indicate the presence of stacking disorders of expandable and nonexpandable layers (Figs. 6.26 and 6.27). Vali et al. (1991) indicated that some structures observed in HRTEM may not be visible in the XRD patterns due to (i) the possibility of peak overlap, (ii) the small amounts present of certain phases, and (iii) the random distribution of very thin packets or layers. In addition, the HRTEM observations indicate that the interfaces of some adjacent packets of non-expanded illite do not respond in a consistent manner to $n_c = 18$, which suggested that some of the basal surfaces did not expand.

7.3.2.2. Chemically-Induced Artifacts

Whereas it is apparent that sodium hexametaphosphate has an inimical effect on the stacking sequences constructing coherent X-ray scattering domains in ethylene-glycol solvated samples, the opposite effect is apparent in samples exchanged with n-alkylammonium ions. All three sets of diffraction patterns of sodium hexametaphosphate-treated and n-alkylammonium ion exchanged specimens, each from a different depth and having different Reichweite values, displayed increased complexity: additional and overlapped reflections, and increased intensity (Figs. 6.7b, 6.8b; 6.9b). To the author's knowledge, these are the first reported examples documenting these changes, although pretreatment is acknowledged as a possible factor influencing *d*-spacing values (Malberg et al. 1989; Ghabru et al 1989). Inconsistensies and contradictions are apparent when comparing the untreated and treated alkylammonium-ion exchanged diffraction profiles, i.e. the presence or absence of reflections. Two explanations are possible for the differences observed: (i) the reflections represent modifications to the expandable components, such as alteration of the interlayer charge densities and/or the arrangement of layers in stacking sequences, or (ii) the reflections may not represent a physical phenomenon derived from the layer structures but rather may be artifacts induced by a chemical reaction between the various components. The second explanation is difficult to verify as the emphasis of this study was to examine and identify the changes in layer structure with depth and an investigation of the reaction products from treatment with a peptizer was not possible.

The additional sharp reflections in the treated samples exchanged with n-alkylammonium ions may correspond to modifications of the interlayer-charge densities or the arrangement of layer structures present in the sample, producing a new series of reflections. If we assume that the integral series of peaks of the untreated and treated samples are somehow related, i.e., that sodium hexametaphosphate has altered the response of mixed-layers to alkylammonium ions then an interesting phenonmenon is discerned. A comparison of the diffraction profiles of the untreated and treated, $n_C=18$ exchanged sample from 12500-12550 ft, which displayed only one series of integral reflections, showed that the untreated sample has a first-order reflection at 5.2 nm, but in the treated sample, this first-order reflection was displaced to a higher 2Θ angle corresponding to a basal spacing of 4.46 nm. This reflection displacement is also observed in the untreated and treated 8700-8750 ft samples. However, the second set of integral reflections in the 8700-8750 ft samples, with a first-order reflection of 3.72 nm in the untreated sample has in fact been displaced in the opposite direction, to a lower 2Θ angle giving a first-order reflection of 4.05 nm.

It is difficult to speculate why the sodium hexametaphosphate treatment responded differently to different layer structures. The contrasting effect that the sodium hexametaphosphate treatment had on these two structures suggests that some form of mineral modification occurs following treatment. However, these modifications are not anomalous but are constant as a comparison between the 8700-8750 and 12500-12550 ft samples revealed, as well as between other samples of intermediate depths (not shown) This phenomenon must be related to the composition or interlayer cation density of the layer structures present and thus may be the reason for the different responses to sodium hexametaphosphate. However, without in-depth geochemical analysis of the layer structures exhibited in the lattice-fringe images, no conclusive answer can be given.

No instances of interactions between chemical treatments and alkylammonium ions have been reported in the literature. Lindgreen and Hansen (1991), however, reported a small sharp peak resulting from the reaction of Mg^{2+}-saturated I/S and adsorbed phosphate, however it did not affect the appearance of other reflections. In the deeper treated samples, diffraction patterns showed a complete new series of reflections. This is to be expected for various pretreatments and has been documented in published XRD studies (for review see Chapter 4)

The question arises whether the differences between untreated and treated samples observed in HRTEM correspond to the additional reflections in XRD (which may very well be the case) or are indeed reflections from chemical complexing or precipitates from the reaction of sodium hexametaphosphate, i.e. phosphate ions, alkylammonium ions, and other adsorbed or interlayer material. Precipitates, however were not imaged in HRTEM

The basis for questioning the validity of XRD patterns of treated samples is that peaks from all three depths, 4800 ft, 8700-8750 ft and 12500-12550 ft depths (as well as the additional samples not shown), have an integral series of remarkably coincident reflections that are difficult to reconcile to known layer structures. This could be explained by assuming that the three depths have similar components (e.g illitic material). The conclusion is that the reflections in the untreated samples correlate with real layer-structure phenomena, and the additional peaks in the treated samples are preparation artifacts of sample pretreatment

In the diffraction patterns of treated and n_c =8 exchanged samples, all samples displayed sharp reflections at remarkably constant spacings of approximately, 2.5-2.4, 1.25 and 0.83 nm. However, with the exception of the 4800 ft sample, the treated samples showed none of the reflections that are present in the untreated samples

The diffraction patterns of the treated and n_c =18 exchanged samples display a more complex series of overlapping reflections making peak position difficult to determine accurately. However, there is a series of nearly integral peaks from all three depths in the ranges of 1.49-1.46 nm, 1.12 nm, 0.91-0.89 nm, 0.76-0.75 nm, and 0.65-0.60 nm The simplest solution is to assume that the sharp peaks of the 12500-12550 ft sample represent artifacts and assume this same set of reflections appears at the other two depths, but is slightly shifted due to peak overlap from other peaks Assuming a first-order reflection of approximately 4.46 nm, the rest of the peaks are exactly integral, and neglecting overlap, the reflections compare favourably to the 4800 and 8700-8750 ft samples. However, the question is still, what happened to the peaks in the untreated sample? The answer may simply be that the treated samples have higher intensity peaks and the reflections of the untreated sample are lost in the background.

Irrespective of either explanation, it is clear that the addition of sodium hexametaphosphate is altering not only the arrangement of layers, but the interlayers as well. This is clearly visible in the lattice-fringe images. If the primary structure is altered or destroyed by chemical pretreatments or peptizers, the disruption may be irreversible. A similar conclusion was evinced in the treated ethylene-glycol solvated samples.

As TEM can directly image the layer structures of the untreated and treated samples exchanged with n-alkylammonium ions, differences are more readily observed. Comparisons between the untreated and treated samples reveal significant differences between the distribution and orientation of layer structures in TEM. Firstly, both the untreated and treated samples displayed the same types of layer structures for each depth. No additional types of layer structures were visible There were, however, modifications to these layer structures. As was to be expected, all treated samples displayed decreased layer aggregation and better orientation of the layer structures within the ultrathin section. In addition, treated samples from all depths displayed increases in the amount and coherency of expanded layers, either high-charge smectite-group layers or expandable illite layers, and a general decrease in the thickness of packets containing non-expanded interlayers Sequences of a high-charged expandable component were much more apparent in the treated than the untreated sample. R1-ordered structures were more apparent in the treated samples. However, these differences can be very subtle, and often changes were more apparent in the XRD patterns. In general, the most common phenomenon was increased expandability in treated samples.

In the 4800 ft sample exchanged with $n_C=18$, sequences of high-charge smectite-group or vermiculite layers were more uniform and displayed thicker sequences of layers (Figs. 6.18 and 6.19), but these modifications were more easily detectable in their respective XRD patterns (Figs. 6.7a,b) However, differences between treated and untreated samples were especially apparent in the 12500-12550 ft depth sample exchanged with $n_C=18$, which exibited significant increases in the amount of packets of expandable illite layers as well as in the number of expanded interlayers in each packet (Figs. 6.25 and 6.28). As well, there were significant increases in the sequences of double layers in the deeper samples (Fig. 6.22). No $n_c = 18$ treated sample was available for the 8700-8750 ft level.

It is difficult to directly compare the XRD profiles and lattice-fringe images for the samples presented in this study for reasons outlined in Section 7.3.2.1. Lattice-fringe images showed the presence of multiple layer structures which differed both in composition and abundance with depth. However, these components were not always easily identifiable or were not present in the respective diffraction patterns. Whereas differences existed between the untreated and treated samples for each analytical technique, e.g. between untreated XRD and treated XRD or between untreated TEM and treated TEM, it is not possible however, to reconcile the differences when comparing between techniques, e.g. between XRD and TEM, except qualitatively. Thus, general changes observed in XRD patterns correspond to changes observed in lattice-fringe images, but it is difficult to be specific.

7.4 Comparison of Ethylene Glycol Solvation and n-Alkylammonium-Ion Exchange for I/S Identification

Solvation with ethylene glycol or glycerol will only show whether a mineral will expand to form a double layer complex or remain as a single layer complex, and thus can only measure expandability. However, ethylene glycol and glycerol thickness, hence expandability, is affected not only by the layer charge but also by the type of interlayer cation and the relative humidity (RH) (Środoń 1980). Glycerol solvation to distinguish between smectite-group minerals and vermiculite may be misleading because the interpretation of the spacings of clay minerals for identification purposes is dependent on the solvation method used (Ross and Kodama 1984; Malla and Douglas 1987a). Smectite-group components and vermiculites encompass minerals with a wide range of layer charges and intermediate expandable minerals may show properties of both minerals when subjected to ethylene glycol and glycerol. In addition, these organic molecules are limited to estimating the proportion of expanding layers in I/S and cannot give evidence of the layer charge. As routine methods for determining the expandable component, they provide no information on the possible heterogeneous composition or layer structure of I/S (Figs. 6.3 and 6.5). These techniques thus cannot be used to distinguish between a smectite-group mineral in I/S and smectite-like behaviour assumed for fundamental illite particles

Reflection intensity is much greater with alkylammonium-ion exchange than with ethylene glycol or glycerol. Alkylammonium ions measure the layer-charge density of layer structures from which the layer charge may be deduced. This reflects the different response of the interlayers to alkylammoniun-ion treatment which is due to differences in the nature of the isomorphous substitution within the 2:1 layer silicates (Vali et al. 1993a). Long-chain alkylammonium ions such as octadecylammonium can differentiate between minerals having similar properties on the basis of layer-charge density, i.e. low- and high-charge smectite or vermiculite components, and expandable high-charge and very high-charge illite. Thus, alkylammionium ions can distinguish between mixed-layer expandable components on the basis of layer-charge differences. In addition, the use of a short alkyl-chain such as octylammonium ions can distinguish between a high-charge vermiculite and a high-charge illite.

Alkylammonium-ion exchange has also revealed that the layer structures making up the components in the <0.05 µm size fractions are much more complex than revealed by ethylene-glycol solvation. This makes interpretations difficult without an in-depth investigation. Alkylammonium ions cannot be used to quantify the proportions of expandable components in mixed-layer I/S samples (Lagaly 1979). Alkylammonium-ion exchange was utilized in this study to characterize the different layer structures of interlayered I/S in a series of samples in which ethylene glycol solvation indicated a two-component I/S Alkylammonium-ion exchange clearly indicated that the components present do not consist exclusively of a low-charge and a high-charge mineral, but rather of layer structures with extensive variation in the layer charge-density of expandable components within a mixed-layer structure. However, to accurately decipher the complexities observed in the XRD patterns of this study, modelling of three- and four-component systems must be used in the future, e.g., NEWMOD 3C

7.5 Discrepancies between XRD and HRTEM

Using NEWMOD (ver. 2) to model the apparent depth-related changes in I/S is not sensitive enough to reveal the heterogeneous composition observed in HRTEM. In addition, these methods cannot be adapted readily to three- or four-component systems. Along the same lines, Drits (1987) emphasized that diffraction patterns characterized with ethylene glycol or glycerol are not sensitive enough to reveal the structural or compositional heterogeneity in I/S.

Determining the precise thickness of layers and coherent scattering domains is a problem in XRD studies. If individual layer structures have a range of compositions (based on differences in layer charge), as this study indicated, then XRD results give only the average compositions of heterogeneous I-S, as previously suggested by Ahn and Peacor (1986a). This is especially obvious when comparing experimental patterns with calculated patterns (Figs. 6.4a,b,c) which indicated a two-component system, yet the lattice-fringe images of the same material just as clearly indicated three and four components of related but differing composition. Thus the significant advantage of the TEM combined with n-alkylammonium ion exchange technique is that it allows the direct imaging of individual layer structures and at a scale of smectite-group and illite layers and interlayers. In addition, as this study has shown, the layer structures in ultrathin-section can be unambiguously identified, in contrast to beam-milled specimens. As well, ultramicrotomy does not induce artificial amorphization.

In general, the diffraction patterns of the n_c=8 exchanged, untreated clay separates displayed features that are characteristic of both the air-dried and ethylene glycol-solvated diffraction patterns (Figs. 6.7a, 6.8a, and 6.9a). The lower-order reflections are broad which is suggestive of a peak containing three components (1.7-1.37-1.0 nm), yet the higher-order reflections corresponding to these components are not present. The corresponding lattice-fringe images clearly indicate mixtures of three and four types of layer structures, which varied in abundance with depth. The diffraction patterns of the n_c=18 exchanged untreated samples clearly indicate the complexity of the components within this size fraction, beyond the ethylene-glycol result of one expandable and one non-expandable component in I/S. The 8700-8750 ft sample implied the presence of R1- and R3-ordered components, and the 12500-12550 ft sample displays just the R3-ordered component, but the thickness of the expandable layers was inconsistent. Both these components were identified in lattice-fringe images.

Attempts to integrate results from XRD and TEM face the problem of adequately characterizing the expandable component in I/S. Implicit in the discussion is the question whether mixed-layer I/S can be detected in TEM or HRTEM. Utilizing the compositional focusing of Guthrie and Veblen (1989, 1990), a number of studies have purported to be able to distinguish between smectite-group interlayers and illite interlayers and to determine periodicity in ordered I/S structures (Ahn and Peacor 1989; Hansen and Lindgreen 1989; Veblen et al. 1990; Środoń et al. 1990; Lindgreen and Hansen 1991; Amouric and Olives 1991; Murakami et al. 1993).

Eberl et al. (1987) suggested that the precise measurement of expandable layers in I/S by XRD depended on acquiring the correct thickness of both illite and smectite-group layers. Eberl and Środoń (1988) suggested that expandabilities measured in TEM images were higher than in XRD due to the presence of non-swelling basal surfaces at the ends of stacks of illite layers. From an investigation of volcanic materials from diagenetic and hydrothermal environments, Środoń et al. (1992) concluded that HRTEM measurements yield similar expandability values to those obtained in XRD when crystal edges were neglected, whereas in considering the crystal edge of disarticulated particles similar expandability values are obtained to those calculated from thickness estimates in Pt-C shadowed images from TEM. However, the preservation of the original texture of the material is questioned as methanol undeniably dehydrates the interlayers. It also neglects the possibility of expandable layers having different layer charges. Other studies attempted to compare XRD and TEM by counting the number of illite and smectite-group layers in lattice fringe images (Veblen et al 1990; Amouric and Olives 1991, Murakami et al 1993). All of the previous approaches of XRD and TEM comparisons are based on a two-component system of illite and smectite-group components, and cannot be applied to this study.

A representative disordered I/S crystallite does not exist and no HRTEM image can be representative of the crystallite distribution that XRD measures, unless all crystallites are identical (Reynolds 1992). This is true for beam-milled specimens or grain mounts, but not for clay separates exchanged with alkylammonium ions which can be representative of the distribution of layer structures as they exist in specimens produced for XRD analysis. Laird et al. (1989a) concluded from a combined XRD and TEM study of octylammonium-ion exchanged clay minerals that only a small part of a specimen needs to be properly oriented to account for coherently diffracted domains depicted in the diffraction reflections. Thus, if there is a problem with a comparison between XRD and TEM results, the problem is inherent to the XRD method which is unable to accurately identify all the expandable components in samples from the Reindeer D-27 well.

7.6 Layer Structures in Mixed-Layer I/S of the Reindeer D-27 Well

There has been much discussion and debate concerning the characterization of smectite-group minerals, illite and I/S with emphasis on the definition of a 'phase', the existence of "interstratification", the composition of the expandable components, the nature of particle boundary coherency, and the relevance of short- and long-range order (Nadeau et al 1984a,b,c; Ahn and Peacor 1986a, 1989; Sass et al. 1987, Altaner and Bethke 1988; Ransom and Helgeson 1989; Rosenberg et al. 1990; Veblen et al 1990; Ahn and Buseck 1990; Aja et al 1991a,b, 1992; Vali et al. 1991; Reynolds 1992) Results from different theoretical and analytical investigations have failed to resolve some of these basic questions Peacor (1992) succinctly summarized much of the recent discussions from a TEM point of view

The classic model of interstratified I/S as a two-component system was originally conceived from diffraction studies (MacEwan 1956, 1958, Reynolds and Hower 1970; Reynolds 1980). As a single unified mineral therefore, I/S cannot be disassembled into its component layers that approach a thickness of one unit layer, nor can it be reconstituted into its original stacking sequence (Reynolds 1992). Mixed-layer I/S is considered to be two thermodynamically distinct phases incorporated into a single coherent mineral (Altaner and Vergo 1988; Altaner and Bethke 1988; Altaner et al. 1988). This model visualizes that layer types within MacEwan crystallites are divided at the center of the octahedral sheets and thus, the interlayer is within the structure unit and not at the boundaries (Hower 1967) Ahn and Peacor (1986b) suggested that assuming illite and smectite layers extend from interlayer to interlayer does not account for the possible presence of two types of interlayers

Analogous to Na-montmorillonite (Norrish 1954), natural three-dimensional MacEwan crystallites which consist of illite and smectite-group layers may separate or dissociate at the smectitic interlayer into thin fundamental particles during grinding or dispersion in liquids, as a result of osmotic swelling (Altaner and Bethke 1988; Ahn and Peacor 1989, Veblen et al. 1990; Ahn and Veblen 1990). Altaner et al. (1988) provided evidence from ^{29}Si NMR studies which indicated that illite-rich I/S contains both a high-charge Al-rich illite and a low-charge Al-poor smectite. Ahn and Peacor (1986b) claimed from TEM studies that rectorite can separate along the smectitic interlayer giving rise to 2.0 nm thick units (fundamental illite particles).

The fundamental-particle model of Nadeau et al. (1984a,b,c) considers sequences of layers within an original rock and in XRD sample mounts as aggregates of fundamental particles of smectite and illite. In this model, an elementary smectite-group particle is defined as one 2:1 layer with a thickness of 1.0 nm and an elementary illite particle as two 2:1 silicate layers coordinated about a K interlayer. It was further proposed that in diffraction studies, fundamental particles of smectite-group and illite were present as random mixtures in disordered

I/S, whereas ordered samples consisted of aggregates of fundamental illite particles (single thermodymanic phase), whose basal surfaces were capable of adsorbing water, cations and organic molecules, giving rise to interparticle diffraction, and thus mimicking the expandable behaviour of a smectite-group mineral (Wilson and Nadeau 1985; Eberl et al. 1987). According to this model, this would result in various ordering types, with 2.0 nm and 4.0 nm thick layers of fundamental illite particles dominating R1- and R3-ordered I/S structures. In addition, Nadeau et al. (1984a,b,c) and Nadeau (1985) concluded from Pt-C shadowed clay separates that fundamental particles of illite and smectite are primary crystallization products and not secondary products from the disarticulation of larger crystals resulting from sample preparation.

From equilibrium studies, Rosenberg et al. (1990) and Aja et al. (1991a, 1991b) proposed that mixed-layer I/S was a mixture of one or more stoichiometric mica-like phases. According to the multiphase model, natural illite is composed of at least four discrete mica-like layers types: S(R0), IS(R1), ISII(R3) and I that behave as discrete, thermodynamic phases (Rosenberg et al. 1990). However, results from this study indicate that these proposed mica-like phases may be applicable to the different types of layer structures imaged in HRTEM rather than to their proposed stacking sequences.

Lattice-fringe images of beam-milled samples of smectite-group minerals, illite and I-S consist of packets of sequences of a few to many tens of layers (Ahn and Peacor 1986a; 1989; Yau et al. 1987, 1988, Jiang et al. 1990a,b; Buatier et al. 1992). Attempts have been made to determine with the aid of TEM images whether layers or packets occur as free or separate particles. The implication in fundamental particle theory is that incoherently stacked particles are separate particles. Vali et al (1991) demonstrated from combined freeze-etch replicas and ultrathin sections that free particles of illite and glauconite consisted of several packets and concluded that the size of free particles of illite is not that of fundamental illite particles. However, free particles of smectite can occur as fundamental smectite particles (Vali and Bachmann 1988) For smectite-group minerals in shales from the Gulf of Mexico, Freed and Peacor (1992) demonstrated that they were incoherently stacked. In lattice-fringe images of beam-milled samples of hydrothermal I/S and burial diagenetic I/S, respectively, Veblen et al. (1990) and Ahn and Buseck (1990) demonstrated that coherency existed between several sequential layers (implying particles thicker than fundamental layers). In contrast, Reynolds (1992) demonstrated using three-dimensional XRD (random mounts) analysis, that turbostratic displacements occurred at the expandable interfaces between fundamental particles, again implying the existence of separate particles. Consequently, XRD and TEM results cannot be directly correlated using conventional methods, e.g. ethylene glycol in XRD or overfocus conditions in TEM.

The I/S debate revolves around the characterization of the expandable component because of the inability at present to determine the chemical composition of the basal surfaces of packets. The determination of a smectite-group mineral must be achieved through indirect methods. For example, Ahn and Peacor (1986b) assumed that because rectorite separated into 2.0 nm thick units, it was a smectite-group layer. However, the charge of the layer is important because it determines the ability of the clays to retain cations, it influences the selectivity of clays for various cations, and it affects the ability of clays to absorb water or organic molecules (Laird et al. 1989a). Image simulations for the TEM assumed a smectitic structural formula for mixed layer I/S (Guthrie and Veblen 1989; Ahn and Busek 1990). However, Veblen et al (1990) indicated from experimental images that smectite interlayers were characterized by dark fringes and illite interlayers by less dark fringes. Ahn and Buseck (1990) deduced from ultrahigh-resolution TEM that simulated images of I/S were also different from the experimental images of I/S, which suggested that the expandable layer was again not a smectite-group phase.

Results from this study indicate that in underfocus conditions with alkylammonium-ion exchange, dispersed smectite-group phases are a single layer thick, but when imaged in overfocused conditions to determine composition, the structures are two layers thick, making distinction between smectite-group and illite impossible. Other results of this study suggest that I/S does not consist of a smectite-group mineral, i.e., the sodium-hexametaphosphate treated <0.05 µm fractions show that smectite-group-rich sediments behave differently in their stacking behaviour in XRD speci[illegible] than illite-rich specimens (Figs. 6.2a, 4800 ft and 12500-12550 ft depth samples). Vali and Hesse (1990) argued that untreated smectite layers in the TEM have a thickness approximately 1.3 nm (Ahn and Peacor 1986a; Bell 1986, Huff et al 1988, Vali and Köster 1986), whereas the expandable layer in mixed-layer I/S collapses to 1.0 nm. They concluded that the layers behaved more like untreated vermiculite with a 0.96-1.0 nm spacing in the TEM (Vali and Köster 1986; Ghabru et al 1989). In addition, if MacEwan crystallites separate along smectitic interlayers, why are smectite layers only imaged in shallow samples and not in deep samples?

Lattice-fringe images from the alkylammonium-ion exchanged <0.05 µm fraction from the Reindeer D-27 well in the Beaufort-Mackenzie Basin generally support the fundamental particle and multiphase illite models, with some distinctions. Clay separates of the <0.05 µm fraction were prepared without chemical pretreatment, but after exchange with $n_c=8$ and $n_c=18$ ions, components with different layer charges could be clearly distinguished in the TEM. In this study, lattice-fringe images revealed five distinct types of layer structures based on the response of the interlayer to n-alkylammonium ions. This interpretation is based on earlier and continuing studies of Dr H Vali and coworkers (see bibliography). Correlations are made between the lattice fringe spacings using values of $d_{(001)}$ for known structure types under constant experimental conditions, after exchange with alkylammonium ions. This study revealed that not only did the proportions of the layer structures change with depth, but that new layer structures were formed (Sears et al 1993a)

The concept of discrete layer structures can be best understood with respect to the P-layer (polar) model as articulated by Güven (1991). Polar layers have been described in earlier studies of Lippman and Johns (1969), Lagaly (1979) and Brown (1984) who detected asymmetrically charged layers adjacent to the interlayer space. Lippman and Johns (1969) suggested that during chemical alteration of an interlayer, modification of the tetrahedial sheets may occur, resulting in the 2:1 layer acquiring a polar character and leaving adjacent layers unmodified Thus, a polar layer has one tetrahedral sheet with low- or no-charge and the other tetrahedral sheet carries a high-charge. This concept was re-articulated for interstratified 2:1 silicate layers observed in the TEM by incorporating the P-layer model (Vali et al. 1993a). Similar to the fundamental particle concept of Nadeau et al. (1984a,b,c), polar layers have component layers which are capable of adsorbing water, inorganic cations or organic molecules, resulting in interparticle diffraction in XRD. The polar layer model describes both the structure and the charge distribution of individual layers P-layers are defined as: (i) non-polar, if the surfaces on both sides of individual 2:1 layers have the same charge density, i.e. upper and lower surface, and (ii) polar, if the surfaces have different charge density.

Thus, the five types of layer structures identified from the Reindeer D-27 well in Beaufort-Mackenzie Basin are. (1) A 2 1 layer silicate with an expandable low-charged interlayer which, when treated with $n_c=8$ or $n_c=18$, is identified in dispersed samples as isolated, bent or wavy single layers, or in aggregated samples as wavy, subparallel and discontinuous layers with irregular interlayer spacings (1 3-3.0 nm) This is defined as a low-charge smectite-group mineral which can exist as single 2 1 layers in dispersion and is a non-polar layer It is equivalent to the fundamental- smectite particle of Nadeau et al. (1984a). However, it is not possible to distinguish between detrital and neoformed smectite-group components.

(2) Packets of 2:1 layer silicates with expanded interlayers consisting of coherent sequences of relatively planar or wavy, subparallel 2:1 silicate layers with relatively uniform interlayer spacing. These sequences are considered to be a high-charged smectite-group or vermiculite mineral, if the layers expand with octylammonium (n_c=8) and octadecylammonium (n_c=18) ions and remain coherent with uniform spacing, in contrast to the first layer structure. The layers are considered to be non-polar.

Layer structures (3), (4) and (5) are considered as illitic material. Structure (3) represents double layers consisting of two 2:1 silicates layer which exist as single units or in sequences or packets with expanded interfaces after n_c=8 exchange, i.e. rectorlike or R1-structure. In order for these sequences to expand, layers adjacent to the interlayer must consist of low- and high-charge layers, i.e. one type of polar 2:1 layer (Lagaly 1979, Ahn and Peacor 1986b; Vali et al. 1993a). The fundamental particle concept of Nadeau et al. (1984a) suggested that fundamental illite particles consisted of two 2:1 silicate layers giving a thickness of 2.0 nm. However because of their polar nature, these double layers cannot convert into packets of four non-expandable layers of illite by simply fixing interlayer K. Thus this layer structure cannot be considered as a fundamental illite particle (see below). However, double layers will form R1-ordered sequences and as they have a unique structure and chemistry, are considered a single phase (Jiang et al. 1990a, 1990b).

(4) Packets of 2:1 silicate layers with expanded interlayers after exchange with n_c=18 and not with n_c=8 are considered expandable illite (Vali et al. 1991). It consists of packets of three to five 2:1 silicate layers with expandable interlayers and exhibits regular, parallel to subparallel coherent sequences of layers, with uniform expansion having a thickness of 2.4 to 2.5 nm. It has been suggested that the difference between the values obtained in HRTEM measurements and the approximate 3.0 nm measured in discrete illitic material in XRD may be the result of radiation damage to the n-alkylammonium-ion under the electron beam resulting in the evaporation of the NH_3 from the alkyl-chains (Dr. H. Vali, pers. comm. 1993). Vali et al. (1991) determined that the mean layer-charge for expandable illite was 0.74 per $O_{10}(OH)_2$.

(5) Regular, discrete packets of homogeneous, straight, parallel 2:1 silicate layers with non-expanded interlayers after exchange with (n_c=18) are considered to be micaceous. The non-expanded component must have interlayer positions filled with K because the layers do not expand after n_c=18 treatment (Vali and Hesse 1990). This type of behaviour has only been

observed in muscovite (Vali and Köster 1986) and biotite (Ghabru et al. 1989). Generally, the discrete packets consist of three to six 2:1 layers which are characteristic of illite and are present as isolated particles, in aggregated stacks, or in coherent stacks of packets with expanded interfaces. This indicates that discrete illite may consist of non-expanded, non-polar layers with possible polar basal surfaces. Contrary to Nadeau et al (1981a), the smallest elementary unit for a fundamental illite particle evinced from this study is three 2:1 silicate layers thick. Thicker packets containing >10 2:1 layers in the <0.05 µm fraction from the Reindeer D-27 well were considered as a detrital micaceous phase.

7.7 Formation of Illitic Material

The diagenetic processes occurring in the Beaufort-Mackenzie Basin appear to be similar to those reported from sedimentary basins such as the Gulf of Mexico Coast (Ahn and Peacor 1986; 1989; Bell 1986; Freed and Peacor 1992), various basins of the North Sea (Pearson and Small 1988; Hansen and Lindgreen 1987, 1989; Jones et al 1989; Glasmann et al. 1989; Lindgreen and Hansen 1991), the Paris Basin (Lanson and Champion 1991) and the Barbados accretionary prism (Buatier et al. 1992). Within the past decade, numerous studies have identified I/S in HRTEM using beam-milled and clay separates from diagenetic, hydrothermal and low-temperature metamorphic environments (Lee and Peacor 1988; Ahn and Peacor 1986a, 1986b, 1989; Yau et al. 1987, 1988; Jiang et al. 1990b; Buatier et al. 1992) in attempt to retain mineralogical textures and fabrics and to elucidate the S-I transition. For example, Peacor and coworkers have identified sequences of mixed-layer I/S using overfocus imaging. Lattice-fringe images of disordered smectite-rich I/S occured as anastomosing, discontinuous and wavy layers (resulting from collapse of expandable layers under high vacuum) and have variable spacings of 1.0 to 1.3 nm, with abundant layer terminations and dislocations within layer packets. Intermediate mixed-layer I/S occurred as packets of relatively straight, continuous, and defect-free layers with a nearly constant spacing of 1.0 nm. The packets have a mottled appearance and are from 5 to a fews 10's of layers thick and laterally extend a few hundred nm. Illite-rich I/S to discrete illite is dominated by contiguous packets with relatively straight lattice fringes having nearly constant spacings of 1.0 nm, and with nearly uniform contrast and free of edge dislocations. Although layer terminations are rare, packets may intersect and abut other packets at small angle boundaries. Packets can become up to 25 nm thick and 0.2 μm long Ahn and Peacor (1986a; 1989) proposed a reaction-rate-dependent model for changes with depth observed in the Gulf Coast whereby the S-I transition proceeded in two steps; (i) cation exchange producing K-rich smectite, and (ii) the dissolution of smectite and the crystallization of illite.

HRTEM results have been use to suggest that lattice-fringe images of clay powders offer direct evidence for the concepts of layer-by-layer transformation and dissolution/reprecipitation (Amouric and Olives 1991; Murakami et al. 1993). Both these papers interpret results in terms of the simulated images of Guthrie and Veblen (1989), but attempt to interpret underfocused (structural) imaging in terms of compositional (or overfocused) imaging. Amouric and Olives (1991) and Murakami et al. (1993) assert that a lateral change in thickness of a single layer is evidence of a layer-by-layer conversion process. However, Guthrie and Veblen (1989) demonstrated that a single layer of variable thickness is not a reliable indicator of layer composition. The thickness of a single layer is variable as a result of operating conditions as well as possible adsorption of organic or inorganic material (which is not detectable in TEM). In addition, in compositional images dark fringes overlie smectite-group interlayers and less dark fringes overlie illite interlayers (Veblen et al. 1990). They do not, however overlie 2:1 silicate layers. Veblen et al. (1990) admitted the distinction between illite and smectite interlayers is subjective. Suggestions that edge dislocations invoke a dissolution/repreciptation process are unproven.

The examination of the layer structures in lattice fringe images and in freeze-etch and freeze-dried replicas from shallow, intermediate and deep samples reflects a complex change in mineralogy which corresponds only superficially to the changes manifested in the diffraction patterns of two-component Mg^{2+}-saturated ethylene-glycol solvated samples. Diffraction patterns of Mg^{2+}-saturated ethylene-glycol solvated samples indicate that the burial diagenetic transition of smectite-group rich I/S to illite-rich I/S involves a structural change from R0- to R1-ordered to R>1-ordered with increasing percent illite (Fig. 6.3). The patterns of Mg^{2+}-saturated glycerol-solvated samples suggest a possible third high-charge expandable component that is fairly constant with depth (Fig. 6.5).

The alkylammonium-ion exchanged samples from XRD analyses are difficult to interpret with any degree of confidence, but they certainly do imply a much more complicated system of layer components than one that can be rationalized using a two-component system. However, the n_c=18 exchanged samples evince a simplification of the layer charge densities with depth, corresponding to the predominance or perhaps neoformation of illite with increasing depth of burial. The lattice-fringe images from each sample depth are compositionally and structurally heterogeneous, in that the individual layer structures have an identifiable and consistent layer structure. However, in the <0.05 µm fraction, a process of layer-by-layer transformation could not be discerned.

The shallow sample consisted of four distinct and separate phases; (i) predominant single-layers or sequences of layers of a low-charged smectite-group mineral, (ii) coherent sequences of expanded layers of high-charged smectite-group mineral or vermiculite, (iii) minor isolated double layers, and (iv) signficant, fairly thick packets of detrital micaceous minerals (Fig. 6.30). The intermediate sample consisted of; (i) minor, single layers of a low-charge smectite-group mineral; (ii) predominant sequences of double layers with expanded interlaces, (iii) moderate proportions of sequences of high-charged smectite-group or vermiculite component, and (iv) packets of three to six 2:1 layers of illite (Fig. 6.31). The deepest sample consisted of three layer structures; (i) predominant packets of three to six 2:1 silicate layers of illite, and (ii) minor amounts of packets containing expandable illite interlayers, and (iii) sequences of double layers (Fig. 6.32).

The S-I conversion in the <0.05 µm fraction from the Reindeer D-27 well is seen in HRTEM as an evolution from randomly mixed smectite-group minerals and detrital micaceous components to predominant discrete illite minerals having different compositions. However, from the limited data set, timing relationships cannot be discerned nor can a mechanism be detected.

Single layers of a low-charge smectite-group mineral and coherent expanded sequences of a high-charged smectite-group mineral are non-existent in the lattice-fringe images of the 12500-12550 ft depth sample. However, ethylene-glycol solvated diffraction patterns of the same material indicate an expanded component of 18 to 20 %. The diffraction pattern of the untreated, octadecylammonium-ion exchanged sample suggests an R3-ordered structure with a high-charge expanded component. Packets of expanded illite are seen in the lattice-fringe images, but a corresponding peak of 2.8-3.1 nm peak is not present in the diffraction patterns. The intermediate sample is composed predominantly of sequences of double layers and packets of illite, with minor amounts of high-charge smectite-group or vermiculite component. Diffraction patterns of ethylene glycol-solvated samples indicate 35 % expandable component, whereas the $n_C=18$ exchanged samples indicate a mixture of R1- and R3-ordered structures. The 4800 ft depth sample consisted predominantly of a low-charge smectite-group mineral and a high-charge smectite or vermiculite component, with a detrital micaceous component. Diffraction patterns of ethylene glycol-solvated samples indicated 76% of expandable component, whereas the $n_C = 18$-exchanged sample gave conflicting results, but may indicate an R0 structure of a non-expandable component and a high-charge expandable component.

Illite or a micaceous component is present at all depths, except that the thickness of the packets changed with depth. In shallow samples, the non-expandable component has a thickness of 8 to 10 layers, suggestive of a detrital micaceous component. In the lattice-fringe images of the 0.1-0.05 μm fraction, these micaceous minerals often show strong dissolution features. Therefore, it is possible that they may dissolve completely and provide the additional K^+ and other ions required for the formation of illite. Velde and Vasseur (1992) suggested that the dissolution of detrital phases which provide K^+ are very important to reactions in diagenesis, whereas those of transformation are more typical of higher energy environments (e.g. hydrothermal). In addition, packets of expandable illite are found only in deep samples, suggesting the development of an illite with different layer charge and thus a different composition to non-expandable illite. Jennings and Thompson (1986) observed that the illitization reaction rates decreased during the formation of R3-ordered structures. The absence of smectite-group minerals at depths has been documented in other sedimentary basins (e.g. Glasmann et al. 1989). However, it is apparent that many phases can coexist over a wide range of burial depth, i.e. 4800 to 12550 ft in the Reindeer D-27 well.

The change in layer structure from smectite-group mineral-rich shallow to exclusively illitic deep samples is difficult to imagine by invoking a layer-by-layer transformation mechanism, but cannot be discussed with lattice-fringe images of clay separates alone. It is difficult to make a case based on only three sample depths, but trends in the < 0.05 μm indicate that layer structures exhibit an increasing charge development (see also Ko 1992). These results are in accordance with the experimental data of Howard (1981) and Howard and Roy (1985) which indicated that I/S evolving in a K-deficient environment can develop a high-charge smectite-group component The low- and high-charged smectite-group minerals give way to the development of predominant double layers consistent with R1-ordering at intermediate depths, which in turn are replaced by packets of expandable interlayers in expandable illite to the predominance of non-expanded interlayers of illite.

Sharp-edged lath-like particles are present on the surface of larger particles in the freeze-etch replicas (Figs. 6.33 and 6.34) and as individual particles in the freeze-dried replicas (Fig. 6.11). Their presence is interpreted as evidence for a dissolution/reprecipitation mechanism. In addition, the presence of anhedral or irregular shaped particles may indicate diagenetic phases that were broken off during sample preparation. However, an equant anhedral morphology for illite may be typical in mud-dominated basins having signficant compaction and may imply that the illite was confined to growth in micropores between adjacent larger detrital particles (Ahn and Peacor 1986a). Freeze-etch replicas also seem to suggest a concomitant process of dissolution at the edges of the larger particles. Glasman et al. (1989a) demonstrated from TEM images of the <0.1 μm size fraction from the North Sea that R1 I/S was formed from illite laths, whereas R3 I/S displayed a platy morphology. Additional evidence for neoformed illite comes from K-Ar ages (Sears et al. 1993b) of the <0.05 μm size fraction. The illitic clays of the deeper samples are found to be younger than the corresponding shale depositional age. The K-Ar ages show a trend of increasing age with depth which is opposite to that reported for other basins (e.g. Gulf of Mexico Coast), suggesting a neoformed component may have been isolated.

CHAPTER 8.0 SUMMARY AND CONCLUSIONS

The emphasis of this research was to characterize the clay material involved in the smectite-to-illite (S-I) conversion in the Beaufort-Mackenzie Basin, and to identify the nature of the effects on the layer structures of mixed-layer I/S resulting from sample treatment, i.e. the addition of sodium hexametaphosphate as a peptizer. This required a combination of XRD and TEM analytical methods using ethylene glycol, glycerol and n-alkylammonium-ion treatments, i.e. octylammonium ($n_C=8$) and octadecylammonium ($n_C=18$) ions.

Analyses of 0.05-0.1 μm and <0.05 μm clay mineral separates collected from shales of the Reindeer D-27 well in the Beaufort-Mackenzie Basin, Arctic Canada, revealed that the S-I conversion cannot be characterized on the basis of a two component I/S system: an expandable and a nonexpandable component. It follows that the S-I conversion cannot be thought of simply as a conversion of a smectite-group-rich I/S to an illite-rich I/S through intermediate compositions.

Analyses of diagenetic clay material treated with $n_C=8$ and $n_C=18$ ions and investigated with XRD and HRTEM have revealed that the components identified in conventional diffraction patterns of Mg^{2+}-saturated ethylene-glycol or glycerol solvated samples are in fact complex mixtures of different types of layer structures. These layer structure are inferred to have differing compositions as a result of their response to alkylammonium-ion exchange. The large organic anisometric ions will expand the interlayer space of 2:1 layer silicates as a function of the layer charge and the alkyl-chain length. Alkylammonium ions are much more sensitive to differing interlayer-charge densities than are other organic molecules such as ethylene glycol and glycerol, which can only detect expandability.

Alkylammonium-ion exchanged clay mineral samples have been shown in X-ray diffraction patterns to consist of complex mixtures of layer structures with varying interlayer-cation densities. The XRD patterns indicated the presence of R1- and R3-ordered structures. However, the responses are difficult to assess with any degree of confidence, as the XRD averages over millions of layer structures with differing stacking sequences. As an analytical method, XRD is not sensitive enough to discern the compositonal and structural heterogeneity of mixed-layer I/S (Drits 1987).

Lattice-fringe images obtained from TEM have revealed the presence of five distinct types of 2:1 silicate layer structures whose existence and abundance varies with depth The types of five layer structures must be viewed in terms of their responses to alkylammonium-ion exchange and are characterized in terms of the P-layer model conceptualized by Guven (1991) and articulated for the TEM by Vali et al (1993a). Stated simply, the P-layer model defines the P-layer as: non-polar, if the tetrahedral sheets of individual 2:1 silicate layers have the same charge density, and polar, if the tetrahedral sheets of individual 2:1 silicate layers have different charge densities, i.e. low- and high-charge interlayers. However, the results of this study are generally consistent with the fundamental particle concept of Nadeau et al. (1984a, 1984b, 1984c) and the multi-phase model of Rosenberg et al (1990) and Aja et al. (1991a, 1991b)

The five types of 2:1 silicate layer structures identified from the Reindeer D-27 well in Beaufort-Mackenzie Basin are: (1) An expandable low-charged 2:1 layer silicate, when treated with $n_C=8$ or $n_C=18$ is identified in dispersed samples as isolated, bent or wavy single layers, or in aggregated samples as wavy, subparallel and discontinuous layers with irregular interlayer spacings. This phase is defined as a low-charge smectite-group phase which can exist as single layers in dispersion. It is equivalent to the fundamental smectite particle of Nadeau et al (1984a) and represents non-polar layers. (2) Packets of 2:1 layer silicates with expanded interlayers consist of coherent sequences of relatively planar or wavy, subparallel 2:1 silicate layers with relatively uniform interlayer spacing. They are considered to be a high-charged smectite-group phase or vermiculite, if the layers expand with solutions of $n_C=8$ and $n_C=18$ ions and remain as coherent sequences with uniform spacing, rather than as single or dispersed layers in contrast to the low-charge smectite-group minerals. They are thus considered to be non-polar 2:1 layer silicates. (3) Double layers consist of two 2:1 silicates layers which exist as single units or in sequences of packets with expandable interfaces forming an R1-ordered structure. These units consist of polar layers having alternating low- and high-charged interlayers. (4) Packets of 2:1 silicate layers with expanded interlayers after exchange with $n_C=18$ and not $n_C=8$ are considered expandable illite. It consists of packets of ≥ 3 2:1 silicate layers with expandable interlayers exhibiting regular, parallel to subparallel coherent sequences of layers with uniform expansion having approximately 2.3-2.6 nm spacing in the TEM. Vali et al. (1991) determined that the mean layer charge for expandable illite was 0.74 per $O_{10}(OH)_2$. Expandable illite may have polar or non-polar basal surfaces. (5) Regular, discrete packets of homogeneous, straight, parallel 2:1 silicate layers with non-expanded interlayers after $n_C=18$ exchange. They consist of three to six layers and are considered illite. Non-expanded illite is considered non-polar but may have polar layers at the basal surfaces of layer packets. If compared to double layers, the smallest elementary unit for a fundamental illite particle evinced from this study is three 2:1 silicate layers thick, as the double layers are the smallest particles for rectorite-like minerals.

Alkylammonium-ion exchanged clay minerals in both XRD and TEM analyses indicate that the layer structures simplify with depth of burial. However, in XRD the proportions of each component layer of the structure cannot be determined, and current modeling programs are incapable of dealing with three- and four- component systems. Lattice-fringe images clearly indicate that smectite-group or vermiculite components are not present at the greatest burial depth (> 12000 ft). Non-expandable illitic (or micaceous) material is present at all depths.

The second major emphasis in this research was to discern the effects of the addition of sodium hexametaphosphate as a peptizer on the components of mixed-layer I-S. The $<0.05\ \mu m$ clay separates were fractionated without treatment and with a dilute sodium hexametamphosphate solution. The samples were then either solvated with ethylene glycol or exchanged with n-alkylammonium ions, i.e. $n_C=8$ or $n_C=18$. In contrast to the untreated samples, diffraction patterns of treated ethylene-glycol solvated samples revealed significant diminished reflection intensity, displacements in reflection position with respect to 2Θ, and extensive reflection broadening which tended to merge with the baseline, giving the appearance that no clay minerals were present. Expandability measurements could not be made with any certitude on treated samples Alkylammonium-ion treated samples gave contradictory results which cannot be explained satisfactorily. Comparison between untreated and treated samples exchanged with $n_C=18$ primarily displayed integral series of reflections which were displaced to either higher or lower 2Θ values for the treated samples. Generally, the reflections in the treated sample displayed better intensity and sharper reflections, but were often affected by signifcant peak overlap However, only in the shallowest sample (4800 ft) were reflections identified in both untreated and treated samples. An alternative explanation for the sharp peaks in the treated sample may be the appearance of a chemical reaction product between the phosphate ions, the alkylammonium ions and any adsorbed material on the clay surface or in the interlayers. This is a reasonable possibility, as similar reflections are visible in all samples regardless of depth. Comparisons between the untreated and treated samples exchanged with alkylammonium ions reveal significant differences between the layer structures. Firstly, both the untreated and treated samples displayed the same types of layer structures for each depth. No new types of layer structures were visible. As was to be expected with the addition of a peptizer, all treated samples displayed decreased layer structure aggregation and better orientation of the layer structures within ultrathin sections. In addition, treated samples from all depths displayed an increase in the amount of, and coherency of expanded layers, either high-charge smectite-group interlayers or expandable illite interlayers, increased abundance of R1-ordered sequences in intermediate and deep samples, and decreases in the thickness of packets containing non-expanded interlayers. In the 4800 ft sample, sequences of high-charge smectite-group or vermiculite interlayers were more uniform and displayed thicker units. Differences were especially apparent in the 12500-12550 ft sample exchanged with $n_C = 18$, which exibited significant increases in the amount of packets of expandable illite interlayers, and increases in the number of expanded interlayers in each illite packet.

The addition of sodium hexametaphosphate to the < 0.05 μm fraction therefore appears to modify not only the interlayers of expandable clay minerals, but also modifies the arrangement of layer structures in stacking sequences. It is possible that if the primary layer structures are altered or destroyed by peptizers, the disruption is irreversible. It is evident that a reliable ratio determination between expandable and nonexpandable components in I/S is dependent on characterizing all the expandable components and resolving the effects of chemical pretreatment. It is especially important to decipher the exact relationship between chemical pretreatments and n-alkylammonium ions. Although, the application of n-aklylammonium-ion techniques to mixed-layer I/S is at present difficult to interpret in diagenetic samples, it is the best method for natural and untreated samples to achieve the most reliable results using a combination of XRD and TEM.

REFERENCES

Aagaard, P. and Helgeson, H.C., 1983, Activity/composition relations among silicates and solutions II. Chemical and thermodynamic consequences of ideal mixing of atoms among energetically equivalent sites in montmorillonites, illites, and mixed layer clays. Clays Clay Min., 31:207-217.

Adams, W.A and Stewart, V.I., 1969, The effect of ultrasonic dispersion on Silurian shale particles. Soil Sci., 108:227-228

Ahn, J.H and Buseck, P.R., 1990, Layer-stacking sequences and structural disorder in mixed-layer illite/smectite: image simulation and HRTEM imaging. Amer. Mineral., 75:267-275.

Ahn, J.H and Peacor, D.R., 1986a, Transmission and analytical electron microscopy of the smectite-to-illite transition. Clays Clay Min., 34:165-179.

Ahn, J.H. and Peacor, D.R., 1986b, Transmission electron microscope data for rectorite: implications for the origin and structure of "fundamental particles". Clays Clay Min., 34:180-186.

Ahn, J.H and Peacor, D.R., 1989, Illite/smectite from Gulf Coast shales: a reappraisal of transmission electron microscope images. Clays Clay Min., 37:542-546.

Aja, S.U., Rosenberg, P.E., and Kittrick, J.A., 1991a, Illite equilibria in solutions: I phase relationships in the system K_2O-Al_2O_3-SiO_2-H_2O between 25°C and 250°C. Geochim. Cosmochim Acta, 37:542-546

Aja, S.U., Rosenberg, P.E., and Kittrick, J.A., 1991b, Illite equilibria in solutions: II. Phase relationships in the system K_2O-MgO-Al_2O_3-Si_2-$_2O$ between 25° and 250°C. Geochim. Cosmochim. Acta, 55:1365-1374.

Allen, F., 1992, Mineral identification by HRTEM: problems and opportunities, in, Buseck, P.R., ed., Minerals and Reactions at the Atomic Scale: Transmission Electron Microscopy. Reviews in Mineralogy: Mineral. Soc. Amer., 27:289-334.

Altaner, S.P and Bethke, C.M., 1988, Interlayer order in illite/smectite. Amer. Min., 73:766-774.

Altaner, S.P and Vergo, N., 1988, Sericite from the Silverton caldera, Colorado: discussion. Amer. Min., 73:1472-1474.

Altaner, S.P., Weiss, C.A., Jr., and Kirkpatrick, R.J., 1988, Evidence from ^{29}Si NMR for the structure of mixed-layer illite-smectite clay minerals. Nature, 331:699-702

Amouric, M. and Olives, J., 1991, Illitization of smectites as seen by high-resolution transmission electron microscopy. Eur. J. Mineral., 3:831-835.

Anderson, J.M., 1963, An improved pretreatment for mineralogical analysis of samples containing organic matter. Clays Clay Min. Proceed. 10th Natl. Conf., 380-388.

April, A.I., Hluchy, M.H., and Newton, R.M., 1986, The nature of vermiculite in Adirondak soils and till. Clays Clay Min., 34:549-556.

Awwiller, D.N., 1993, Illite/smectite formation and potassium mass transfer during burial diagenesis of mudrocks: a study from the Texas Gulf Coast Paleocene-Eocene. J. Sediment. Petrol., 63:501-512.

Barber, D.J., 1970, Thin foils of non-metals made for electron microscopy by sputter etching. J. Mater. Sci., 5:1-8.

Bailey, S.W., 1980, Summary of recommendations of AIPEA nomenclature committee. Clays Clay Min., 28:73-78.

Bailey, S.W., 1982, Nomenclature for regular interstratifications. Amer. Mineral., 67:394-398.

Bailey, S.W., 1988, X-ray diffraction identification of the polytypes of mica, serpentine, and chlorite. Clays Clay Min., 36:193-213.

Bailey, S.W., Brindley, G.W., Kodama, H., and Martin, R.T., 1982, Report of the Clay Minerals Society Nomenclature Committee for 1980-1981: Nomenclature for regular interstratifications. Clays Clay Min., 30:76-78.

Bain, D.C. and Smith, B.F.L., 1987, Chemical analysis, in, Wilson, M.J., ed., A Handbook of Determinative Methods in Clay Mineralogy, Blackie, Glasgow and London. 6:248-274.

Barberis, E., Ajmone Marsan, F., Boero, V., and Arduino, E., 1991, Aggregation of soil particles by iron oxides in various size fractions of soil B horizons. J. Soil Sci., 42:535-542.

Barefoot, R.R. and Van Elsberg, J.N., 1975, The role of adsorbed or structured water in the diagenesis of the Tertiary sediments in the Mackenzie Delta: a preliminary report. Geol. Surv. Can., Paper 75-1c, 303-309.

Baronnet, A., 1972, Growth mechanisms and poltypism in synthetic hydroxyl-bearing phlogopite. Amer. Mineral., 57:1272-1293.

Baronnet, A., 1973, Sur les origines des dislocations vis des spirales de croissance dans les mica. J. Crystal Growth, 19:193-198.

Baronnet, A., 1992, Polytypism and stacking disorder, in, Buseck, P.R., ed., Minerals and Reactions at the Atomic Scale: Transmission Electron Microscopy. Reviews in Mineralogy. Mineral. Soc. Amer., 27:231-282.

Basset, G., 1958, A new technique for decoration of cleavage and slip steps on ionic crystal surfaces. Phil. Mag., 3:1042-1045.

Bayliss, P. and Levinson, A.A., 1970, Clay mineralogy and boron determination of the shales from Reindeer Well, Mackenzie River delta, N.W.T., Canada. Can. Petrol. Geol. Bull., 18:80-83.

Bell, T.E. 1986, Microstructure in mixed-layer illite-smectite and its relationship to the reaction of smectite to illite. Clays Clay Min., 2.146-154.

Berligen, B.A., Sinha, A.K., and Fertl, W.H., 1988. Estimation of productivity of Lobo 6 sand, Lower Wilcox, Texas, by identifying diagenetic clays with well log data. SPE Formation Evaluation, June 393-406

Bethke, C.M. and Altaner, S.P., 1986, Layer-by-layer mechanism of smectite illitization and application to a new rate law. Clays Clay Min., 34.136-145.

Bethke, C.M., Vergo, N., and Altaner, S.P., 1986, Pathways of smectite illitization. Clays Clay Min., 34 125-135

Bish, D.L. and Reynolds, R.C. Jr., 1989, Sample preparation for x-ray diffraction, in Bish, D.L. and Post, J.E., eds., Modern Powder Diffraction: Reviews in Mineralogy, Mineral Soc. Amer p 73-99.

Bloch, J.M., 1950, The chemical and physical properties of montmorillonite. Thesis Nancy, France.

Bloch, J. and Hutcheon, I.E., 1992, Shale diagenesis: a case study from the Albian Harmon Member (Peace River Formation), Western Canada. Clays Clay Min., 40:682-699

Bodine, M.W., Jr. and Fernald, T.H., 1973, EDTA dissolution of gypsum, anhydrite, and Ca-Mg carbonates. J. Sediment. Petrol., 43:1152-1156.

Boles, J.R. and Franks, S.G., 1979, Clay diagenesis in Wilcox Sandstones of southwest Texas: Implications of smectite diagenesis on sandstone cementation. J. Sed. Petrol., 49 55-70

Bourget, S.J. and Tanner, C.B., 1953, Removal of organic matter with sodium hypobromite for particle-size analysis of soils. Can. J. Agr. Sci., 33:579-585.

Brewster, G.R., 1980, Effect of chemical pretreatment on X-ray powder diffraction characteristics of clay minerals derived from volcanic ash. Clays Clay Miner., 28:303-319.

Brindley, G., 1965, Nomenclature and liason committee of the clay minerals society, 1963-4, in, Bradley, W.F. and Bailey, S.W., eds., Clays Clay Min., Proc. 13th Natl. Conf. Madison, Wisconsin, 1964, Pergamon Press, New York, 429-432.

Brindley, G.W., 1966, Ethylene glycol and glycerol complexes of smectite and vermiculite. Clay Miner., 6.237-259.

Brindley, G.W., 1980, Order-disorder in clay mineral structures, in, Brindley, G.W and Brown, G., eds., Crystal Structures of Clay Minerals and their X-ray Identification. Mineralogical Society, London, 125-195

Brindley, G.W. and Ray, S., 1964, Complexes of Ca-montmorillonite with primary monohydric alcohols (clay-organic studies-VIII), Amer. Mineral., 49:106-115

British American Oil Company, 1966, Well Reports for the Reindeer D 27 well, Richards Island, Mackenzie Delta, N W T

Brooks, P W , 1986, Biological marker geochemistry of oils from the Beaufort-Mackenzie region, Arctic Canada Bull Can Petrol Geol , 34 490-505

Brown, G, 1984, Crystal structures of clay minerals and related phyllosilicates Phil Trans R Soc Lon , A 311 221-240

Brown, G and Brindley, G W , 1980, X-ray diffraction procedures for clay mineral identification, in Brindley, G.W. and Brown, G , eds , Crystal Structures of Clay Minerals and their X-ray Identification. Mineralogical Society, London, 305-359

Brown, J L and Jackson, M L , 1973, Chlorite examination by ultramicrotomy and high resolution electron microscopy Clays Clay Min , 21 1-7

Bruce, C H , 1984, Smectite dehydration - its relation to structural development and hydrocarbon accumulation in Northern Gulf of Mexico Amer Assoc Petrol Geol Bull , 68 673-683

Bruce, C.J and Parker, E R , 1975, Structural features and hydrocarbon deposits in the Mackenzie Delta Proc. 9th Wld Petrol Congr London, Applied Science Publishers, 2 251-261

Buatier, M D , Peacor, D R , and O'Neil, J R , 1992, Smectite-illite transition in Barbados accretionary wedge sediments: TEM and AEM evidence for dissolution/crystallization at low temperature Clays Clay Min , 40 65-80

Bühmann, C , 1992, Smectite-to-illite conversion in a geothermally and lithologically complex Permian sedimentary sequence Clays Clay Min , 40 53-64

Bujack, J P. and Davies, E H , 1981, Neogene dinoflagellate cysts from the Hunt Dome Kopanoar M-13 well, Beaufort Sea, Canada. Bull Can Petrol Geol , 29 420-425

Burst, J.F., 1959, Post diagenetic clay mineral environmental relationships in the Gulf Coast Eocene Clays and Clays Minerals, Proc 6th Conf Pergamon Press, New York, 327-341

Burst, J.F., 1969, Diagenesis of Gulf Coast clayey sediments and its possible relation to petroleum migration Amer Assoc Petrol Geol Bull , 53 73-79

Buseck, P R., 1992, Principles of transmission electron microscopy, in, Buseck, P R , ed , Minerals and Reactions at the Atomic Scale: Transmission Electron Microscopy Reviews in Mineralogy Mineral Soc Amer , 27 1-36

Carroll, D., 1959, Ion exchange in clays and other minerals Bull Geol Soc Am 70 749-780

Carey, 1958, The tectonic approach to continental drift, in Proceedings, Continental drift, A symposium, Hobart, March 1958: Hobart, University of Tasmania, 177-355

Chamney, T.P., 1969, Abnormally thick Tertiary-Cretaceous sequence, Mackenzie delta, District of Mackenzie. Geol. Surv. Can., Paper 69-1, Part B, 1:69-72.

Chamney, T.P., 1970, Tertiary and Cretaceous biostratigraphic divisions in the Reindeer D-27 borehole, Mackenzie River Delta. Geol. Surv. Can., Paper 70-30. 45 p.

Chen, C.C., Turner, F.T., and Dixon, J.B., 1989, Ammonium fixation by high-charge smectite in selected Texas Gulf coast soils. Soil Sci. Soc. Amer. J., 53:1035-1040.

Chichester, F.W., Youngberg, C.T., and Harward, M.E., 1969, Clay mineralogy of soils formed on Mazama pumice Soil Sci. Soc. Amer. Proc., 33:115-120.

Cook, F.A., Coflin, K.C., Lane, L.S., Dietrich, J.R., and Dixon, J., 1987, Structure of the southeast margin of the Beaufort-Mackenzie basin, Arctic Canada, from crustal seismic-reflection data. Geol., 15:931-935.

Cook, R.J., 1992, A comparison of methods for the extraction of smectites from calcareous rocks by acid dissolution techniques. Clay Min., 27:73-80.

Corbató, C. and Tettenhorst, R., 1987, Analysis of illite-smectite interstratification. Clay Min., 22:269-285.

Cullity, B.D. 1978, Elements of x-ray diffraction: Addison-Wesley Publ. Co., Reading, Massachusetts, 555 pp.

de Lange, G.J., 1976, Röntgen diffractie aan kleimineralen van enkele Noordzee monsters. Internal Report N I O.Z., 1976-6, 25 p.

Dean, R.S., 1985, Burial diagenesis of weathered illite. Beaufort Sea, Canada [abstr.] Proc. 8th Inter. Clay Conf., Denver, 51.

Dickinson, W R. and Suczek, C.A., 1979, Plate tectonics and sandstone composition. Amer. Assoc. Petrol. Geol Bull., 63:2164-2182.

Dietrich, J.R., Dixon, J., and McNeil, D.H., 1985, Sequence analysis and nomenclature of Upper Cretaceous to Holocene strata in the Beaufort-Mackenzie Basin. In Current Research, Part A, Geol. Surv Can., Paper 85-1G, 133-157.

Dietrich, J.R, Dixon, J., McNeil, D.H., and Snowdon, L.R., 1989a, Geology, biostratigraphy and organic geochemistry of strata in the Beaufort-Mackenzie area, Arctic Canada. Brief supplementary notes to accompany a one-day short course sponsored by the Canadian Society of Petroleum Geologists, Calgary, 15 June, 1989.

Dietrich, J.R., Coflin, K.C., Lane, L.S., Dixon, J., and Cook, F.A., 1989b, Interpretation of deep seismic reflection data, Beaufort Sea, Arctic Canada: Can. Geol. Surv. Open-File Report 2106, 15 p.

Dietrich, J.R., Dixon, J., McNeil, D.H., McIntyre, D.J., Snowdon, L.R., and Cameron, A.R., 1989c, The geology, biostratigraphy and organic geochemistry of the Natsek E-56 and Edlok N-56 wells, western Beaufort Sea; in Current Research, Part G, Geol. Surv. Can., Paper 89-1G, 133-157

Dixon, J., 1979, The Lower Cretaceous Atkinson Point Formation (new name) on the Tuktoyaktuk Peninsula, N.W.T.: a coastal fan-delta to marine sequence. Bull. Can. Petrol. Geol., 27 163-182

Dixon, J., 1980, Sedimentology of the Eocene Taglu Delta, Beaufort-Mackenzie Basin: example of a river-dominant delta. Geol. Surv. Can., Paper 80-11, 11 p.

Dixon, J., 1982, Upper Oxfordian to Albian Geology, Mackenzie Delta, Arctic Canada, in Embry, A.F. and Balkwill, H.R., eds., Arctic Geology and Geophysics: Can. Soc. Petrol. Geol. Memoir 8:29-42.

Dixon, J., 1982, Jurassic and Lower Cretaceous subsurface stratigraphy of the Mackenzie Delta-Tuktoyaktuk Peninsula, N.W.T. Geol. Surv. Can., Bull. 349, 52 p

Dixon, J., 1986, Cretaceous to Pleistocene stratigraphy and paleogeography, northern Yukon and northwesten district of Mackenzie. Bull. Can. Petrol. Geol., 34:49-70

Dixon, J, 1991, The Neocomian Parsons Group, northern Yukon and adjacent Northwest Territories. Geol. Surv. Can. Bull. 406, 54 p

Dixon, J. and Dietrich, 1985, Geology, in Dixon, J., Dietrich, J.R, McNeil, D.H., McIntyre, D.J., Snowdon, L.R., and Brooks, P., Geology, biostratigraphy and organic geochemistry of Jurassic to Pleistocene strata, Beaufort-Mackenzie area, northwest Canada; Course Notes: Can. Soc. Petrol. Geol., 3-30.

Dixon, J. and Dietrich, J.R., 1988, The nature of depositional and seismic sequence boundaries in Cretaceous-Tertiary strata of the Beaufort-Mackenzie Basin, in, James, D.P. and Leckie, D.A., eds., Sequences, Stratigraphy, Sedimentology: Surface and Subsurface: Can. Soc. Petrol. Geol. Memoir 15:63-72.

Dixon, J. and Dietrich, J.R., 1990, Canadian Beaufort Sea and adjacent land areas, in Grantz, A., Johnson, L., and Sweeney, J.F., eds., The Arctic Ocean Region, Boulder, Colorado, Geological Society of America, The Geology of North America, v.L., 239-256.

Dixon, J., Dietrich, J.R., and McNeil, D.H., 1992a, Upper Cretaceous to Pleistocene sequence stratigraphy of the Beaufort-Mackenzie and Banks Island areas, Northwest Canada. Geol. Surv. Can., Bull. 407., 90 p.

Dixon, J., McNeil, D.H., Dietrich, J.R., and McIntyre, 1989, Barremian to Albian stratigraphy Tuktoyaktuk Peninsula and south MacKenzie Delta, Northwest Territories. Geol. Surv. Can. Paper 89-15, 16 p.

Dixon, J., Dietrich, J., Snowdon, L.R., Morell, G., and McNeil, D.H., 1992b, Geology and petroleum potential of Upper Cretaceous and Tertiary strata, Beaufort-Mackenzie area, northwest Canada. Amer. Assoc. Petrol. Geol. Bull., 76:927-947.

Dixon, J.D., McNeil, D.H., Dietrich, J.R., Bujak, J.P., and Davies, E.H., 1984, Geology and biostratigraphy of the Dome Gulf et al. Hunt Kopanoar M-13, Beaufort Sea. Geol. Surv. Can., Paper 82-13, 28 p.

Dixon, J., McNeil, D.M., Dietrich, J.R., and McIntyre, D.J., 1988, Petroleum resources of the MacKenzie-Delta-Beaufort Sea. Geol. Surv. Can., Open File Rep. 1926.

Douglas, L.A., 1967, Sodium-citrate-dithionite-induced alteration of biotite. Soil Sci., 103:191-195.

Douglas, L.A., 1977, Vermiculites. in, Dixon, J.B. and Weed, S.B., eds., Minerals in Soil Environments. Soil Sci. Soc. Amer., Madison, Wisconsin, 259-292.

Douglas, L.A., 1982, Smectites in acidic soils, in, Van Olphen, H. and Veniale, F., eds., Proc. Int. Clay Conf., Bologna and Pavia, Italy, 6-12 Sept. 1981. Elsevier Scientic Publishing Co., Amsterdam, 635-640.

Douglas, L.A. and Fiessinger, F., 1971, Degradation of clay minerals by H_2O_2 treatments to oxidize organic matter. Clays Clay Miner., 19:67-68.

Drever, J.I., 1973, The preparation of oriented clay mineral specimens for x-ray diffraction analysis by a filter-membrane peel technique. Amer. Mineral., 58:553-554.

Drits, V.A., 1987, Mixed-layer minerals: diffraction methods and structural features, in Schultz, L.G., van Olphen, H and Mumpton, F.A., eds., Proc. Int. Clay Con., Denver, 1985: The Clay Minerals Society, Indiana, 33-45.

Drits, V.A. and Tchoubar, C., 1990, X-ray diffraction by disordered lamellar structures, theory and applications to microdivided silicates and carbons. Springer-Verlag, Berlin. 371 p.

Drits, V.A., Plançon, B.A., Sakharov, B.A., Besson, G., Tsipursky, S.L., and Tchoubar, C., 1984, Diffraction effects calculated for structural models of K-saturated montmorillonite containing different types of defects. Clays Clay Min., 19:541-561.

Drosdoff, M. and Miles, E.F., 1938, Action of hydrogen peroxide on weathered mica. Soil Sci., 46:391-395.

Dudas, M.J. and Harward, M.E., 1971, effect of dissolution treatment on standard and soil clays. Soil Sci. Soc Amer Proc., 35:134-140.

Dümmler, H. and Schroeder, D., 1965, Zur qualitativen und quantitativen röntgenographischen Bestimmung von Dreischicht-Tonmineralen in Böden. Z. Pflänzenernährung. Düng. Bodenk., 109:35-47.

Dypvik, H., 1981, Drilling mud contamination of samples in X-ray diffraction and atomic absorption analyses Amer Assoc. Petrol. Geol. Bull., 65:744-748.

Dypvik, H., 1983, Clay mineral transformations in Tertiary and Mesozoic sediments from North Sea. Amer. Assoc. Petrol. Geol. Bull., 67:160-165.

Eberhart, J.P., S.P. and Triki, R., 1972, Description d'une technique permetant d'obtenir des coupes minces de minéraux argileux par ultramicrotomie. Application à l'étude des minéraux argileux interstratifiés. J. Microscopie., 15:111-120.

Eberl, D.D., 1993, Three zones for illite formation during burial diagenesis and metamorphism. Clays Clays Clay Min.,(in press).

Eberl, D.D. and Środoń J., 1988, Ostwald ripening and interparticle-diffraction effects for illite crystals. Amer. Mineral., 73:1335-1345.

Eberl, D.D., Velde, B., and McCormick, T., 1993, Synthesis of illite/smectite from smectite at earth surface temperatures and high pH. Clay Min., 28:49-60.

Eberl, D.D., Środoń, J., Lee, M., Nadeau, P., and Northrup, R., 1987, Sericite from the Silverton caldera, Colorado· correlation among structure, composition, origin, and particle thickness Amer. Mineral., 72:914-934.

Edwards, A.P. and Bremner, J.M., 1967, Dispersion of soil particles by sonic vibration. J Soil Sci., 18:47-63.

Ellingboe, J. and Wilson, J., 1964, A quantitative separation of non-carbonate minerals from carbonate minerals. J. Sediment. Petrol., 34:412-418.

Elliot, W.C., Aronson, J.L., Matisoff, G., and Gautier, D.L., 1991, Kinetics of the smectite to illite transformation in the Denver basin: clay mineral, K-Ar, and mathematical model results: Amer Assoc. Petrol. Geol. Bull., 75:436-462.

Embry, A.H. and Dixon, J., 1990, The breakup unconformity of the Amerasia Basin, Arctic Ocean: evidence from Arctic Canada. Geol. Soc. Amer. Bull., 102:1526-1534

Emerson, W.W., 1971, Determination of the contents of clay-size particles in soils J. Soil Sci., 22:50-59.

Enachescu, M., 1990, Structural setting and validation of direct hydrocarbon indicators for Amauligak oil field, Canadian Beaufort Sea. Amer. Assoc. Petrol. Geol., 74.41-59

Ergun, S., 1970, X-ray by very defective lattices. Phys Rev. B,131 3371-3380

Eslinger, E. and Pevear, D., 1988, Clay minerals for petroleum geologists and engineers Soc Econ. Paleon. Min. Short Course Notes no.22, Soc Econ. Paleon. Mineral., Oklahoma City, OK A-31

Farmer, V.C. and Mitchell, B.D., 1963, Occurrence of oxalates in soil clays following hydrogen peroxide treatment. Soil. Sci., 96:221-229.

Farrington, J.W. and Quinn, J.G., 1971, Comparison of sampling and extraction techniques for fatty acids in recent sediments. Geochim. Cosmochim. Acta, 35:735-741.

Fenner, P., 1966, Clay mineral studies: results of investigation of pretreatment. Proc. Int. Clay Conf. 1966, Jerusalem, 1:401-406.

Follet, E.A.C., McHardy, W.J., Mitchell, B.D., and Smith, B.F.L., 1965a, Chemical dissolution techniques in the study of soil clays. 1. Clay Min., 6:23-24.

Follet, E.A., McHardy, W.J., Mitchell, B.D., and Smith, 1965b, Chemical dissolution techniques in the study of soil clays. Part II. Clay Min., 6:35-43.

Freed, R.L. and Peacor, D.R., 1992, Diagenesis and the formation of illite-rich I/S crystals in Gulf Coast shales: TEM study of clay separates. J. Sediment. Petrol., 62:220-234.

Foscolos, A.E. and Powell, T.G., 1980, Mineralogical and geochemical transformation of clays during catagenesis and their relation to oil generation, in, Miall, A.D., ed., Facts and Principles of World Petroleum Occurrence: Can. Soc. Petrol. Geol., Memoir 6:153-172.

Garrels, R.M., 1984, Montmorillonite/illite stability diagrams. Clays Clay Min., 32:161-166.

Gee, G.W. and Bauder, J.W., 1986, Particle-size analysis, in, Klute, A., ed., Methods of Soil Analysis:Part 1-Physical and Mineralogical Methods, Amer. Soc. Agro., Inc. and Soil Sci. Amer.,Inc. 2nd edition. 383-411.

Ghabru, S.K., Mermut, A.R., and St. Arnaud, R.J., 1989, Layer-charge and cation-exchange characteristics of vermiculite (weathered biotite) isolated from a gray luvisol in northeastern Saskatchewan. Clays Clay Min., 37:164-172.

Gipson, M., Jr., 1962, Ultrasonic disaggregation of shale. J. Sed. Petrol., 33:955-958.

Glasmann, J.R., Lartner, S., Briedis, N.A., and Lundegard, P.D., 1989a, Shale diagenesis in the Bergen High Area, North Sea. Clays Clay Min., 37:97-112.

Glasmann, J.R., Lundegard, P.D., Clark, R.A., Penny, B.K., and Collins, I.D., 1989b, Geochemical evidence for the history of diagenesis and fluid migration: Brent sandstone, Heather Field, North Sea. Clay Min., 24:255-284.

Gluskoter, H.J., 1965, Electronic low-temperature ashing of bituminous coal. Fuel, 44:285-291.

Grantz, A, Eittreim, S., and Dinter, D.A., 1979, Geology and tectonic development of the continental margin north of Alaska. Tectonophys., 59:263-291.

Grantz, A., May, S.D., Taylor, P.T. and Lawver, L.A., 1990, Canada Basin, in Grantz, A., Johnson, L., and Sweeney, J.F., eds., The Arctic Ocean Region, Boulder Colorado, Geological Society of America, The Geology of North America, v.L., 379-403.

Grim, R.E., Lamar, J.E., and Bradley, W.F., 1937, The clay minerals in Illinois limestones and dolomites. J. Geol., 45:828-843.

Gunther, P.R., 1975, Palynomorph color and dispersed coal particle reflectance from three Mackenzie delta boreholes. Geosci. Man., 15:35-39.

Guthrie, G.D. Jr. and Veblen, D.R., 1989, High-resolution transmission electron microscopy of mixed-layer illite/smectite: computer simulations. Clays Clay Min., 37:1-11

Guthrie, G.D. Jr. and Veblen, D.R., 1990, Interpreting one-dimensional high-resolution transmission electron micrographs of layer silicates by computer simulation. Amer Mineral., 75:276-288

Güven, N, 1988, Smectite, in, Bailey, S.W., ed., Hydrous Phyllosilicates (Exclusive of Micas): Reviews of Mineralogy, Mineral. Soc. Amer., 497-559.

Güven, N., 1991, On a definition of illite/smectite mixed-layer. Clays Clay Min., 39:661-662.

Haimila, N.E., Kirschner, C.E, Nassichuk, W.W., Ulmichek, G., and Procter, R.M, 1990, Sedimentary basins and petroleum resource potential of the Arctic Ocean region, in Grantz, A., Johnson, L., and Sweeney, J.F., eds, The Arctic Ocean region: Boulder, Colorado, Geol. Soc. Amer., The Geology of North America, v.L.503-538.

Halma, G., 1969, The separation of clay mineral fractions with linear heavy liquid density gradient columns. Clay Min., 8:59-69.

Hancock, N.J. and Taylor, A.M., 1978, Clay mineral diagenesis and oil migration in the Middle Jurassic Brent Sand Formation. J. Geol. Soc. Lon., 135:69-72.

Hansen, P.L. and Lindgreen, H., 1987, Structural investigations of mixed-layer smectite-illite clay minerals from North Sea oil rocks. Proc. 45th Ann. Meet. Electron Microsc Soc. Amer., 374-375.

Hansen, P.L. and Lindgreen, H., 1989, Mixed-layer illite/smectite diagenesis in Upper Jurassic Claystones from the North Sea and onshore Denmark. Clay Min., 24:197-213

Harward, M.E., Theisen, A.A., and Evans, D.D., 1962, Effect of iron removal and dispersion methods on clay mineral identification by X-ray diffraction. Soil Sci. Soc. Amer. Proc., 26:535-541.

Hatch, G.B. and Rice, O., 1938, Surface-active properties of hexametaphosphate. Indus Eng. Chem , 31:51-57.

Hawkings, T.J. and Hatlelid, W.G., 1975, The regional setting of the Taglu gas field, in, Yorath, C.J., Parker, E.R., and Glass, D.J., eds., Canada's continental margins. Can. Soc. Petrol. Geol Memoir 6:30-45.

Heling, D., 1974, Diagenetic alteration of smectite in argillaceous sediments of the Rhinegraben (SW Germany). Sediment., 21:463-472.

Heling, D., 1978, Diagenesis of illite in argillaceous sediments of the Rhinegraben. Clay Min., 13:211-220.

Hendricks, S.B. and Alexander, L.T., 1939, Minerals present in soil colloids: description and methods for identification. Soil Sci., 48:257-271.

Hitchon, B., Underschultz, J.R., Bachu, S., and Sauveplane, C.M., 1990, Hydrogeology, geopressures and hydrocarbon occurrences, Beaufort-Mackenzie basin. Bull. Can. Petrol. Geol., 38:215-235.

Hoffman, J. and Hower, J., 1979, Clay mineral assemblages as low grade metamorphic geothermometers, in, Scholle, P.A. and Schluger, P.R., eds., Applications to the thrust faulted disturbed belt of Montana, U.S.A, Aspects of Diagenesis, Soc. Econ. Paleon. Mineral. Special Pub., no. 26:55-79.

Horton, R.B., Johns, W.D., and Kurzweill, H., 1985, Illite diagenesis in the Vienna Basin, Austria. Tschermaks Min. Petr. Mitt., 34:239-260.

Howard, J.J., 1981, Lithium and potassium saturation of illite/smectite clays from interlaminated shales and sandstones. Clays Clay Min., 29:136-142.

Howard, J.J. and Roy, D.M., 1985, Development of layer charge and kinetics of experimental smectite alteration. Clays Clay Min., 33:81-88.

Hower, J., 1967, Order of mixed-layering in illite/montmorillonites. Clays Clay Min. 15:63-74.

Hower, J., Eslinger, E.V., Hower, M.E., and Perry, E.A., 1976, Mechanism of burial metamorphism of argillaceous sediment: 1. Mineralogical and chemical evidence. Bull. Geol. Soc. Amer. 87:725-737.

Hubbard, R.J, 1988, Age and significance of sequence boundaries on Jurassic and early Cretaceous rifted continental margins. Amer. Assoc. Petrol. Geol. Bull., 72:49-72.

Hubbard, R.J., Edrich, S.P., and Rattey, R.P., 1987, Geologic evolution and hydrocarbon habitat of the 'Arctic Alaska Microplate'. Mar. Petrol. Geol., 4:1-92.

Huff, W.D. and Whiteman, J.A. and Curtis, C.D., 1988, Investigation of a K-bentonite by x-ray powder diffraction and analytical transmission electron microscopy. Clays Clay Min., 36:83-93.

Ingersoll, R.V. and Suczek, C.A., 1979, Petrology and provenance of Neogene sand from Nicobar and Bengal Fans, DSDP sites 211 and 218. J. Sed. Petrol., 49:1217-1228.

Inoue, A., Kohyama, N., Kitagawa, R., and Watanabe, T., 1987, Chemical and morphological evidence for the conversion of smectite to illite. Clays Clay Min., 35:111-120.

Inoue, A., Velde, B., Meunier, A., and Touchard, G., 1988, Mechanism of illite formation during smectite-to-illite conversion in a hydrothermal system. Amer. Mineral., 73:1325-1334.

Jackson, M.L., 1969, Soil Chemical Analysis - Advanced Course. 2nd ed., publ. by author, Dept. Soil Sci., Univ. Wisconsin, Madison, Wisconsin, 895 pp.

Jackson, R.H., Johnson, G.L., Sundvor, E., and Myhre. A.M., 1984, The Yermak Plateau, formed at a triple junction. J. Geophys. Res. 89:3223-3232.

Jennings, S. and Thompson, G.R., 1986, Diagenesis of Plio-Pleistocene sediments of the Colorado River Delta, Southern California. J Sed. Petrol., 56:88-98

Jiang, W.-T., Essene, E.J., and Peacor, D.R., 1990a, Transmission electron microscopic study of coexisting pyrophyllite and muscovite: direct evidence for the metastability of illite. Clays Clay Min., 38:225-240.

Jiang, W.-T., Peacor, D.R., Merriman, R.J. and Roberts, B., 1990b, Transmission and analytical electron microscopic study of mixed-layer illite/smectite formed as an apparent replacement product of diagenetic illite. Clays Clay Min., 38:449-468.

Johns, W.D. and Kurzweill, H., 1979, Quantitative estimation of illite-smectite mixed phases formed during burial diagenesis. Tschermaks Min. Petr. Mitt., 26:202-215.

Johns, W.D. and McKallip, T.E., 1989, Burial diagenesis and specific catalytic activity of illite-smectite clays from Vienna Basin, Austria. Amer. Assoc. Petrol. Geol., 73:472-482

Johns, W.D. and Sen Gupta, P.K., 1967, Vermiculite-alkylammonium complexes. Amer. Mineral., 52:1706-1724

Jones, P.B., 1980, Evidence from Canada and Alaska on plate tectonic evolution of the Arctic Ocean basin. Nature, 285:70-84.

Jones, P.B., Brache, J., and Lentin, J.K., 1980, The geology of the 1977 offshore hydrocarbon discoveries in the Beaufort-Mackenzie Basin, N.W.T. Bull Can. Petrol. Geol , 28:81-102.

Jones, R.L. and Beavers, A.H., 1963, Silt-size whewellite and weddellite by soil peroxidation Soil Sci Soc. Amer. Proc., 27:356-357.

Jones, T.G., Hughes, T.L., and Tomkins, P., 1989, The ion content and mineralogy of a North Sea Cretaceous shale formation. Clay Min., 24:393-410.

Juhász, A.Z., 1990, Some surface properties of Hungarian bentonites. Colloids Sur., 49:41-55.

Jurik, P., 1964, Quantitative insoluble residue procedure. J. Sediment. Petrol., 34.666-668.

Kohyama, N., Fukushima, K., and Fukami, A., 1982, Interlayer hydrates and complexes of clay minerals observed by electron microscopy using an environmental cell., in, van Olphen, H. and Veniale, F., eds., Proc. Inter. Clay Conf., Bologna and Pavia, 1981, Elsevier, Amsterdam, 373-384.

Kittrick, J.A. and Hope, E.W., 1963, A procedure for the particle-size separation of soils by X-ray analysis. Soil Sci., 96:319-325.

Klimentidis, R.E. and Mackinnon, I.D.R., 1986, High-resolution imaging of ordered mixed-layer clays Clays Clay Min., 34:155-164.

Klug, H.P. and Alexander, L.E., 1974, X-Ray Diffraction Procedures, 2nd Ed, J. Wiley and Sons Inc., New York, 996 p.

Ko, J. 1992, Illite/smectite diagenesis in the Beaufort-Mackenzie Basin, Arctic Canada. Ph.D. Thesis, McGill University, Montreal, 184 p.

Ko, J. and Hesse, R., 1992, Illite/smectite diagenesis in overpressured and normally pressured environments, Beaufort-Mackenzie Basin, Arctic Canada, in, Kharaka, Y.K and Meast, A.S., eds., Proc. 7th Int. Symp. Water-Rock Interaction: Park City, Utah, 1173-1176.

Kodama, H., Gatineau, L., and Mering, J., 1971, An analysis of X-ray diffraction line profiles of microcrystalline muscovites. Clays Clay Min., 19:405-413.

Kunze, G.W. and Dixon, J.B., 1986, Pretreatment for mineralogical analysis, in, Klute, A., ed., Methods of Soil Analysis:Part 1-Physical and Mineralogical Methods, Amer. Soc. Agro., Inc. and Soil Sci. Amer.,Inc. 2nd edition, 91-99.

Lag, J., 1953, Observations on dispersing in the preparation of soil samples for mechanical analysis. Acta Agr. Scand., 3:113-119.

Lagaly, G., 1979, The "layer charge" of regular interstratified 2:1 clay minerals. Clays Clay Min., 27:1-10.

Lagaly, G., 1981, Characterization of clays by organic compounds. Clay Min., 16:1-21.

Lagaly, G., 1982, Layer charge heterogeneity in vermiculites. Clays Clay Min., 30:215-222.

Lagaly, G., 1984, Clay-organic interactions. Phil. Trans. R. Soc. Lond. A., 311:315-332.

Lagaly, G., 1987, Clay-organic interactions: Problems and recent results, Schultz, L.G., van Olphen, H., and Mumpton, F.A., Proc. Int. Clay Con. Denver, The Clay Minerals Society, Bloomington, Indiana, 343-351.

Lagaly, G. and Weiss, A., 1969, Determination of the layer charge in mica-type layer silicates, in, Heller, L., ed., Proc. Int. Clay Conf., Tokyo, Israel Univ. Press, Jerusalem, 61-80.

Lagaly, G. and Weiss, A., 1970, Inhomogeneous charge distribution in mica-type layer silicates, in, J.M. Serratosa, ed., Reunion Hispano-Belga de Minerales de la Arcilla, Consejo Superior de Investigaciones Cientificas, Madrid, 179-187.

Lagaly, G. and Weiss, A., 1976, The layer charge of smectitic layer silicates, in, Bailey, S.W., ed., Proc. Int. Clay Con., Mexico City, Applied Publishing, Wilmette, Illinois, 157-172.

Lagaly, G., Gonzalez, M.F., and Weiss, A., 1976, Problems in layer-charge determination of montmorillonites. Clay Min., 11:173-186.

Laird, D.A., Fenton, T.E. and Scott, A.D., 1988, Layer charge of smectites in an Argiaboll-Argiquoll sequence. Soil Sci. Soc. Amer. J., 52:463-467.

Laird, D.A., Scott, A.D., and Fenton, T.E., 1987, Interpretation of alkylammonium characterization of soil clays. Soil. Sci. Soc. Am. J., 51:1659-1663.

Laird, D.A., Scott, A.D., and Fenton, T.E., 1989a, Evaluation of the alkylammonium method of determining layer charge. Clays Clay Min., 37:41-46

Laird, D.A., Thompson, M.L., and Scott, A.D., 1989b, Technique for transmission electron microscopy and x-ray powder diffraction analyses of the same clay mineral specimen. Clays Clay Min., 37:280-282.

Laird, D.A., Barak, P., Nater, E.A., and Dowdy, R.H., 1991, Chemistry of smectitic and illitic phases in interstratified soil smectite. Soil Sci. Soc. Am. J., 55:1499-1504.

Lane, F.H. and Jackson, K.S., 1980, Controls on occurrence of oil and gas in the Beaufort-Mackenzie Basin, in, Miall, A.D., ed., Facts and Principles of World Petroleum Occurrence, Can. Soc Petrol. Geol., Memoir 6:489-507.

Lanson, B. and Champion, D., 1991, The I/S-to-illite reaction in the late stage diagenesis. Am. J. Sci., 291:473-506.

Laveulich, L.M. and Wiens, J.H., 1970, Comparison of organic matter destruction by hydrogen peroxide and sodium hypochlorite and its effects on selected mineral constituents. Soil Sci. Soc. Amer. Proc., 34:755-758.

Lawver, L.A. and Scotese, 1990, A review of tectonic models for the evolution of the Canadian Basin, in Grantz, A., Johnson, L., and Sweeney, J.F., eds., The Arctic Ocean Region, Boulder, Colorado, Geological Society of America, The Geology of North America, v. L, 593-618

Lawver, L.A., Grantz, A., Meinke, L., 1984, The tectonics of the Arctic Ocean, in, Dyer, I. and Chryssostomidis, C., Arctic Technology and Policy, Proc. 2nd Ann. MIT Sea Grant Coll. Prog. Lec. Sem. 3rd Ann. Hemisphere Publ. Co., 147-158

Lee, J.H. and Peacor, D.R., 1986, Expansion of smectites by laurylamine hydrochloride: ambiguities in transmission electron microscope observations. Clays Clay Min., 34:69-73

Lee, J.H., Ahn, J.H., and Peacor, D.R., 1985, Textures in layered silicates: progressive changes through diagenesis and low-temperature metamorphism. Jour, Sed. Petrology, 55:532-540

Lee, S.Y., Jackson, M.L., and Brown, J.L., 1975, Micaceous occlusions in kaolinite observed by ultramicrotomy and high resolution electron microscopy. Clays Clay Min., 23:125-129

Liewig, N., Clauer, N., and Sommer, F., 1987, Rb-Sr and K-Ar dating of clay diagenesis in Jurassic Sandstone Oil Reservoir, North Sea. Amer. Assoc. Petrol. Geol. Bull., 71:1467-1474.

Lindgreen, H., 1985, Diagenesis and primary migration in Upper Jurassic claystone source rocks in North Sea. Amer. Assoc. Petrol. Geol., 69:525-536.

Lindgreen, H. and Hansen, P.L., 1991, Ordering of illite-smectite in Upper Jurassic claystones from the North Sea. Clay Min., 26:105-125.

Lippmann, F. and Johns, W.D., 1969, Regular interstratification in rhombohedral carbonates and layer silicates Neues Jahrb. Mineral. Geol. Palaeontol. Monatsh. Abt. 1:212-221.

Love, K.M. and Woronow, A., 1991, Chemical changes induced in aragonite using treatments for the destruction of organic material. Chem. Geol., 93:291-301.

MacEwan, D M C., 1956, Fourier transform methods for studying scattering from lamellar systems. I. A direct method for analyzing interstratified mixtures. Kolloidzeitschrift, 149:96-108.

MacEwan, D.M.C., 1958, Fourier transform methods for studying X-ray scattering from lamellar systems II. The calculation of X-ray diffraction effects for various tyoes of interstratification. Kolloidzeitschrift, 156:61-67.

MacEwan, D M.C. and Wilson, M.J., 1980, Interlayer and intercalation complexes of clay minerals, in, Brindley, G.W. and Brown, G., Crystal Structures of Clay Minerals and their X-ray Identification, Mineral. Soc., 197-248.

Mackintosh, E.E., Lewis, D.G. and Greenland, D.J., 1971, Dodecylammonium-mica complexes - I. Factors affecting the exchange reaction. Clays Clay Min., 19:209-218.

Mackintosh, E E., Lewis, D.G., and Greenland, D.J, 1972, Dodecylammonium-mica complexes-II Characterization of the reaction products. Clays Clay Min., 20, 125-134.

Majorowicz, J.A. and Dietrich, J.R. 1989, Comparison of the geothermal and organic maturation gradients of the central and southwestern Beaufort-Mackenzie Basin, Yukon and Northwest Territories; in Current Research, Part G, Geological Survey of Canada, Paper 89-1G:63-67.

Majorowicz, J.A., Jones, F.W., and Jessop, A.M., 1988, Preliminary geothermics of the sedimentary basins in the Yukon and Northwest Territories (60 N-70 N) - estimation from petroleum bottom-hole temperature data. Bull. Can. Soc. Petrol. Geol., 36:39-51.

Majorowicz, J.A., Jones, F.W., and Judge, A.S., 1990, Deep subpermafrost thermal regime in the Mackenzie Delta basin, northern Canada - analysis from petroleum bottom-hole temperature data. Geophys., 55:362-371.

Malberg, R., Dekany, I. and Lagaly, G., 1989, Short-chain alkylammonium montmorillonites and alcohols: gas adsorption and immersional wetting. Clay Min., 24:631-647.

Malla, P.B, 1987, Characterization of layer charge, expansion behaviour, and weathering of 2:1 layer silicate clays. PhD. Thesis, Rutgers The State University of New Jersey, 205 p.

Malla, P.B. and Douglas, L.A., 1987a, Identification of expanding layer silicates: layer charge vs. expansion properties, in, Shultz, L.G., van Olphen, H., and Mumpton, F.A., eds., Proc. Int. Clay Conf., Denver, 1985, The Clay Minerals Society, Bloomington, Indiana, 277-283.

Malla, P.B. and Douglas, L.A., 1987b, Layer charge properties of smectites and vermiculites Tetrahedral vs. octahedral. Soil Sci Soc Am. J., 51 1362-1366

Malla. P.B. and Douglas. L.A., 1987c, Problems in identification of montmorillonite and beidellite Clays Clay Min., 35:232-236.

Marcks, Ch., Wachsmuth. H. and Graf von Reichenbach, H., 1989, Preparation of vermiculites for HRTEM. Clay Min., 24:23-32.

Martin, R.T., 1954, Calcium oxalate formation in soils from hydrogen peroxide treatment Soil Sci., 77:143-145

Mathers, A.C., Weed, S B., and Coleman, N.T., 1955, The effect of acid and heat treatment on montmorillonoids. Proc. 3rd Nat Conf Clays Clay Min., 3:403-412

McCarty, D.K. and Thompson, G R., 1991, Burial diagenesis in two Montana Tertiary basins Clays Clay Min., 39:293-305

McKee, T.R. and Brown, J.L., 1977, Preparation of specimens for electron microscopic examination, in, Dixon, J.B. and Weed, S.B., eds, Minerals in Soil Environments, Soil Sci Soc Amer, Madison, Wisconsin, 809-846.

McLaren, A.C., 1991, Transmission electron microscopy of minerals and rocks Cambridge University Press, Cambridge, 387 p.

McNeil, D.H., 1989, Foraminiferal zonation and biofacies analysis of Cenozoic strata in the Beaufort-Mackenzie Basin of Arctic Canada; in Current Research, Part G, Geological Survey of Canada, Paper 89-1G:203-223.

McNeil, D.H., 1990, Stratigraphy and paleoecology of the Eocene Stellarima assemblage zone (pyrite diatom steinkerns) in the Beaufort-Mackenzie Basin, Arctic Canada Bull Can Petrol Geol, 38:17-27.

McNeil, D.H., Ionnides, N.S., and Dixon, J., 1982, Geology and biostratigraphy of the Dome Gulf et al. Ukalerk C-50 well, Beaufort Sea. Geol Surv. Can Paper 80-32, 17 p

McWhae, J.R., 1986, Tectonic history of northern Alaska, Canadian Arctic, and Spitsbergen regions since Early Cretaceous. Amer. Assoc. Petrol. Geol Bull., 70:430-450

Mehra, O.P. and Jackson, M.L., 1960, Iron oxide removal by a dithionite-citrate system buffered with sodium bicarbonate, in, Swineford, A ,ed., Clays and Clay Minerals, Proc 7th Natl Conf, Washington, D C., 1958, Pergamon Press, New York, 317-327

Meunier, A. and Velde, B., 1989, Solid solutions in I/S mixed-layer minerals and illite Amer Mineral, 74:1106-1112

Mikhail, E.H. and Briner, G.P., 1978, Routine particle size analysis of soils using sodium hypochlorite and ultrasonic dispersion. Aust. J. Soil Res, 16:241-244

Mitchell, B.D., Farmer, V.C., and McHardy, W.J., 1964, Amorphous inorganic materials in soils. Advance Agron., 16 327-383

Mitchell, B.D. and Smith, B.F.L., 1974, The removal of organic matter from soil extracts by bromine oxidation. J. Soil Sci., 25.239-241

Moore, D.M. and Reynolds, R.C., Jr., 1989, X-Ray Diffraction and the Identification and Analysis of Clay Minerals. Oxford University Press, New York 332 p.

Morton, J.P., 1985, Rb-Sr evidence for punctuated illite/smectite diagenesis in the Oligocene Frio Formation, Texas Gulf Coast. Geol. Soc. Amer. Bull., 96-114-122.

Murakami, T., Sato, T., Watanabe, T., 1993, Microstructure of interstratified illite/smectite at 123 K: a new method for HRTEM examination. Amer. Mineral., 78 465-468.

Nadeau, P.H., 1985, The physical dimensions of fundamental clay particles. Clay Min., 20:499-514.

Nadeau, P.H. and Bain, D.C., 1986, Composition of some smectites and diagenetic illitic clays and implications for their origin. Clays Clay Min., 34:455-464

Nadeau, P.H. and Tait, J.M., 1987, Transmission electron microscopy, in, Wilson, M.J., ed., A Handbook of Determinative Methods in Clay Mineralogy. Blackie Glasgow, London, 6:209-247

Nadeau, P.H., Tait, J.M., McHardy, W.J., and Wilson, M.J., 1984a, Interstratified XRD characteristics of physical mixtures of elementary clay particles. Clay Min., 19:67-76.

Nadeau, P.H., Wilson, M.J., McHardy, W.J., and Tait, J.M., 1984b, Interstratified clays as fundamental particles. Sci., 225:923-925.

Nadeau, P.H., Wilson, M.J., McHardy, W.J., and Tait, J.M., 1984c, Interparticle diffraction: A new concept for interstratified clays. Clay Min., 19:757-769

Nadeau, P.H., Wilson, M.J., McHardy, W.J., and Tait, J.M., 1985, The conversion of smectite to illite during diagenesis: evidence from some illitic clays from bentonites and sandstones. Mineral. Mag., 49.393-400

Nadeau, P., Wilson, M., McHardy, W., and Tait, J., 1987, The fundamental nature of interstratified illite/smectite clay particles: A reply. Clays Clay Min., 35:77-79.

Nentwich, F.W., 1980, Sedimentology and stratigraphy of the Reindeer Formation (Early Tertiary) in the subsurface, Mackenzie Delta-Beaufort Sea area, Northwest Territories. M.Sc. thesis, Carleton University, Ottawa 125 p.

Nentwich, F.W., 1989, Petrography of Kugmallit sequence sandstones, Beaufort-Mackenzie Basin. Contract report prepared for the Department of Energy, Mines and Resources, Canada. 62 p.

Nentwich, F.W., and Yole, R.W., 1982, Sedimentary petrology and stratigraphic analysis of the

Nentwich, F.W., and Yole, R.W., 1982, Sedimentary petrology and stratigraphic analysis of the subsurface Reindeer Formation (Early Tertiary) Mackenzie Delta-Beaufort Sea area, Canada, in, Embry, A.F. and Balkwill, H.R., eds., Arctic Geology and Geophysics, Can. Soc. Petrol. Geol., Memoir 8 55-82

Newman, A.C.D. and Brown, G., 1987, The chemical constitution of clays, in, Newman, A.C.D., ed., Chemistry of Clays and Clay Minerals, Mineral. Soc. Monograph 6, Longman Scientific & Technical, 1-128.

Norris, D.K., 1985, Eastern Cordilleran foldbelt of northern Canada, its structural geometry and hydrocarbon potential. Amer. Assoc. Petrol. Geol. Bull., 69 788-808

Norrish, K., 1954, The swelling of montmorillonite. Trans. Faraday Soc., 19 120-134

Norrish, K. and Tiller, K.G., 1976, Subplasticity in Australian soils. V. Factors involved and techniques of dispersion. Aust. J. Soil Res., 14 273-289.

Ohr, M., Halliday, A.N., and Peacor, D.R. 1991, Sr and Nd isotopic evidence for punctuated clay diagenesis, Texas Gulf Coast. Earth Planet. Sci. Let., 105 110-126

Olis, A.C., Malla, P.B., and Douglas, L.A., 1990, The rapid estimation of the layer charges of 2 1 expanding clays from a single alkylammonium ion expansion. Clay Min., 25 39-50

Omueti, J.A.I. and Lavkulich, L.M., 1988, Identification of clay minerals in soil. the effect of sodium pyrophosphate. Soil Sci. Soc. Amer. J., 52 285-287

Page, R. and Wenk, H.-R., 1979, Phyllosilicate alteration studied by transmission electron microscopy. Contrib. Mineral. Petrol., 75:393-397

Peacor, D.R., 1992, Diagenesis and low-grade metamorphism of shales and slates, in, Buseck, P.R., ed., Minerals and Reactions at the Atomic Scale: Transmission Electron Microscopy. Reviews in Mineralogy. Mineral. Soc. Amer., 27 335-380

Pearson, M. and Small, J., 1988, Illite-smectite diagenesis and paleotemperatures in northern North Sea Quaternary to Mesozoic shale sequences. Clay Min., 23 109-132

Perez-Rodriguez, J.L. and Wilson, M.J., 1969, Effects of pretreatment on a 14A swelling mineral from Gartly, Aberdeenshire. Clay Min., 8:39-45.

Perry, E.A.,Jr., 1974, Diagenesis and K-Ar dating of shales and clay minerals. Geol. Soc. Amer. Bull., 85:827-830.

Perry, E.A. and Hower, J., 1970, Burial diagenesis in Gulf Coast pelitic sediments. Clays Clay Min., 18:165-177.

Perry, E. A. and Hower, J., 1972, Late-stage dehydration in deeply buried pelitic sediments. Amer. Assoc. Petrol. Geol. Bull., 56:2013-2021

Plançon, A., 1981, Diffraction by layer containing different kinds and stacking faults. J. Appl. Cryst. 16:62-69.

Plançon, A., Drits, V.A., Sakharov, B.A., Gilan, Z., I., and Ben-Brahim, J., 1983, Powder diffraction by layered minerals containing layers and/or stacking defects. Comparsion between Markovian and non-Markovian models. J. Appl. Cryst., 16:62-69.

Plançon, A., Sakharov, B.A , and Drits, V.A., 1984, Diffractional effects from homogenous mixed-layer crystals. Crystallograpr., 29:657-662.

Pollastro, R , 1982, A recommended procedure for the preparation of clay mineral specimens for X-ray diffraction analysis - Modifications to Drever's filter membrane peel technique. U.S. Geol. Surv., Open File Report 82-71, 10 p.

Pollastro, R , 1985, Mineralogical and morphological evidence for the formation of illite at the expense of illite/smectite Clays Clay Min., 33:265-274.

Pollastro, R.M., 1990, The illite/smectite geothermometer - concepts, methodology, and application to basin history and hydrocarbon generation, in, Nuccio, V.F. and Barker, C.E., eds., Applications of Thermal Maturity Studies to Energy Exploration. RMS-SEPM, 1-18.

Powell, T.G., Foscolos, A E., Gunther, P.R., and Snowdon, L.R , 1978, Diagenesis of organic matter and fine clay minerals: a comparative study. Geochim. Cosmochim. Act., 42:1181-1197.

Powers, M.C., 1967, Fluid release mechanisms in compacting marine mudrocks and their importance in oil exploration. Bull. Amer. Assoc. Petrol Geol., 51:1240-1254.

Price, F R. and Jenkins, D.A., 1980, Removal of resin from standard soil thin-sections by low temperature ashing as a means of following transmitted optical by scanning electron microscopy. Clay Min , 15:309-315.

Protz, R. and St. Arnaud, R.J., 1964, The evaluation of four pretreatments used in particle-size distribution analyses. Can. J. Soil Sci., 44:345-351.

Pusch, R., 1966, Ultrasonic dispersion of clay suspensions for granulometric and morphological investigations. Geol. Fören. Stockholm, 88:395-403

Pye, K., Krinsley, D.H. and Burton, J.H., 1986, Diagenesis of US Gulf Coast shales. Nature, 324:557-559

Ramseyer, K. and Boles, J.R., 1986, Mixed-layer illite/smectite minerals in Tertiary sandstones and shales, San Joaquin Basin, California. Clays Clay Min., 34:115-124.

Ransom, B. and Helgeson, H.C., 1989, On the correlation of expandability with mineralogy and layering in mixed-layer clays. Clays Clay Min., 37:189-191.

Reynolds, R.C., Jr., 1968, The effect of particle size on apparent lattice spacings. Acta Cryst., A24:319-320.

Reynolds, R.C. Jr., 1980, Interstratified clay minerals, in, Brindley, G.W. and Brown, G., eds., Crystal Structures of Clay Minerals and Their X-Ray Identification, Mineralogical Society, London, 249-303.

Reynolds, R.C. Jr., 1985, NEWMOD a computer program for the calculation of one dimensional diffraction patterns of mixed-layered clays R.C. Reynolds, 8 Brook Rd., Hanover, New Hampshire 03755.

Reynolds, R.C. Jr., 1989a, Diffraction by small and disordered crystals, in, Bish, D.L and Post, J.E., Modern Powder Diffraction: Reviews in Mineralogy, Mineral. Soc. Amer., 20 145-188

Reynolds, R.C.,Jr., 1989b, Principles and techniques of quantification analysis of clay minerals by X-ray powder diffraction, in, Pevear, D.R., and Mumpton, F.A., eds., CMS Workshop Lectures, Vol. 1, Quantitative Mineral Analysis of Clays, The Clay Minerals Society, Evergreen, Colorado, 4-37.

Reynolds, R.C. Jr., 1991, One- and three-dimensional x-ray powder diffraction studies of illite/smectite subjected to different sample preparation methods [abstr.] Prog. with Abs., 28th Ann. Meet. Clay Minerals Soc., 133.

Reynolds, R.C., 1992, X-ray diffraction studies of illite/smectite from rocks, < 1 µm randomly oriented powders, and <1 µm oriented powder aggregates. the absence of laboratory-induced artifacts. Clays Clay Min., 40:387-396.

Reynolds, R.C. Jr. and Hower, J., 1970, The nature of interlayering in mixed-layer illite-montmorillonites. Clays Clay Min., 18:25-36.

Robards, A.W., and Wilson, A.J., eds., 1993, Procedures in Electron Microscopy John Wiley & Sons Ltd, New York, 900 p.

Rosenberg, P.E., Kittrick, J.A., and Aja, S.U., 1990, Mixed-layer illite/smectite: a multiphase model. Amer. Mineral., 75:1182-1185.

Ross, G.J. and Kodama, H., 1984, Problems in differentiating soil vermiculites and soil smectites Agron. Abstr., 1984 Ann. Meet. ASA, CSSA, SSSA, Las Vegas, 275

Ross, M, 1968, X-ray diffraction effects by non-ideal crystals of biotite, muscovite, montmorillonite, mixed-layer clays, graphite, and periclase. Zeitschr. Kristall., 126 80-97

Rühlicke, G. and Kohler, E., 1981, Note: A simplified procedure for determining layer charge by the n-alkylammonium method. Clay Min., 16:305-307.

Rühlicke, G. and Niederbudde, E.A , 1985, Determination of layer-charge density of expandable 2:1 clay minerals in soils and loess sediments using the alkylammonium method Clay Min , 20:291-300.

Šaly, R., 1967, Use of ultrasonic vibration for dispersing soil samples. Sov. Soil Sci., 7:1547-1559.

Sass, B.M., Rosenberg, P.E., and Kittrick, J.A., 1987, The stability of illite/smectite during diagenesis: An experimental study. Geochim. Cosmochim. Acta, 51:2103-2115.

Sawhney, B.L., 1960, Weathering and aluminum interlayers in a soil catena: Hollis-Charlton-Sutton-Leicester Soil Sci. Soc. Amer. Proc., 24:221-226.

Schmidt, V., 1987, Petrological/diagenetic study of Upper Cretaceous and Tertiary strata, Beaufort-Mackenzie Basin. Geol. Surv. Can., Open File 1534, 49 p.

Schramm, L.L. and Kwak, J.C.T., 1980, Application of ultrafiltration/dialysis to the preparation of clay suspensions. Clays Clay Miner., 28:67-69.

Sears, S.K. and Hesse, R., 1992, Factors affecting the reliable ratio determinations of expandable to non-expandable components in mixed-layer illite-smectite. [abstr.] V M. Goldschimdt Conference, Reston, Va., Prog. with Abs., A-98.

Sears, S K., Hesse, R., and Vali, H., 1993a, Effects of pretreatment on layer structure of mixed-layer illite-smectite in XRD and TEM as revealed by n-alkylammonium-ion saturated samples [abstr.], Prog. with Abs., Geol. Assoc. Can. & Min. Assoc. Can., Joint Ann. Meet. Edmonton, A-95.

Sears, S.K., Hesse, R., Vali, H., Aronson, J.L., and Elliot, W.C., 1993b, Burial-diagenetic(?) K/Ar ages from the <0.05 µm fraction of illite/smectite mixed-layer clays, Reindeer D-27 well, Beaufort-Mackenzie Basin, Arctic Canada [abs.], Geol. Soc. Amer. Abs. with Prog. (in press).

Sella, C., Conjeaud, P., and Trillat, J., 1958, Nouvelle méthode d'étude par microscopie électronique de la structure superficielle des faces de clivages dalogénures alcalins. IV Inter. Kongr. Elektronenmikroskopie, 1:508-512.

Senkayi, A.L., Dixon, J.B., Hossner, L.R., and Kippenberger, L.A., 1985, Layer charge evaluation of expandable soil clays by an alkylammonium method. Soil Sci. Soc. Am. J., 49:1054-1060.

Senkayi, A.L., Dixon, J.B., Hossner, L.R., and Viani, B.E., 1983, Mineralogical transformations during weathering of lignite overburden in east Texas. Clays Clay Min., 31:49-56.

Smart, G. and Clayton, T., 1985, The progressive illitization of interstratified illite-smectite from carboniferous sediments of northern England and its relationship to organic maturity indicators. Clay Min., 20:455-466.

Smith, D.G., 1987, Late Paleozoic to Cenozoic reconstruction of the Arctic, in Tailleur, I.L., and Weimer, P., eds., Alaska North slope geology, Soc. Econ. Paleon. Min. Pacific Section and AK Geol. Soc., 102-111.

Spurr, A.R., 1969, A low viscosity epoxy resin embedding medium for electron microscopy. J. Ultrastructure Res., 26:31-43.

Środoń, J., 1980, Precise identification of illite/smectite interstratification by x-ray powder diffrraction. Clays Clay Min., 28:401-411.

Środoń, J. and Eberl, D.D., 1987, Illite, in Bailey, S.W., ed., Micas:Reviews in Mineralogy, Mineral Soc. Amer., 13:495-544.

Środoń, J., Andreoli, C., Elsass, F., and Robert, M., 1990, Direct high-resolution transmission electron microscopic measurement of mixed-layer illite/smectite in bentonite rock. Clays Clay Min., 38:373-379.

Środoń, J., Elsass, F., McHardy, W.J., and Morgan, D.J., 1992, Chemsitry of illite/smectite inferred from TEM measurements of fundamental particles. Clay Min., 27:137-158.

Środoń, J., Morgan, D.J., Eslinger, E.V., Eberl, D.D., and Karlinger, M.R., 1986, Chemistry of illite/smectite and end-member illite. Clays Clay Min., 34:368-378

Stanjek, H., Niederbudde, E.A., and Häusler, W., 1992, Improved evaluation of layer charge of n-alkylammonium-treated fine soil clays by Lorentz- and polarization-correction and curve-fitting. Clay Miner. 27:3-19.

Starkey, H.C., Blackmon, P.D., and Huff, P.L., 1984, The routine mineralogical analysis of clay-bearing samples. U.S. Geol. Surv. Bull. 1563, 32 p.

Stuhl, M. and Mortier, W., 1974, The heterogeneity of the charge density in montmorillonites. Clays Clay Min., 22:391-396.

Suquet, H. and Pezerat, A., 1987, Parameters influencing layer stacking types in saponite and vermiculite: a review. Clays Clay Min., 35:353-362.

Suquet, H. and Pezerat, H., 1988, Comments on the classification of trioctahedral 2:1 phyllosilicates. Clays Clay Min., 36:184-186.

Suquet, H., de la Calle, C., and Pezerat, H., 1975, Swelling and structural organization of saponite. Clays Clay Min., 25:231-242.

Sweeney, J.F., 1985, Comments about the age of the Canada Basin. Tectonophys., 114:1-10.

Tailleur, I.L., 1973, Probable rift origin of Canada Basin, in, Fitcher, M.G., ed., Arctic Geology, Amer. Assoc. Petrol. Geol. Mem., 19:526-535.

Tailleur, I.L. and Brosge, W.P., 1970, Tectonic history of northern Alaska, in, Adkinson, W.L. and Brosge, M.M., Proceedings of the Geological Seminar on the North Slope of Alaska. Amer. Assoc. Petrol. Geol., Pacific Sec., Los Angeles, E:1-19.

Tchoubar, C., 1984, X-ray studies of defects in clays. Phil. Trans. R. Soc. Lond. A 311:259-269

Tchoubar, C., Rautureay, M., Clinard, C., and Ragot, J.P., 1973, Technique d'inclusion appliquée à l'étude des silicates lamellaires et fibreux. J. Microscopie, 18:147-154.

Tessier, D. and Pédro, G., 1987, Mineralogical characterization of 2:1 clays in soils: importance of the clay texture, in, Schultz, L.G., van Olphen, H., and Mumpton, F.A., eds., Proc. Inter. Clay Conf., Denver, 1985, The Clay Minerals Society, Bloomington, Indiana, 78-84.

Tettenhorst, R. and Roberson, H.E., 1973, X-ray diffraction aspects of montmorillonites. Amer. Mineral., 58:73-80.

Tettenhorst, R T., Corbató, C.E., and Haller, R.I., 1990, The I-S contact in 10-Å/17-Å interstratified clay minerals. Clays Clay Min., 25:437-445.

Thorez, J., 1975, Phyllosilicates and clay minerals - a laboratory handbook for their X-ray diffraction analysis. Dison, Belgium, 604 p.

Thorez, J , 1985, Qualitative clay mineral analyses biased by sample treatments, in, 5th Meet. Europ. Clay Groups, 1983, 383-389.

Townsend, F.C. and Reed, L.W., 1971, Effects of amorphous constituents on some mineralogical and chemical properties of a Panamanian latosol. Clays Clay Miner., 19:303-310.

Troell, E , 1976, The use of sodium hypobromite for the oxidation of organic matter in the mechanical analysis of soils. J. Agric. Sci. Cambz., 21:476-483.

Trunz, V., 1976, The influence of crystallite size on the apparent basal spacings of kaolinite. Clays Clay Min., 24:84-87.

Tyner, E.H., 1939, The use of sodium metaphosphate for dispersion of solid for mechanical analysis. Soil Sci. 48:106-113.

Vali, H. and Bachmann, L., 1988, Ultrastructure and flow behaviour of colloidal smectite dispersions. J. Colloid. Interface Sci., 126:278-291.

Vali, H and Hesse, R., 1990, Alkylammonium ion treatment of clay minerals in ultrathin section: a new method for HRTEM examination of expandable layers. Amer. Mineral., 75:1445-1448.

Vali, H. and Hesse, R., 1992, Identification of vermiculite by transmission electron microscopy and x ray diffraction. Clay Min., 27:185-192.

Vali, H. and Köster, H.M., 1986, Expanding behavior, structural disorder, regular and random irregular interstratification of 2:1 layer silicates studied by high-resoluion images of transmission electron microscopy. Clay Min., 21:827-859.

Vali, H., Hesse, R., and Kodama, H., 1992, Arrangement of alkylammonium ions in phlogopite and vermiculite: an XRD- and TEM-study. Clays Clay Min., 40:240-245.

Vali, H., Hesse, R., and Kohler, E.E., 1991, Combined freeze-etched replicas and HRTEM images as tools to study fundamental-particles and multi-phase nature of 2:1 layer silicates. Amer. Mineral., 76:1953-1964.

Vali, H., Hesse, R., and Martin, R., 1993a, On a TEM-based definition of 2:1 layer silicates and their interstratified constituents. Amer. Mineral. (submitted)

Vali, H., Martin, R.F. Amarantidis, G., and Morteani, G., 1993b, Smectite-group minerals in deep-sea sediments: Monomineralic solid-solutions or multiphase mixtures. Amer. Mineral., 78:1217-1230.

van Langeveld, A.D., van der Gaast, S.J., and Eisma, D., 1978, A comparison of the effectiveness of eight methods for the removal of organic matter from clay. Clays Clay Min., 26:361-364

van Olphen, H., 1977, An Introdution to Clay Colloid Chemistry, 2nd Ed., John Wiley & Sons, New York, 318 p.

van Olphen, H., 1987, Dispersion and flocculation, in Newman, A.C.D., ed., Chemistry of Clays and Clay Minerals. Mineral. Soc. Monograph No. 6, Longman Scientific & Technical, 203-224

Veblen, D.R., 1983, Microstructures and mixed layering in intergrown wonesite, chlorite, talc, biotite, and kaolinite. Amer. Mineral., 68:566-580.

Veblen, D., Guthrie, G.,Jr., Livi, K., and Reynolds, R.,Jr., 1990, High-resolution transmission electron microscopy and electron diffraction of mixed-layer illite/smectite: experimental results Clays Clay Min., 38:1-13.

Velde, B. and Vassuer, G., 1992, Estimation of the diagenetic smectite to illite transformation in time-temperature space. Amer. Mineral., 77:967-976.

Veneman, P.L.M., 1977, "Calgon" still suitable. Soil Sci. Soc. Amer. J., 41:450.

Walker, G.F., 1957, On the differentiation of vermiculites and smectites in clays Clay Min. Bull., 3:154-163.

Walker, G.F., 1958, Reactions of expanding-lattice clay minerals with glycerol and ethylene glycol. Clay Min. Bull., 3:302-313.

Walker, G.F., 1967, Interactions of n-alkylammonium ions with mica-type layer silicates. Clay Min., 7:129-143.

Walker, P.H. and Hutka, J., 1973, Grain fragmentation in preparing samples for particle-size analysis Soil Sci So. Amer. Proc., 37:278-280.

Warren, B.E. and Averbach, B.L., 1950, The effect of cold-work distortion on X-ray patterns J Appl Phys., 21:595-599.

Warren, E.A. and Ransom, B., 1992, The influence of analytical error upon the interpretation of chemical variations in clay minerals. Clay Min , 27.193-209.

Weir, A.H. and Rayner, J.H., 1974, An interstratified illite-smectite from Denchworth series soil in weathered Oxford clay. Clay Min., 10:173-187

Weiss, A., 1963, Mica-type layer silicates with alkylammonium ions. Clays Clay Min., 10:191-224.

Whitehouse, U. and Jeffrey, L., 1955, Peptization resistance of selected samples of kaolinitic montmorillonitic and illitic clay minerals. Clays Clay Min., Natl. Acad. Sci., Nation. Res. Council Pub., 3:260-281.

Whittig, L.D. and Allardice, W.R., 1986, X-ray diffraction techniques, in Methods of Soil Analysis:Part 1-Physical and Mineralogical Methods, Klute, A., ed., Amer. Soc. Agro., Inc. and Soil Sci. Sci. Amer.,Inc. 2nd edition, 331-359.

Wielens, J.B.W., 1988, A brief outline of the pre-Mesozoic stratigraphy and structure of Tuktoyaktuk Peninsula, Northwest Territories, in, James, D.P. and Leckie, D.A., eds., Sequences, Stratigraphy, Sedimentology: Surface and Subsurface. Can. Soc. Petrol. Geol., Memoir 15:517-524.

Wilson, M.J. and Nadeau, P.H., 1985, Interstratified clay minerals and weathering processes, in, Drever, J.I., ed., Chemistry of weathering, D. Reidel Publ. Co., Dordrecht, Holland, 97-118.

Yaalon, D.H., 1976, "Calgon" no longer suitable. Soil Sci. Soc. Amer. J., 40:333.

Yau, Y.-C., Peacor, D.R., and McDowell, S.D., 1987, Smectite-to-illite reactions in Salton Sea shales: a transmission and analytical electron microscopy study. J. Sed. Petrol., 57:335-342.

Yau, Y.-C., Peacor, D.R., Beane, R.E., Essene, E.J., and McDowell, S.D, 1988, Microstructures, formation mechanisms, and depth-zoning of phyllosicicates in geothermally altered shales, Salton Sea, California. Clays Clay Min., 36:1-10.

Yoshida, T., 1973, Elementary layers in the interstratified clay minerals as revealed by electron microscopy. Clays Clay Min., 21:413-420.

Young, F.W., Myhr, D.W., and Yorath, C.J., 1976, Geology of the Beaufort-Mackenzie Basin. Geol. Surv. Can., Paper 76-11. 63 p.